ADVANCED REMOTE SENSING JOURNAL

Volume 2 Issue 2 DECEMBER 2022

ADVANCED REMOTE SENSING

(VOLUME: 2, ISSUE: 2)

DECEMBER, 2022

Aim

Advanced Remote Sensing Journal (ARSEJ) publishes regular research papers, reviews, letters, and communications covering all aspects of remote sensing science, from sensor design, validation/calibration, to its application in geosciences, environmental sciences, ecology, and civil engineering. Our aim is to publish novel / improved methods/approaches and/or algorithms of remote sensing to benefit the community, open to everyone in need of them. There is no restriction on the length of the papers or colors used. The method/approach must be presented in detail so that the results can be reproduced. There are, in addition, three unique features of this Journal:

- Manuscripts regarding research proposals and research ideas are welcome
- Electronic files and software regarding the full details of the calculation and experimental procedure, if unable to be published in a normal way, can be deposited as supplementary material
- We also accept manuscripts communicating to a broader audience with regard to research projects financed with public funds

(ARSEJ) is a **Blind Review** and a **free journal**. All of the responsibilities belong to authors.

Scope

Basic remote sensing applications
Multi-spectral and Hyperspectral remote sensing
Active and passive microwave remote sensing (RADAR/SAR)
Lidar and laser scanning
Geometric reconstruction
Image classification and analysis methods
Image processing and pattern recognition
Data fusion and data assimilation
Improvement of atmospheric modelling for radiometric correction
Modelling of parameters obtained from satellite data
Global modelling, monitoring and global database for sustainable development
Checking validity of data by using laboratory and in-situ test methods
Integration of remote sensing and GIS methods
Information utility for reducing disaster and risk effects: Early warning system, Impact assessment, monitoring, flexibility and risk reduction studies
Environmental pollution: Assessment and impact studies
Integration of remote sensing inputs and Earth surface applications
Monitoring growth of agricultural products for sustainable agriculture
Physical modeling and signatures
Change detection
Climate change studies
Global and regional dynamic of land use/biodiversity
Desertification and aridity studies
Soil, vegetation and carbon arc in shore and ocean water
Water quality studies
Dedicated satellite missions
Operational processing facilities
Spaceborne, airborne, unmanned aerial vehicle (UAV) and terrestrial platforms

Contents

Advanced Remote Sensing

http://publish.mersin.edu.tr/index.php/arsej

e-ISSN 2979-9104

Investigation of Land Use/Land Cover change in Mersin using geographical object-based image analysis (GEOBIA)

Raziye Hale Topaloğlu *[1]

[1]*Yıldız Technical University, Geomatics Engineering Department, Türkiye, haletopaloglu48@gmail.com*

Cite this study: Topaloğlu, R. H. (2022). Investigation of Land Use/Land Cover change in Mersin using geographical object-based image analysis (GEOBIA). Advanced Remote Sensing, 2(2), 40-46

Keywords
Remote sensing
GEOBIA
CORINE
Sentinel-2
Land Use/Land Cover

Research Article
Received: 25.05.2022
Revised: 08.09.2022
Accepted: 09.09.2022
Published: 28.12.2022

Abstract

In a rapidly changing and developing world, progressive urbanization with a growing population is inevitable. With the migration of people from rural areas to urban areas, both in Turkey and in the world, growth is continuously occurring even in small cities. Remote Sensing technologies provide fast and reliable data and methods for the examination of urban areas, and with these methods, it allows to produce highly accurate Land Use/ Land Cover (LU/LC) maps to examine the temporal changes of urban areas. This study aimed to interpret the changes in Mersin province in the last six years by using LU/LC maps. In this context, Sentinel-2 images of the years 2015 and 2021 with 10 m spatial resolution, including Mersin city center, were obtained. Highly accurate LULC maps of two different years were produced using geographic object-based image analysis (GEOBIA). During the object-based classification, Level 2 of the CORINE project terminology was used for the LU/LC classes. In this process, open-source geographic data (Open Street Map, Wikimapia) were also included in the classification. The LU/LC changes that were occurred in the study area in the last six years were evaluated by comparing the classification results, the areas of the detailed LU/LC classes were examined and the changes were put forward objectively.

1. Introduction

The increasing population in our country as well as all over the world lead to significant changes in urban areas. It is important to observe the past and current status of urban areas for the design of rapidly expanding cities. Remote sensing techniques are widely used to detect and monitor the change in urban areas [1, 2]. Satellite images with medium resolution optical satellite images such as Sentinel-2, and Landsat are widely used to produce Land Use/ Land Cover (LU/LC) maps. The maps are an important resource for accessing Earth Observation information and understanding the dynamics of urbanization and allow for analysis of developments over the years in urban [3]. Monitoring and mapping of LU/LC change and detailed analysis of these changes provide useful information to planners and decision-makers [3-5]. There are several methods of generating LC/LU maps. Geographic Object-Oriented Image Analysis (GEOBIA) is a widely used approach recently. GEOBIA is a technique that uses the analysis of image objects while traditional pixel-based classification uses pixels. It is possible to take into account topological relationships and use different functions and indexes, other than just spectral information with GEOBIA. Since different geographical data sources obtained from different platforms can be integrated into the GEOBIA classification, the method allows for obtaining detailed thematic classes with high accuracy [3, 6-8].

In this research, LU/LC maps were created from Sentinel-2 images of the 2015 and 2021 years of Tarsus, Toroslar, Mezitli, Yenişehir, and Mersin Central districts, and their changes in the last 6 years were analyzed. Sentinel-2 images were chosen because they were open-source data with 10-m spatial resolution in the RGB and

NIR bands. Furthermore, there were no recent studies investigating LU/LC change in Mersin by using Sentinel-2 images. In this study, the GEOBIA approach was used, rule sets were determined based on functions, indexes, and topological relations, and 2015 and 2021 LU/LC maps were created. During the classification, Open Street Map (OSM) and Wikimapia open-source geographic data were also used. Totally 14 classes in the second CORINE level were used to create LU/LC maps.

2. Study Area

Mersin province is located between 36-37° north latitude and 33-35° east longitude and the mid-south region of the Anatolian Peninsula. This province, which is one of the important cities in Turkey, has 13 districts in total and trade is highly developed due to being a port city [9,10].

Tarsus, Toroslar, Mezitli, Yenişehir, and Mersin Central districts, which are among the important districts of Mersin and constantly developing, were chosen as the study area. This District is located in the eastern part of Mersin, Turkey, and has approximately 3.880 km^2 surface area and various landscape characteristics including forest, agricultural areas, urban areas, and water bodies (Figure 1).

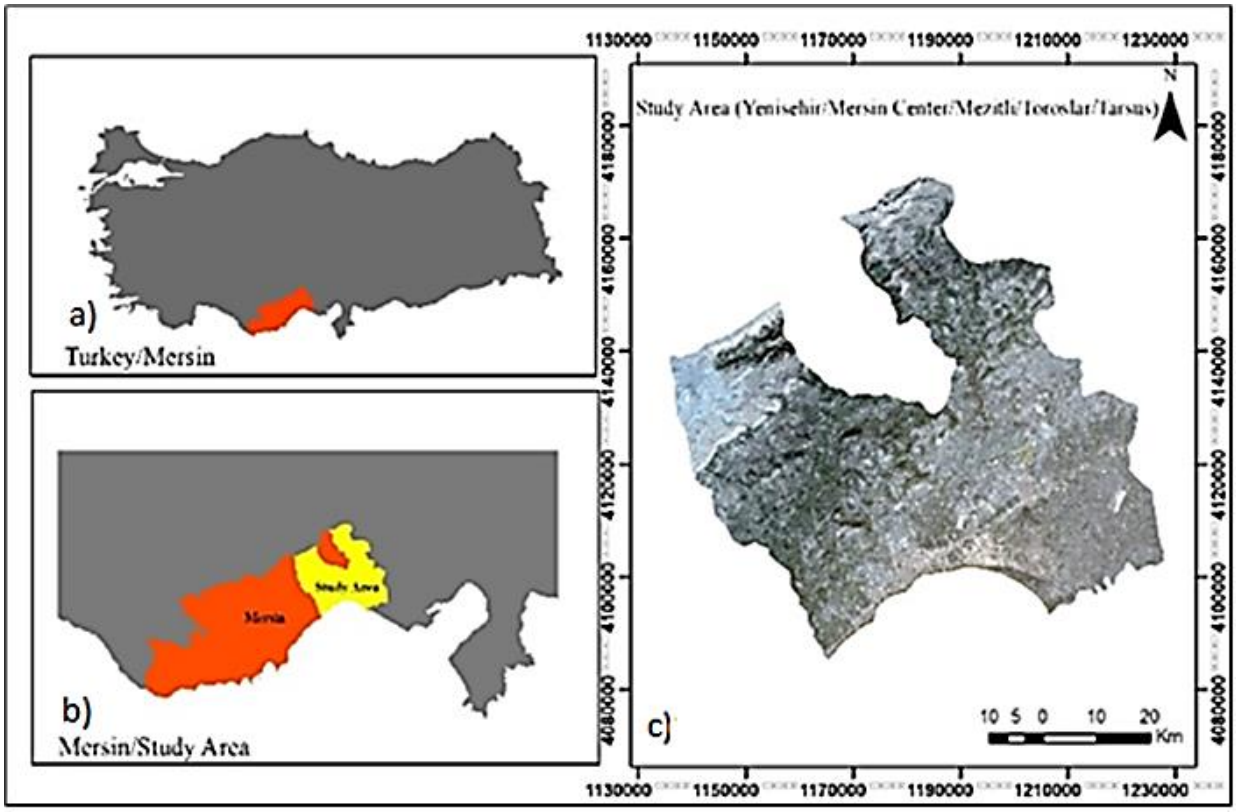

Figure 1. Location of the Study Area **(a)** Turkey (grey)/Mersin (orange); **(b)** Mersin(orange)/Study Area(yellow); **(c)** Tarsus, Toroslar, Mezitli, Yenişehir, and Mersin Central districts (Sentinel-2)

3.Method

3.1. Data

Four Sentinel-2 Level 2A images acquired on 02 September 2015 and 21 October 2021 are used. Sentinel-2 has 13 spectral bands with 10, 20, and 60-meter spatial resolution [11]. In this study, only the 10-meter spectral bands which are Red (665 nm), Green (560 nm), Blue (497 nm), and Near-Infrared (835 nm) are used. The images were ortho-rectified tiles of 100 km x 100 km in UTM WGS84 projections.

Open-source vector data were used to determine a more detailed class and increase accuracy. Open Street Map (OSM) and Wikimapia were used for extraction of land-use classes such as transport units and industrial areas and mine, dump, and construction sites. In addition, Imperviousness maps which are obtained from the Copernicus website were used to control the determined urban fabric classes. In this study, second-level CORINE classes for defining LU/LC classes.

Figure 2 illustrates the flowchart of the process chain. GEOBIA was performed using various indices, and features to create CORINE-based Level 2 LU/LC maps of the study area. Finally, an accuracy assessment was conducted to determine the accuracy of these two maps and evaluated change between 2015 and 2021.

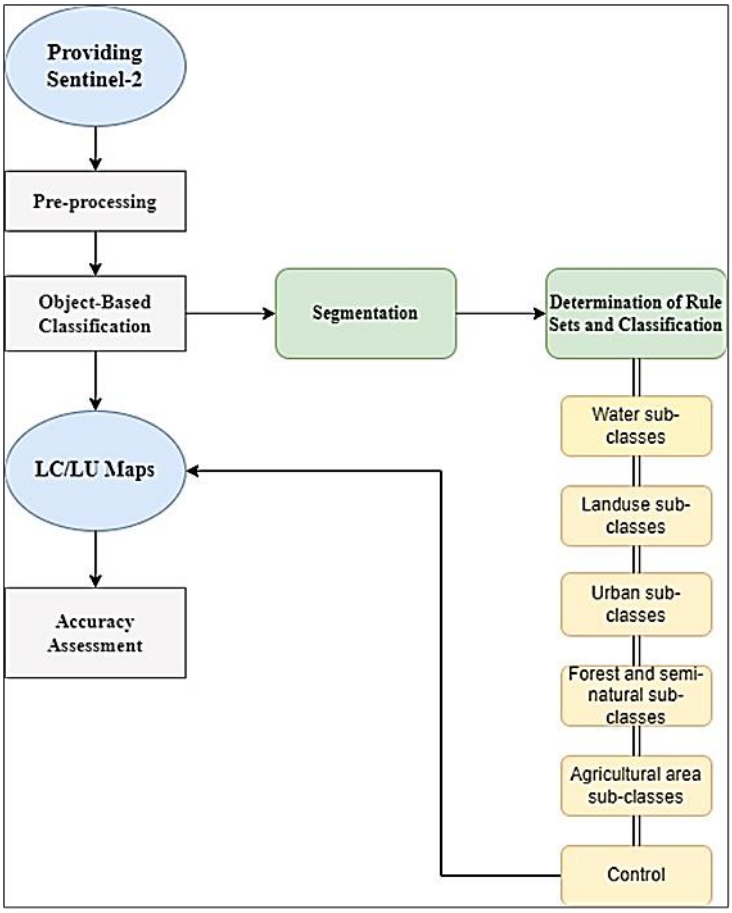

Figure 2. Flowchart of this study

3.2. Image Preprocessing

Sentinel images were obtained at the 2A level which constitutes ToA reflectance values. This shows that there is no need for geometric correction. 4 full frames that cover the study area were downloaded and RGB and NIR bands were layers stacked. Then, mosaic satellite images were created using the histogram matching method for the 2 frames of 2015, 2021 and both images were separately subsetted according to the study area borders.

A total of 14 classes were created according to the 2nd level CORINE nomenclatures and Figure 3 shows these classes.

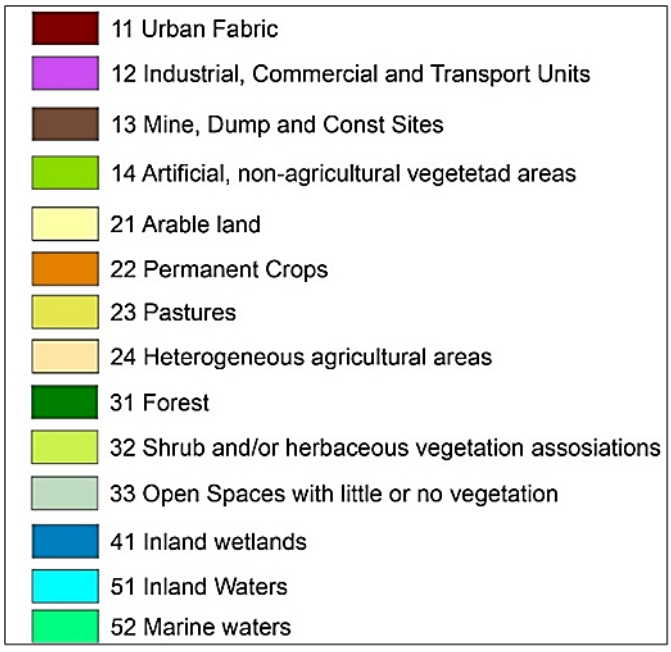

Figure 3. LU/LC classes used

3.3. Classification

The GEOBIA approach was used in the classification phase. The most important and first stage of Classification is the segmentation stage to obtain high accuracy classification results. There are many segmentation methods in the literature, the most used is multiresolution segmentation. Scale, shape, color, compactness, and smoothness, which are the control parameters of the method, should be chosen carefully considering the spatial resolution of the satellite image used [8,12,13]. In this study, the multiresolution segmentation method was used and the appropriate parameters were carefully selected. While the scale parameter varied between 700 and 100, the shape and compactness parameters differed between 0.9 and 0.4 for each LU/LC.

During the segmentation and classification phase, 3 open-source data were used to obtain better results for some of the LU/LC classes. These data were first checked for compatibility with the images and then included in the process. Some vectors were manually fixed since considering the image resolution some parts of the data were too detailed to be used. OSM for Road and Industrial Areas (12) (land use sub-class), Imperviousness Maps for urban fabric (11) class, and Wikimapia for other land-use classes (12,13, and 14) were used as supplementary open-source geo-information. Roads were used with a 10-meter buffer, as suggested in the Urban Atlas Mapping Guide [14]. The supplementary data were integrated into the recognition project as thematic layers and used in the GEOBIA procedure.

Different indices and functions that are defined in the recognition software were used in the classification step and explained in Table 1.

The classification phase was started with vegetated and artificial surface areas for two periods via NDVI and water sub-classes (41,51,52) were determined using Normalized Difference Water Index (NDWI) and Area and Distance to and Texture after Haralick functions.

Table 1. Indices and features used in this study [3,8,15]

Features/Indices	Explanations
NDVI	Normalized difference vegetation index; NDVI = (Layer 4 - Layer 1)/ (Layer 4 + Layer 1)
NDWI	Normalized difference water index; NDWI = (Layer 2 - Layer 4)/ (Layer 2 + Layer 4)
Brightness	Mean of the brightness values in an image
Maximum difference	Calculates the mean difference between the feature value of an image object and its neighbors of a selected class
Standard deviation of NIR	The standard deviation of the NIR band is derived from the intensity values of all pixels in this channel
Shape index	The measure of overall shape complexity
Border index	Describes how jagged an image object is; the more jagged, the higher its border index
Asymmetry	Compares an image object with an approximated ellipse around the given image object
Density	The distribution in space of the pixels of an image object
Area	The total number of pixels in the object
Length/Width	The length-to-width ratio of the mainline of an object
Coordinate (X, Y Center)	X-position and Y-position of the center of an image object. The calculation is based on the center of gravity (geometric center) of the image object in the internal map.
Related border to	Determines the relative border length an object shares with neighbor objects of a certain class
Distance to	The distance (in pixels) of the image object's center concerned to the closest image object's center assigned to a defined class
Texture after Haralick (GLCM)	Texture features are used to evaluate the texture of image objects. Texture after Haralick features is calculated from the gray level co-occurrence matrix.

Secondly, Industrial, commercial, and transport units (12) were determined using Open Street Map (OSM) and Wikimapia vector data and the geometric functions Asymmetry, Length /Width, Brightness, Related border to and Border Index, Shape index, Coordinate, and Maximum difference were used in addition to these vector data. Then the other step, the other land use sub-classes Mine, dump, and construction sites (13) and Artificial, non-agricultural vegetated areas (14) were identified using Wikimapia vector data including Border Index, Shape index, Coordinate (X, Y Center) and Maximum difference and Area functions.

In the third step, Urban fabric (11) was determined between unclassified areas in artificial surfaces with the help of imperviousness vector data and Brightness" and "Area function values.

In the next step, after applying a bigger scale segmentation to the unclassified areas, the classification of Forest (31) was classified by using NDVI, Texture after Haralick (GLCM), Standard deviation, and Maximum difference. Then, Scrub and/or herbaceous vegetation associations (32) and Open spaces with little or no vegetation fields were identified with a smaller scale factor and with the help of NDVI, Coordinate, Area, Maximum Difference, Density, and Standard Deviation functions.

In order to define agricultural sub-classes (21,22,23,24) Texture after Haralick (GLCM) functions were used. Firstly NDVI, Related border to, Standard deviation, Coordinate, Maximum difference feature, and indices, were

used to obtain the Arable Land. In addition to the NDVI index, Permanent Agriculture, Pastures, and Heterogeneous agricultural areas were recognized with the use of various Texture after Haralick. After the classification was completed and was controlled in all LU/LC classes, some areas were corrected by manual editing.

After classification processes, an error matrix was created by using 160 randomly selected reference points for each year. Results were evaluated based on the producer's and user's accuracies.

4. Results and Discussion

4.1. LU/LC Maps

In this study, LU/LC maps of Mersin metropolitan city were produced according to 2nd level CORINE nomenclature using the GEOBIA technique on Sentinel-2 dated 2015 and 2021 images. Classification results are shown in Figure 4. Totally 14 LU/LC classes each year were created. The class areas are represented in Table 2.

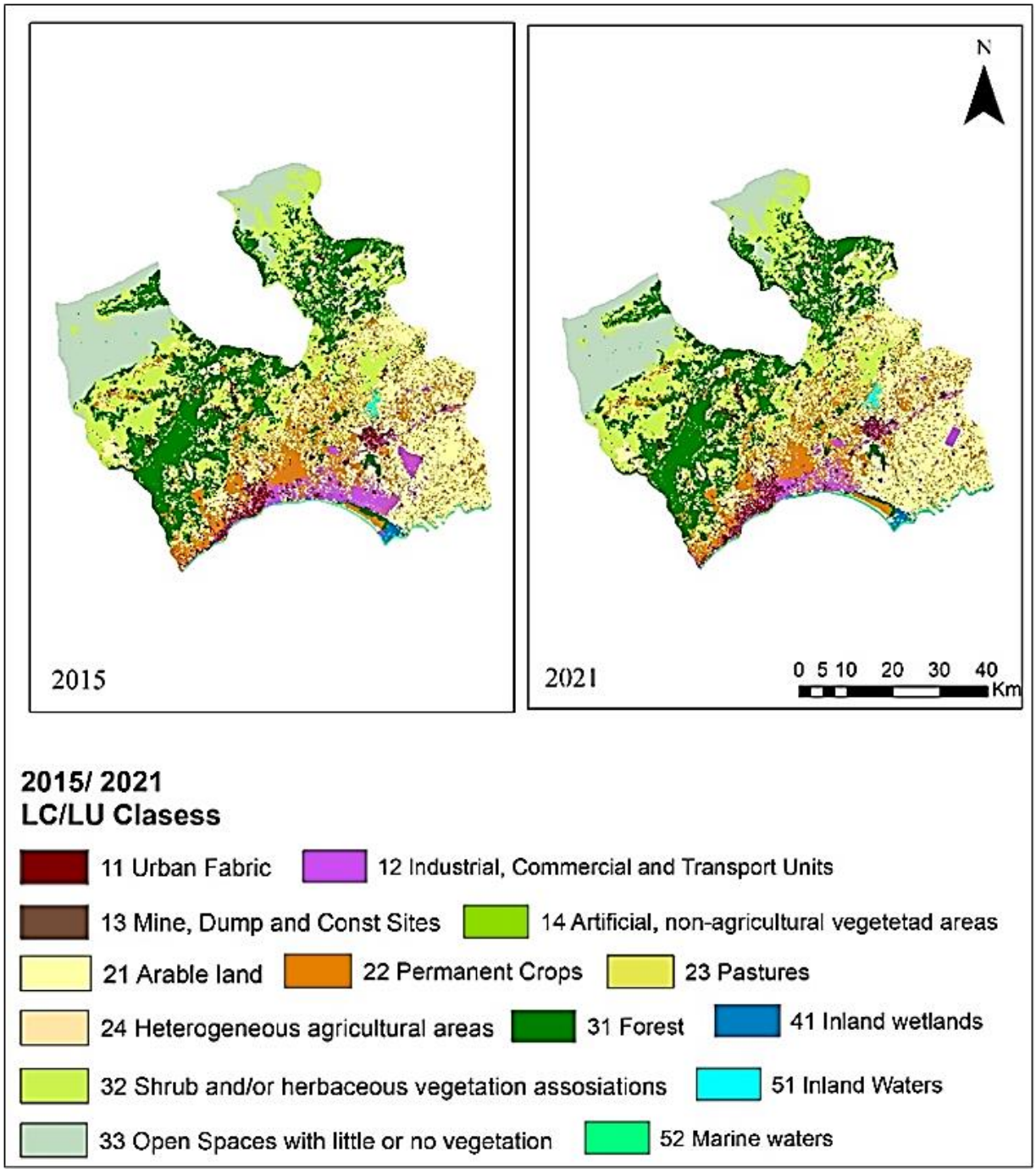

Figure 4. LU/LC maps of two years

According to the results, it is seen that there is an increase in urban fabric (11) in 2021 compared to 2015. In addition, the increase in other artificial areas (12,13,14) also shows that there is urbanization in the districts. Despite the increase in urban areas, the increase in agricultural areas (21,22) indicates that agriculture is also effective in 2021 among the livelihoods of the districts.

The decrease in the shrub and/or herbaceous vegetation associations (32) together with the increase in the open spaces with little or no vegetation (33) may mean that thinning has occurred in some native classes.

A decrease in the total area of wetland and water-related (expect 52) (41,51) classes in 2021 may indicate that there is a slight drought.

Table 2. Class areas in classified images

Class Code	Classes	2015 (km²)	2021 (km²)
11	Urban fabric	107,07	115,37
12	Industrial, commercial and transport units	161,12	180,49
13	Mine, dump and construction sites	19,78	20,18
14	Artificial, non-agricultural vegetated areas	6,94	7,79
21	Arable land	940,07	962,34
22	Permanent crops	466,04	470,24
23	Pastures	11,78	9,57
24	Heterogeneous agricultural areas	1,86	0,23
31	Forest	851,32	851,19
32	Shrub and/or herbaceous vegetation associations	799,54	748,54
33	Open spaces with little or no vegetation	448,83	452,28
41	Inland wetlands	11,34	9,81
51	Inland waters	32,89	30,28
52	Marine water	20,88	21,15
	Total	3879,46	3879,46

4.2. Accuracy Assessment

A point-based accuracy assessment was applied to determine the thematic accuracies of 14 LC/LU classes. To generate reference polygons, open-source geospatial data such as Google Earth, and Yandex Maps were used each year. 160 randomly selected points according to proportionally the class area in the study area were used in this phase. The accuracy assessment was completed and error matrixes were produced using ArcGIS software. Table 3 shows the overall and class level accuracy values. The overall accuracy of the 2015 and 2021 LU/LC maps were found as 80.63% and 82.50 %, respectively.

Table 3. Accuracy assessment results of LU/LC maps

Class Code	Producer's Accuracy (%)	User's Accuracy (%)	Producer's Accuracy (%)	User's Accuracy (%)
	2015		2021	
11	80.00	72.73	75.00	81.82
12	75.00	75.00	75.00	75.00
13	75.00	75.00	80.00	72.73
14	77.78	70.00	77.78	70.00
21	82.35	87.50	87.50	93.33
22	81.25	76.47	82.35	82.35
23	85.71	75.00	85.71	75.00
24	66.67	80.00	71.43	83.33
31	84.21	88.89	87.50	87.50
32	82.35	77.78	82.35	77.78
33	83.33	83.33	83.33	83.33
41	77.78	87.50	80.00	88.89
51	87.50	87.50	87.50	87.50
52	100.00	100.00	100.00	100.00
Overall Accuracy	80.63		82.50	
Kappa Statistics	0.7890		0.8100	

5. Conclusion

LC/LU maps provide accurate, reliable, and up-to-date geographic information important for the current status, change, effective management, and future planning of cities. To produce an efficient LC/LU map with accurate and detailed LU/LC classes, it is necessary to prefer the GEOBIA approach.

In this study, thanks to the use of Sentinel-2 images together with open-source geo-information, which can be obtained free of charge, detailed LU/LC maps were produced and the change in the study area were examined. In addition, detailed identification of agricultural areas was made possible by the GEOBIA approach. Thanks to the Texture of Haralick (GLCM) functions, many green areas can be distinguished.

The importance of using open-source data for the determination of land use classes is demonstrated by the ability to produce high accuracy from data with 10 m spatial resolution. However, it is extremely important to be able to analyze the satellite image and vector data compatibility well before proceeding to the classification stage.

Funding

This research received no external funding.

Conflicts of interest

The authors declare no conflicts of interest.

References

1. Joshi, N., Baumann, M., Ehammer, A., Fensholt, R., Grogan, K., Hostert, P., ... & Waske, B. (2016). A review of the application of optical and radar remote sensing data fusion to land use mapping and monitoring. *Remote Sensing*, *8*(1), 70.
2. Yılmaz, E. Ö., Varol, B., Topaloğlu, R. H., & Sertel, E. (2019, June). Object-based classification of Izmir Metropolitan City by using Sentinel-2 images. In *2019 9th international conference on recent advances in space technologies (RAST)* (pp. 407-412). IEEE.
3. Topaloğlu, R. H., Aksu, G. A., Ghale, Y. A. G., & Sertel, E. (2021). High-resolution land use and land cover change analysis using GEOBIA and landscape metrics: a case of Istanbul, Turkey. *Geocarto International*, 1-27.
4. Thapa, R. B., & Murayama, Y. (2009). Urban mapping, accuracy, & image classification: A comparison of multiple approaches in Tsukuba City, Japan. *Applied Geography*, *29*(1), 135-144.
5. Sertel, E., & Akay, S. S. (2015). High resolution mapping of urban areas using SPOT-5 images and ancillary data. *International Journal of Environment and Geoinformatics*, *2*(2), 63-76.
6. Weng, Q. (2012). Remote sensing of impervious surfaces in the urban areas: Requirements, methods, and trends. *Remote Sensing of Environment*, *117*, 34-49.
7. Chen, G., Weng, Q., Hay, G. J., & He, Y. (2018). Geographic object-based image analysis (GEOBIA): Emerging trends and future opportunities. *GIScience & Remote Sensing*, *55*(2), 159-182.
8. Sertel, E., Topaloğlu, R. H., Şallı, B., Yay Algan, I., & Aksu, G. A. (2018). Comparison of landscape metrics for three different level land cover/land use maps. *ISPRS International Journal of Geo-Information*, *7*(10), 408.
9. Alphan, H., & Çelik, N. (2016). Monitoring changes in landscape pattern: Use of Ikonos and Quickbird images. *Environmental monitoring and assessment*, *188*(2), 1-13.
10. Göksel, C., & Balçik, F. B. (2019). Land Use and Land Cover Changes Using Spot 5 Pansharpen Images; A Case Study in Akdeniz District, Mersin-Turkey. *Turkish Journal of Engineering*, *3*(1), 32-38.
11. ESA (2015). Sentinel-2 User Handbook, https://sentinel.esa.int/documents/247904/685 11/
12. Witharana, C., & Civco, D. L. (2014). Optimizing multi-resolution segmentation scale using empirical methods: Exploring the sensitivity of the supervised discrepancy measure Euclidean distance 2 (ED2). ISPRS Journal of Photogrammetry and Remote Sensing, 87, 108-121.
13. Hossain, M. D., & Chen, D. (2019). Segmentation for Object-Based Image Analysis (OBIA): A review of algorithms and challenges from remote sensing perspective. *ISPRS Journal of Photogrammetry and Remote Sensing*, *150*, 115-134.
14. European Union, (2016). Urban Atlas Mapping Guide, https://land.copernicus.eu/user-corner/technicallibrary/urban-atlas-mapping-guide, accessed 20.04.2021.
15. eCognition. (2017). Trimble eCognition© Developer 9.3 for Windows Operating System Referans Book, Trimble: Germany GmbH, Munich.

Advanced Remote Sensing

http://publish.mersin.edu.tr/index.php/arsej

e-ISSN 2979-9104

An assessment of physical development prediction in Shiraz (Iran) and its relationship with geomorphological factors

Khalil Valizadeh Kamran[*1], Abuozar Nasiri[2], Rahman Zandi[3], Najmeh Shafiei[2], Rababeh Farzin Kia[2]

[1]University of Tabriz, Department of Remote Sensing and GIS, Iran, valizadeh.tabrizu.ac.ir
[2]Firouzabad Institute of Higher Education, Faculty of Geography, Iran, abuzarnasiri@gmail.com, najmeh@yahoo.com, r.farzinkiya@gmail.com
[3]Hakim Sabzevari University, Department of Remote Sensing and GIS, Iran, r.zandi@hsu.ac.ir

Cite this study: Kamran, K. V., Nasiri, A., Zandi, R., Shafiei, N., & Kia, R. F. (2022). An assessment of physical development prediction in Shiraz (Iran) and its relationship with geomorphological factors. Advanced Remote Sensing, 2 (2), 47-57

Keywords
Satellite images
Land use
Markov chain model
Shiraz
OLS model

Research Article
Received: 20.08.2022
Revised: 26.09.2022
Accepted: 01.10.2022
Published:28.12.2022

Abstract

The development of cities and their environmental impacts have adverse consequences. However, it is possible to move toward sustainable development through knowledge and awareness of the urban areas, investigation, application, and optimal use of modern technologies and sciences. The current study examined the land-use changes of the city of Shiraz using remote sensing (RS) and geographical information system (GIS) to estimate the increase in the urban area, the reduction in agricultural and horticultural lands, the abuse of rangelands, and unauthorized construction in mountainous areas during 2000-2018. City development was determined in the time interval of 2025 using the maximum likelihood algorithm, supervised method, and Markov chain model. The relationship between land use and geomorphological factors was examined using the OLS method, the results of which showed an increase in the area of built-in land use and a decrease in the area of barren and agricultural lands in Shiraz during 2000-2018. Over the 7-year period, the area of built-in (36%), horticultural and agricultural (11%), barren (19%), and rangeland (46%) land use will change. According to the output of the OLS method, distance from the fault and distance from the channel had the highest impact on urban development risk compared to other parameters with the probability of 83% and 72% and error of 0.007 and 0.008, respectively.

1. Introduction

The contemporary urban world has, unfortunately, caused a distance from the natural environment and the unwanted acceptance of imbalances that stem from the asymmetric relationships between humans and urban space [1]. Urban land use is one of the most critical issues of modern life [2]. Urban development, which affects large areas of land, is important in low latitudes and particularly in developing countries whose urban growth has overtaken Europe and North America [3].

Physical development in Iranian cities has always been associated with changes in the urban structure due to geographical features, human density, population growth, and rural migration, leading to unbalanced urban development. Accordingly, the growth of urbanization over the past decades has been disproportionate to the ability to equip urban spaces and expand infrastructure, creating severe problems such as expensive housing, unemployment, and informal housing represented in the urban physical body [4]. It is necessary to consider hazards and seek risk-free conditions in urban planning and models of urban physical development to reduce the

vulnerability of the population and ensure future developments. Urban sprawl is a dominant phenomenon that has caused the occupation of more land in low-density compared to dense and compact cities [5]. Although man-made areas cover only 3% of the Earth's surface, they have had a significant environmental impact on a global and local scale [6]. For example, the proximity of urban areas to agricultural lands has resulted in very unfavorable environmental consequences such as desertification and soil erosion. Thus, access to up-to-date and accurate information on land-use change is necessary to understand and manage the outcomes of such changes [7-8]. The area of the city of Shiraz has increased significantly in recent years, and urban sprawl has caused various economic, environmental, and social consequences. The current study aims to investigate the urban development of Shiraz and the related risks in recent years.

Alansi et al. [9] investigated the land hazards of urban development in the Malaysian river basin using the GIS technique. Guan et al. [10] used the cellular automata model and Markov chain to model land-use changes and examine the balance of urban growth and environmental protection by 2069. The results of this study showed an increase in urban land use and a decrease in agricultural lands and forest coverage in the study area. Václavík and Rogan [11] used the Land Change Modeler to examine land use/land cover changes in the Olomouc Region of the Czech Republic. According to their results, 9% of the mixed forest had been transformed into a broadleaf forest, and the residential areas increased by 35%. Kuldeep and Kamlesh [12] prepared a land-use map for Uttarakhand using Landsat satellite images between 2000 and 2009. After classification and validation, the results showed a significant decrease in the forest and agricultural lands and a considerable increase in residential land use in less than a decade. Iqbal [13] examined the trend of land-use changes in the urban area of Chittagong in Bangladesh from 1989 to 2011 using Landsat TM. The results showed a 27% change in the area under study. De Oliveira Silveira et al. [14] used the object-based method and images of Landsat 8 and Sentinel to classify forest landscape vegetation in Brazil. Huo et al. [15] used Landsat satellite data and object-based classification method to study deforestation in the United States from 2003-2011. They reported an overall accuracy of 88.1% image classification and introduced the object-based method as a suitable method for monitoring forest land degradation.

2. Material and Method

2.1. Study area

Shiraz is one of the metropolises of Iran, the capital of Fars province, and located in southwestern Iran. This city is at an altitude of 1550 meters above sea level in the mountainous region of Zagros with a temperate climate. The city of Shiraz is the third largest city in Iran with an area of 348 km^2 and a population of 1547129. Shiraz is in longitude of 52°20’ to 52°47’ and latitude of 29°22’ to 29°42’. The city is located on a plane with a mild slope (5%) from the west to the east, limited to Baba Kuhi, Kaftarak, and Bemo Mountains from the north, Sabzpooshan mountains from the south, Derak Mountain from the west, and Maharloo Lake from the east. The city is connected to Marvdasht from the north, Firoozabad from the south, Arsanjan and Sarvestan from the east, and Kazerun from the west (Figure 1).

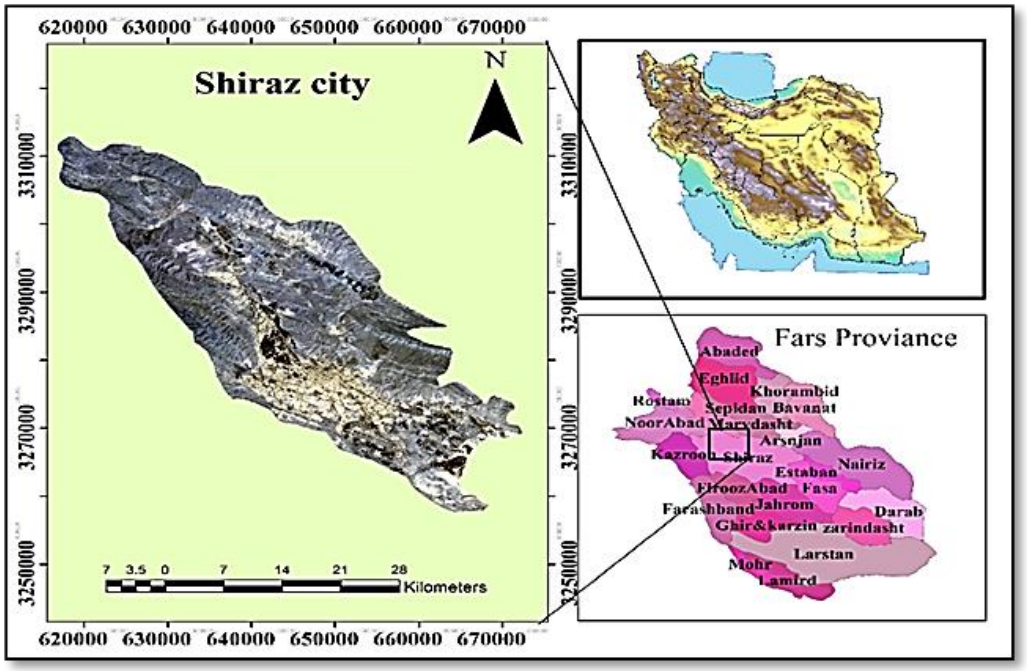

Figure 1. Location of the study area

This study used the images of the ETM sensor for 2000 and 2006 and the OLY sensor from Landsat 7 and 8 for 2018. The layer of distance from the fault and lithology from the 1:100000 geological map of Iran was used. The layer of distance from the channel, height, slope, and aspect provided from the DEM layer was used to examine the hazard and its role in urban physical development.

The dates of the images were 28.05.2000, 24.05.006, and 27.11.2019, respectively, and training samples were used to classify the pixels. Accordingly, the classification operation is performed in the form of intended training classes by defining specific pixels of the image for each class. The supervised algorithm (maximum likelihood) was used for classification. This method classifies the value of each unknown pixel based on its variance and covariance, after which its specific spectral response is analyzed. It is assumed that data of each class are distributed based on the normal distribution around the mean pixel of that class. In practice, the variance, covariance, and the mean of the different classes of each satellite image are calculated to classify the phenomena and assign each pixel to a class in which it is most likely to be present. Markov chain model was used to determine the changes in the land use in the study area (Shiraz), including horticultural and agricultural lands, urban areas, barren lands, and rangeland. The general flowchart of the research is shown in Figure 2.

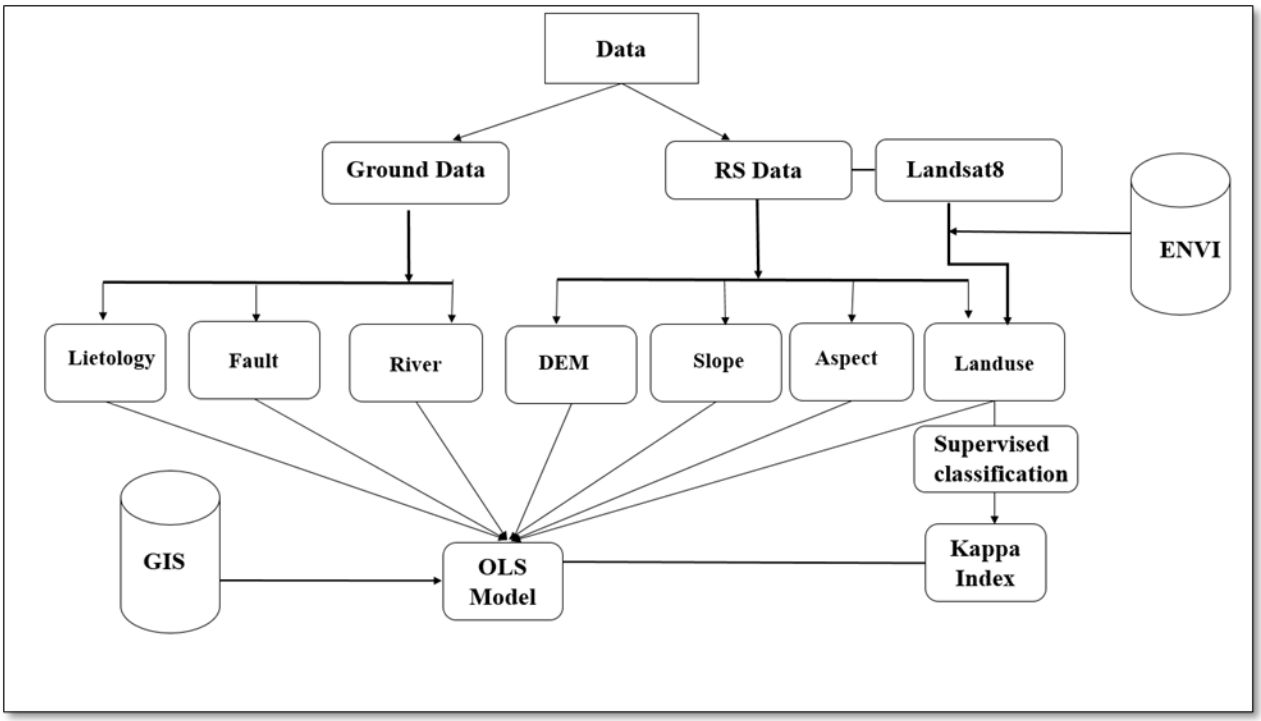

Figure 2. The general flowchart of the research

2.2. Markov Chain Model and CA-Markov

The Markov chain model operates as a random process in which the future state of a pixel depends only on its previous state, based on which it is predicted. The state transition probability matrix is the direct result of this model; however, there are no geographical interpretations in this model, and the model does not produce a single map indicating the spatial distribution of classes. John Von Neumann designed the CA-Markov model in the 1950s to add a spatial feature to the Markov model and address this problem [16]. Equation (1) is used to calculate prediction on the Markov model.

$$S(t+1) = P_{ij} \times s(t) \quad (1)$$

In which s(t) and s(t+1) indicate the system states at the time of t and t+1, respectively, and P_{ij} represents the transition probability matrix in a state, calculated by Equation (2).

$$p_{ij} = \begin{matrix} p_{11} & p_{12} & \cdots & p_{1n} \\ p_{21} & p_{22} & \cdots & p_{2n} \\ \cdots & \cdots & \cdots & \cdots \\ p_{n1} & p_{n2} & \cdots & p_{nn} \end{matrix} \quad (2)$$

In the Markov chain, land-cover classes are used as chain states. This analysis always uses 3-raster maps called models. In addition to these two maps, the CA Markov model also considers the time interval between the two images and the forecast time interval in the 2025 horizon. The output of the Markov model also includes the transition probabilities between states, the matrix of transitioned areas in each class, and finally the potentially conditional images for land use changes. Also, this study has used the Kappa index, which is calculated from the Equation 3, to ensure the classification.

$$Kappa = (P\_0-P\_C) / (1-P\_C) * 100 \quad (3)$$

P0: Observed agreement
PC: Expected agreement

2.3. The Results of Classification Accuracy

The calculation of the error matrix is one of the most widely used methods to assess classification accuracy. After the classification of the images, the kappa index and the overall accuracy of the classified maps were calculated based on the error matrix, indicating good agreement of the classification and the types of land-use classes. Table 1 shows the assessment of the classification accuracy of the satellite images. Accordingly, the overall accuracy is more than 90%, and the kappa index is between 0.88 and 0.9.

Table 1. The assessment of the classification accuracy of the satellite images

Years	Image	Kappa Index	Accuracy coefficient
2000	ETM	90/0	92%
2006	ETM	93%	94%
2018	OLI	88/0	91%

2.4 The Regression Model of Ordinary Least Squares (OLS)

The ordinary least square method (OLS) is the simplest and most common among the common regression models.

The idea behind the ordinary least square method is to assign values to the model coefficients that make the regression model closest to the observations, which means the least deviation from the observations. In spatial modeling with the OLS method, the coefficients or parameters of the statistical model are assumed constant concerning location (geographical coordinates). Therefore, the value of the dependent variable estimated by this model is for the whole study area. However, one of the drawbacks of this method in spatial modeling is the estimation of the same value for different parts of the area. The simple univariate linear regression model is as Equation 4:

$$\gamma i=\beta 0+\beta 1xi+\varepsilon i \quad (4)$$

In which, γ, x, εi, β_0, and β_1 represent dependent variable (estimated), independent variable (estimator), error or model deviation in estimation, and model parameters or coefficients, respectively. the values of β_0 and β_1 are assumed to be constant for all the basin area. The statistical model of OLS and the matrix of model coefficient estimation are expressed by the following relations:

$$\beta \hat{} =(XTX)-1XTy \quad (5)$$

$$y=X\beta+\varepsilon \quad (6)$$

In which T, XTX (-1), and X indicate Matrix Transpose, inverse of variance-covariance matrix, and matrix of independent variables, respectively. The coefficients of the OLS multivariate regression model are constant across the location. It is not possible to map the spatial changes of the parameters or coefficients of the model using this model. Besides, this model is incompatible with ARC GIS software and does not consider spatial correlation [17].

3. Results

Given the changes in the city from 2000 to 2018, most of the urban development has occurred in the northwest direction. Barren land has undergone insignificant changes because most of the growth has been on horticultural, agricultural, and rangeland. According to the output of the maps in the three time periods of 2000, 2006, 2018, the

most land-use changes have been related to the built-in areas as a result of excessive construction, particularly from 2006 to 2018 in Shiraz, affecting other land uses adversely (Figures 3-5).

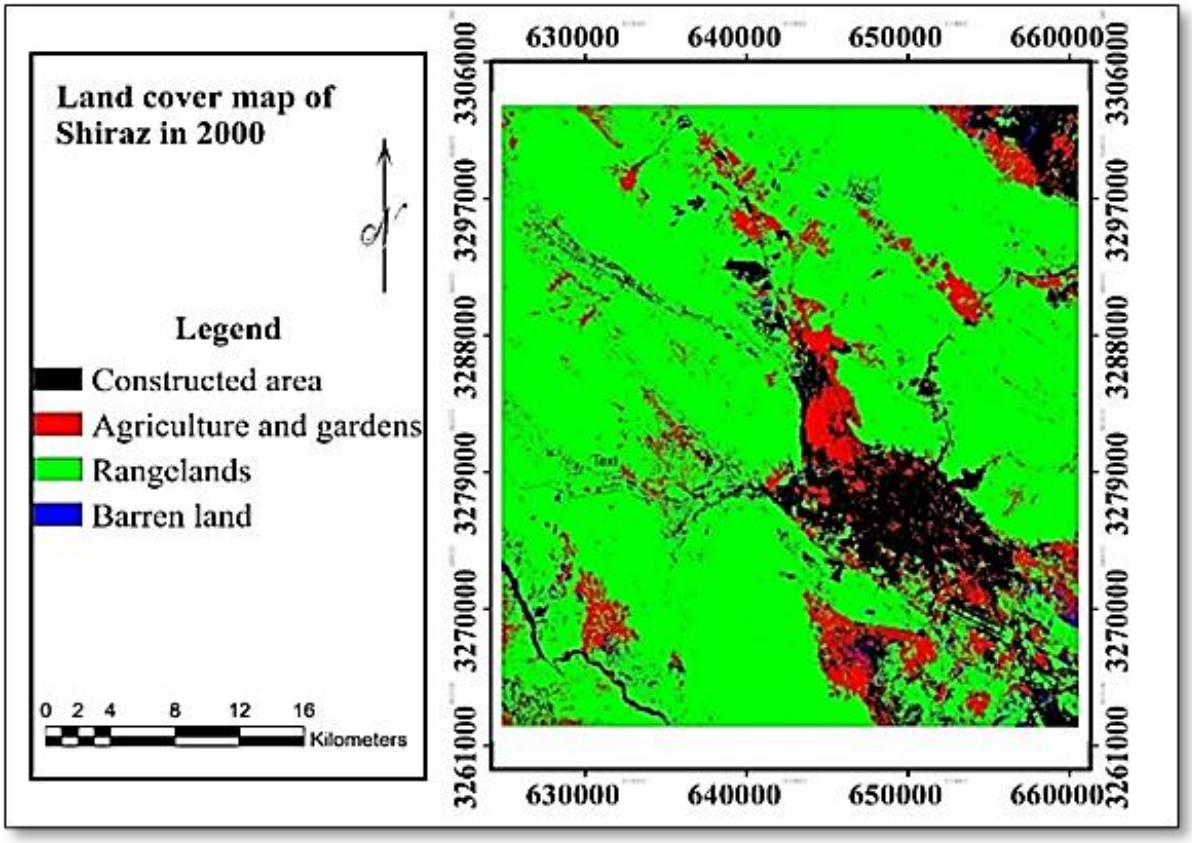

Figure 3. Land cover map of Shiraz city in 2000

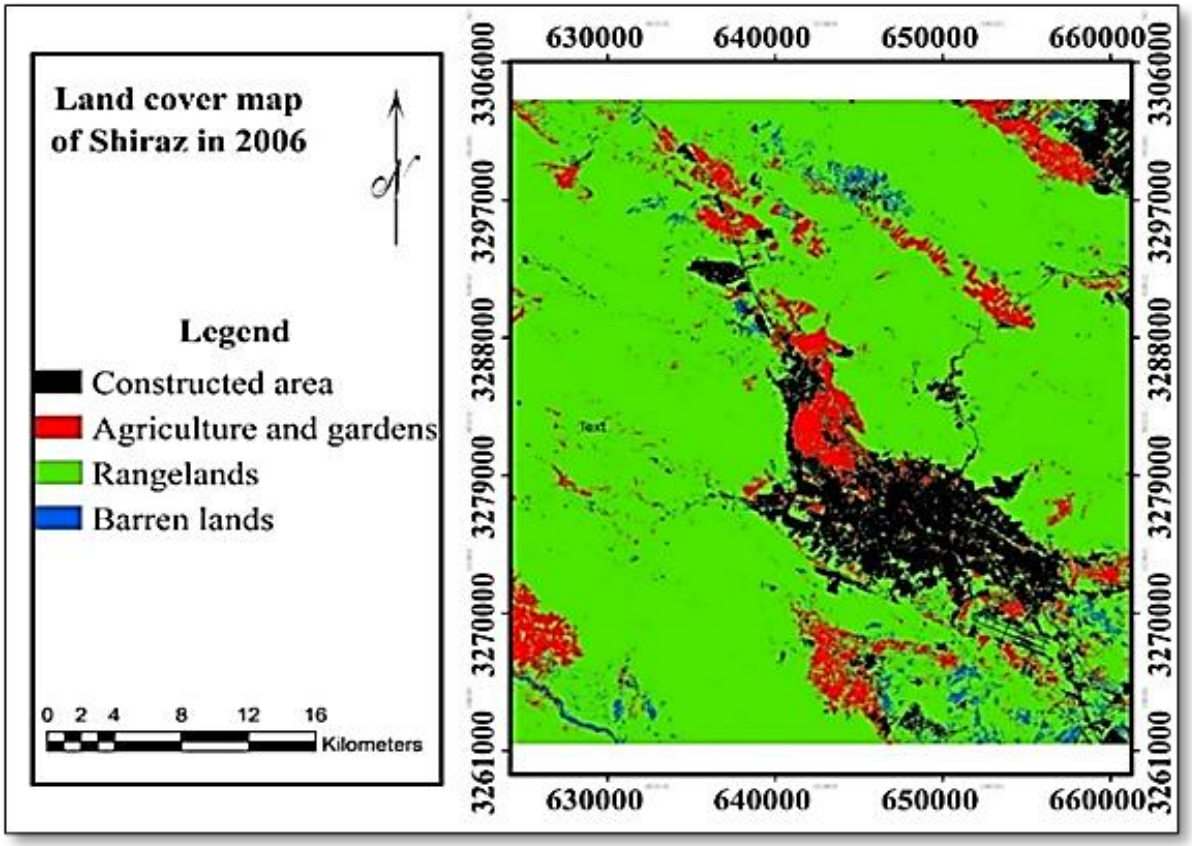

Figure 4. Land cover map of Shiraz city in 2006

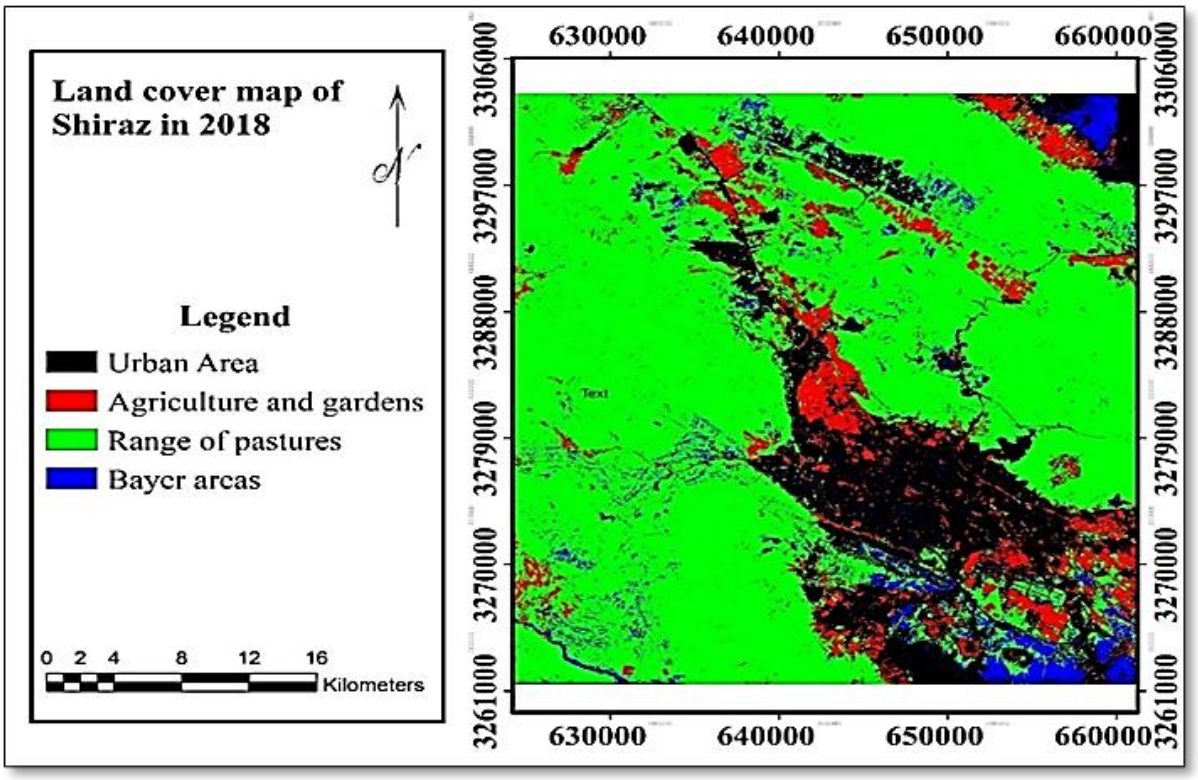

Figure 5. Land cover map of Shiraz city in 2018

3.1 State Transition Matrix

As shown in Table 2, the state transition matrix between 2000 and 2006 indicates that most changes have been from rangeland to horticultural and agricultural land use (84586 m^2) and rangeland to built-in land use (83589 m^2). Most agricultural land in Shiraz is allocated to horticulture; thus, rangeland has changed into built-in land use during this period.

Table 2. State Transition area matrix between 2000 and 2006 (in square meters)

Land cover	Built-in area	Gardens and Agriculture	Rangelands	Barren lands
Built-in area	160601	10935	16579	2422
Gardens and Agriculture	7547	108381	33851	1544
Rangelands	83589	84589	1499752	10064
Barren lands	11956	2410	24431	5229

According to Table 3, the highest probability of land use transition in the period 2006 to 2018 is related to the change of rangeland into horticultural and agricultural land use (and vice versa). From 2006 to 2018, the horticultural, agricultural, barren, and rangeland area has decreased, while urban area has increased to around 164477 m^2.

Table 3. State Transition area matrix between 2006 and 2018 (in square meters)

Land cover	Built-in area	Gardens and Agriculture	Rangelands	Barren lands
Built-in area	164477	22249	14926	15337
Gardens and Agriculture	7845	82282	66343	3047
Rangelands	6813	46075	139767	14262
Barren lands	11402	717	64707	11380

According to Table 4, the built-in area has followed an increasing trend in Shiraz from 2000 to 2018. The urban development of Shiraz is in the form of extensive and horizontal sprawl. Accordingly, the built-in area in Shiraz was 237, 271, and 316 km^2 in 2000, 2006, and 2018, respectively, indicating an approximately 79 km^2-increase in the built-in area of Shiraz. On the other hand, the areas of horticultural and agricultural land, barren land, and rangeland have reduced from 2000 to 2018 due to the urban development of Shiraz. Table 4 indicates the area of each land use in 2000, 2006, and 2018. The table shows an increase in the area of built-in land and a decrease in

the area of rangeland from 2000 to 2018. The land uses of horticultural and agricultural on the one hand and barren land, on the other hand, have had reverse changes. From 2000 to 2006, the area of agricultural, horticultural, and barren lands has decreased while the area of rangeland has increased. However, in the next 10-year period, the urban area has increased, and the area of agricultural, barren, and rangeland has decreased. These changes are associated with the concentration of population and migration of people from the surrounding suburbs to the city of Shiraz, leading to the development of residential and commercial complexes by destroying horticultural and agricultural lands.

Table 4. Land area in 2000, 2006 and 2018 (in square meters)

Land cover	2000	2006	2018
Built-in area	237	271	316
Gardens and Agriculture	185	136	143
Rangelands	1471	1510	1318
Barren lands	173	39	79

3.2 Prediction of Land Use Classes by 2025

The Markov chain model was used to predict changes in the mentioned classes. The classification classes are used as chain states in this model. Also, the transition area matrix represents the area of the land use changed into another land use during 2000-2018. The area of the four land use classes was determined in the 2025 horizon using the output of the tables and the Markov chain model. These data determine the extent of built-in, horticultural and agricultural, barren, and rangeland classes in 2025 for the city of Shiraz (Figure 6). According to the area of land uses in 2018 and the prediction of their changes by 2025, the most changes have been in the built-in area with a 36% increase, after which the areas of barren land (19%), agricultural and horticultural land (11%), and rangeland (46%) have decreased. Among these, the changes in horticultural, agricultural, and barren lands are not significant (Table 5).

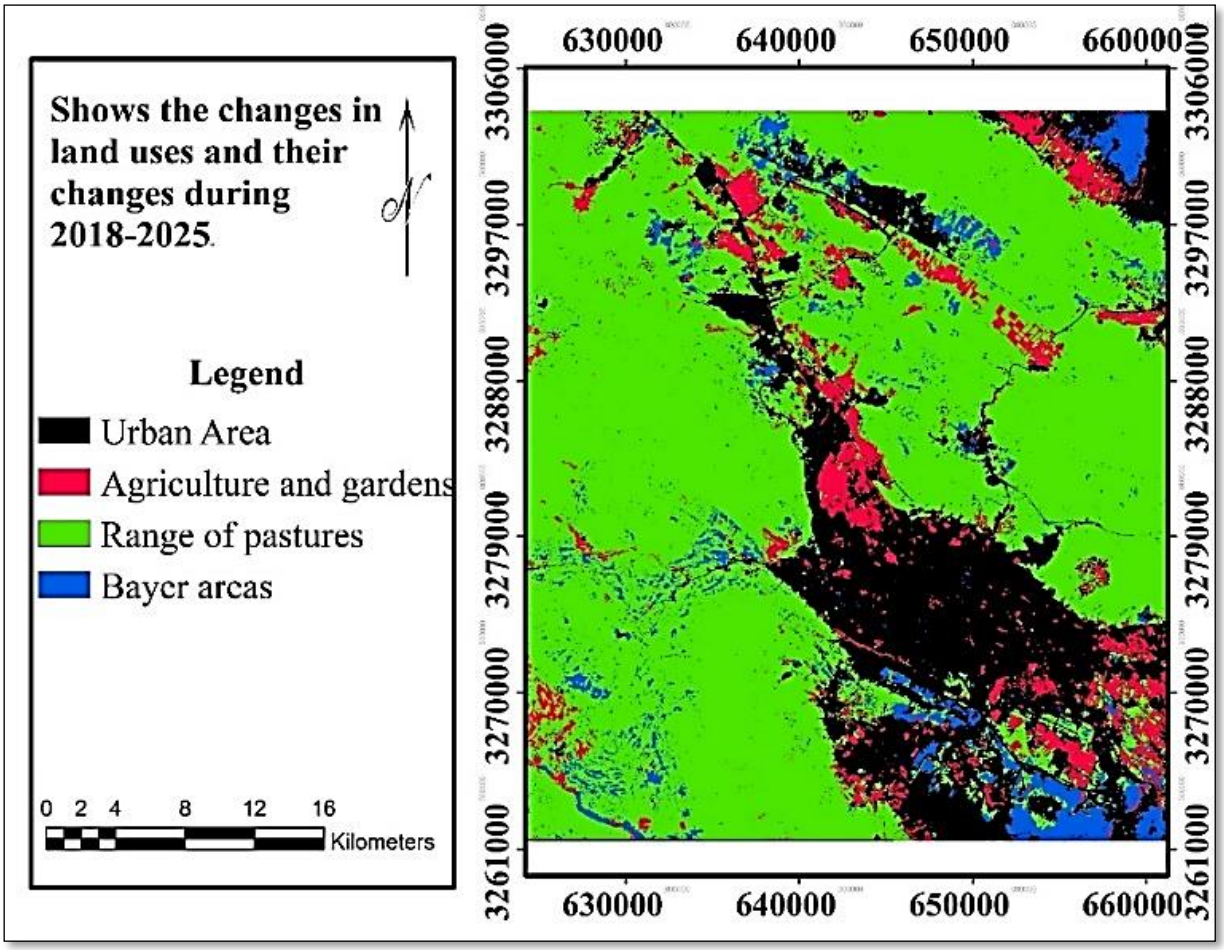

Figure 6. Different land uses and their changes in the study area during 2018-2025

Table 5. Prediction of Land Use Classes in the 2018- 2025 horizon

Land cover	2018	2025	Increase in changes in the 2025 horizon (in percent)
Built-in area	316197000	391657500	36%
Gardens and Agriculture	143565300	147025800	11%
Rangelands	1318344300	122972800	46%
Barren lands	79385400	89055900	19%

3.3 Elevation and Slope

Usually, the maximum suitable slope for urban planning is 9%, and values exceeding 9% increase urban development costs. Slopes close to zero bring about problems in terms of sewage disposal, leading to water pollution and area saturation when the groundwater level is high.

Therefore, urban development costs increase in these areas. The city of Shiraz has a normal slope in the range of 0-6 degrees, indicating that no serious hazards threaten the city. The city of Shiraz is located at an altitude of 1458 to 1892 meters, which is almost high. The central and southern parts of the city are much lower in height, and the northern areas have recently built towns at higher altitudes (Figure 7).

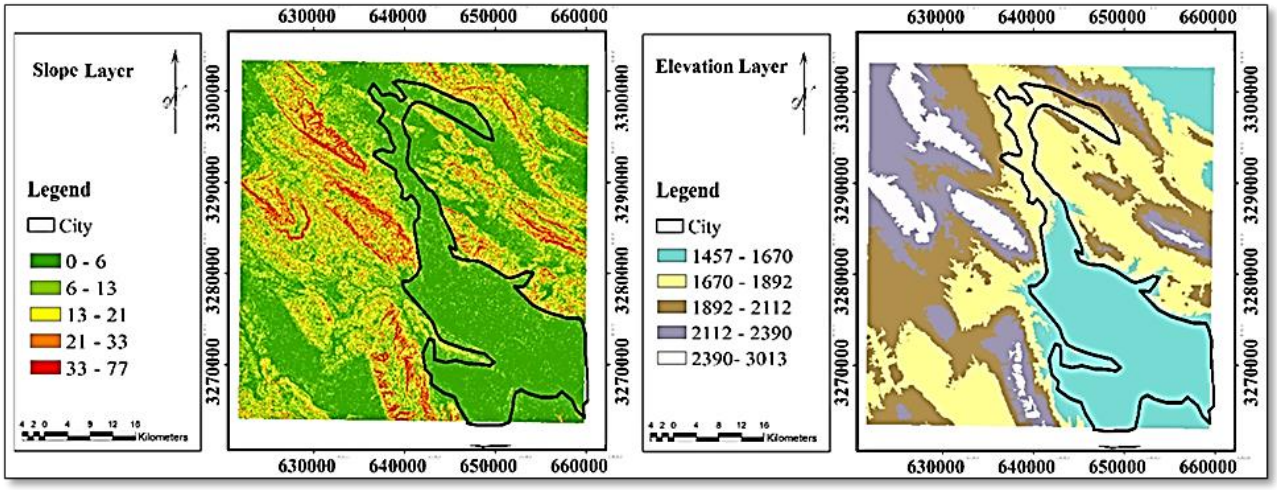

Figure 7. Layer of elevation and slop of Shiraz city

3.4 Lithology and Geomorphology

According to the lithology of the city, the southern, northern, and western parts are limited to calcareous formations, and the north and northwest of the city are limited to the Jahrom Lime Formation with resistant materials. According to satellite images in different years, the city has developed toward sediments inside calcareous formations in the mountainous areas, leading to adverse effects for the residents and different hazards such as earthquakes and landslides. Geomorphology is another influential parameter in the discussion of urban development. The geomorphology map of Shiraz indicated that the city has been formed in an alluvial fan and is suitable for urbanization (Figure 8).

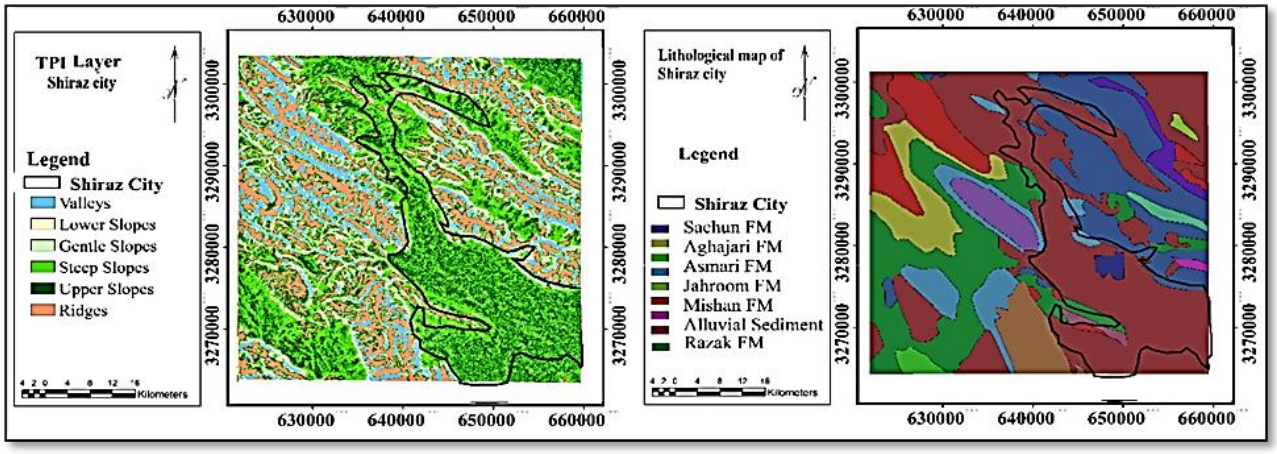

Figure 8. Lithology and geomorphology layer of Shiraz city

3.5 Fault and Channel

The fault is an influential factor in creating hazards, particularly in urban areas. Construction in the fault area and failure to avoid the proximity of fault can result in irreparable damage in the city of Shiraz. The current state of the city is the result of the changes in its urban physical body from 2000 to 2017. This fault, which was once far from the urban area of Shiraz, now passes through the new neighborhoods under construction in the north of the city because of the development of construction and towns on its territory. The development of the city toward the north is greatly important. The main river of Shiraz, which passes through the city center, has been dry in recent years due to successive droughts, but there are sometimes heavy rains in the area. However, the city has developed toward the river in recent years due to the failure to consider the appropriate distance from the channel. Construction in this direction leads to problems in the case of heavy rains and floods, along with the destruction of the buildings and irreparable damages due to the high speed of the flood. Another problem that can gradually lead to a crisis concerning these constructions is the inrush of sewage into residential and commercial units (Figure 9).

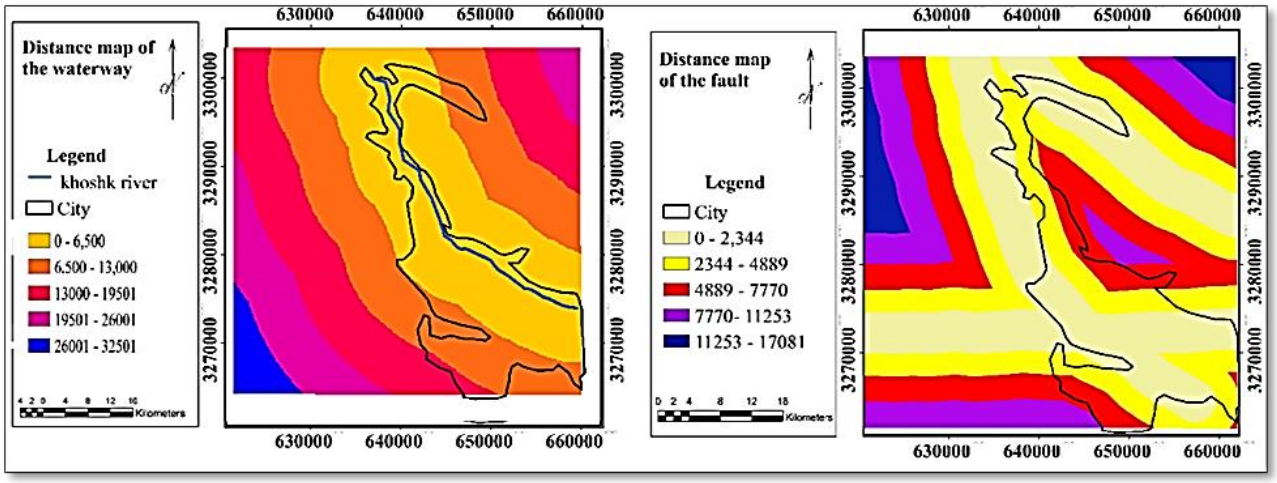

Figure 9. Distance map of the fault and distance map of the waterway of Shiraz city

3.6 Aspect

Aspect is an influencing factor in urban development. According to the aspect in the region, the southern slopes seem suitable for residential purposes and streets because of receiving more sunlight and appropriate airflow in the study area (Figure 10).

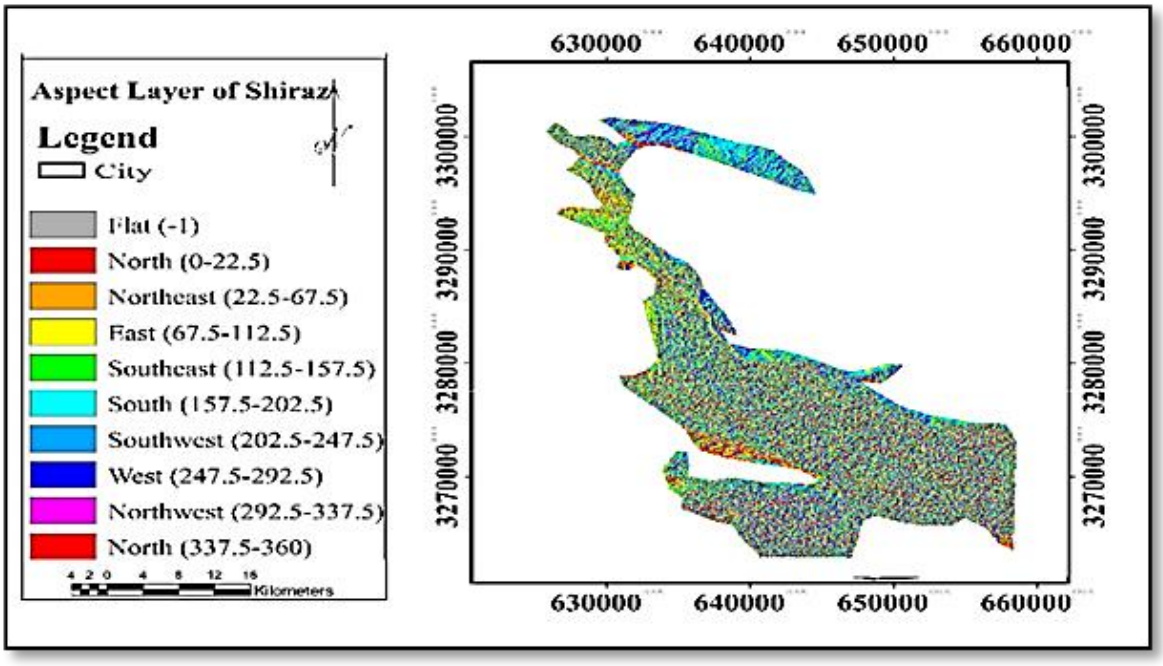

Figure 10. Aspect layer of Shiraz city

3.7 OLS Spatial Analysis

According to the results of the correlation between the land use layer and 7 parameters (height, slope, aspect, distance from the river, distance from the fault, lithology, and geomorphology), distance from the fault and distance from the channel had the greatest impact as environmental hazards on the development of Shiraz. Distance from the faults and distance from the channel had R^2 values of 83% and 72% with error percentages of 0.007 and 0.008, respectively, reflecting an effective role in the risk of urban development in Shiraz (Table 6).

Table 6. OLS model output

Variable	Coefficient [a]	Std Error	t-Statistic	Probability [b]	Robust SE	Robust_t	Robust Pr [b]	VIF [C]
Intercept	2.378635	0.819854	2.901293	0.006304*	0.889275	2.674803	0.011178*	.....
Slope	-0.09494	0.107925	-0.87963	0.384893	0.072067	-1.317313	0.196057	1.248277
Dem	-0.07648	0.091327	-0.83746	0.407858	0.060733	-1.259324	0.216018	1.464532
Distance of River	0.075248	0.008121*	0.942644	0.352146	0.063551	1.184067	0.72067	1.278774
TPI	-0.11997	0.131355	-0.91332	0.367153	0.093836	-1.278485	0.20926	1.168513
Distance of Fault	-0.03502	0.007982*	-0.43123	0.668874	0.085108	-0.41151	0.83138	1.099606
Aspect	-0.04579	0.049534	-0.92449	0.361388	0.034198	-1.339092	0.188935	1.136334
Lithology	0.138147	0.143937	0.959775	0.343571	0.22907	0.603078	0.550237	1.352305

4. Discussion and Conclusion

Urban life is expanding rapidly worldwide at a much faster pace in developing than developed countries. The process of urbanization in Iran is increasingly growing, leading to different problems and challenges. The horizontal development of cities leads to the destruction of lands around cities along with significant costs for the construction of towns and neighborhoods. It is possible to establish the dynamism and vitality of old neighborhoods by considering the neighborhood development capacities. It is also possible to prevent the destruction of suitable agricultural lands and the imposition of excessive costs through the application of sustainable urban development models. This study used satellite images from 2000 to 2018, supervised classification method (maximum likelihood algorithm), and Markov chain model to examine the changes in land coverage in horticultural, agricultural, built-in, barren, and rangeland uses. The study also investigated the relationship with geomorphological parameters such as height, slope, aspect, geomorphology, fault, channel, and lithology. In 2000, 2006, and 2018, the area of built-in land uses has changed in Shiraz with built-in, agricultural and horticultural, barren, and rangeland uses allocating 36%, 11%, 19%, and 46% to themselves, respectively. Considering the decentralized development of Shiraz, leading to urban sprawl and approaching the fault line and the main river, the risk of flood increases.

Over the 25-year period, agricultural land has become barren and vice versa. Residential land use had its maximum in 2018 (316000 km^2) and is expected to reach 391000 km2 by 2025. Shiraz has approached the main fault in the area because of horizontal expansion and unbalanced physical development, leading to erosion and destruction of buildings with weak infrastructure with a value of 88% and percentage error of 0.0007. These hazards cause irreparable damage; hence, the lands around the city of Shiraz (rainfed and irrigated agricultural land and rangeland) are considered critical areas in the future. In the case of incorrect planning, these areas will soon change their use, which is contrary to sustainable development. Thus, this important issue needs more attention from managers, planners, and those in charge of urban affairs. More control over urban areas, the use of mass and high-rise construction (compact city), the use of barren lands across the city (infill development), and directing urban development toward areas other than agricultural land should have priority to reduce the horizontal sprawl and the resulting problems and address the adverse environmental impacts, such as conversion and destruction of agricultural lands into urban lands, soil and water pollution, soil erosion, etc. According to the research findings, the following suggestions are the most important practical issues in urban and regional planning (urban engineering).

Funding

This research received no external funding.

Author contributions

Khalil Valizadeh Kamran: Data curation, Writing-Original draft preparation **Abouzar Nasiri:** Conceptualization, Methodology, Software. **Rahman Zandi:** Visualization, Investigation. **Najmeh Shafiei:** Visualization, Investigation, Writing-Reviewing and Editing. **Rababeh Farzin Kia:** Software, Validation.

Conflicts of interest

The authors declare no conflicts of interest.

References

1. Farid, Y. (1996). New Attitudes in the Context of Urban Geography. Journal of Geographical Research, Tehran, 33, 5-14.
2. Seif al-Dini, F. (2002). A dictionary of urban and regional planning. Shiraz, Iran: Shiraz University Pres 1-507.
3. Chengtai D. (1999). Urban geomorphology in Chinese, 391.
4. Abedini, M., & Moghimi, E. (2012). the role of geomorphological bottlenecks in the physical development of metropolis of Tabriz for optimal use. *Geography and environmental planning*, *23*(1), 147-166.
5. Bullard, R. D., Johnson, G.S., & Torres, A.O. (2000). Sprawl City: Race, Politics, and Planning in Atlanta, Island Press, Island, Washington, DC.
6. Herold, M., Goldstein, N. C., & Clarke, K. C. (2003). The spatiotemporal form of urban growth: measurement, analysis and modeling. *Remote sensing of Environment*, *86*(3), 286-302.
7. Nasiri, A., Shirocova, V. A., & Zareie, S. (2019). Zoning of groundwater quality for plain Garmsar in Iran. *Water Resources*, *46*(4), 624-629. https://doi.org/10.1134/S009780781904002X
8. Nasiri, A., Shafiei, N., & Farzin Kia, R. (2021). Investigation of Fahlian aquifer subsidence and its effect on groundwater loss. *Arabian Journal of Geosciences*, *14*(7), 1-12. https://doi.org/10.1007/s12517-021-06917-7
9. Alansi, A. W., Amin, M. S. M., Halim, G. A., Shafri, H. Z. M., Thamer, A. M., Waleed, A. R. M., ... & Ezrin, M. H. (2009). The effect of development and land use change on rainfall-runoff and runoff-sediment relationships under humid tropical condition: Case study of Bernam watershed Malaysia. *European Journal of Scientific Research*, *31*(1), 88-105. http://psasir.upm.edu.my/id/eprint/17077
10. Guan, D., Gao, W., Watari, K., & Fukahori, H. (2008). Land use change of Kitakyushu based on landscape ecology and Markov model. *Journal of Geographical Sciences*, *18*(4), 455-468. https://doi.org/10.1007/s11442-008-0455-0
11. Václavík, T., & Rogan, J. (2009). Identifying trends in land use/land cover changes in the context of post-socialist transformation in central Europe: a case study of the greater Olomouc region, Czech Republic. *GIScience & Remote Sensing*, *46*(1), 54-76. https://doi.org/10.2747/1548-1603.46.1.54
12. Tiwari, K., & Khanduri, K. (2011). Land use/land cover change detection in Doon valley (Dehradun tehsil), Uttarakhand: using GIS & Remote sensing technique. *International journal of Geomatics and Geosciences*, *2*(1), 34-41.
13. Sarwar, M. I., Billa, M., & Paul, A. (2016). Urban land use change analysis using RS and GIS in Sulakbahar ward in Chittagong city, Bangladesh. *International Journal of Geomatics and Geosciences*, *7*, 1-10.
14. de Oliveira Silveira, E. M., de Menezes, M. D., Júnior, F. W. A., Terra, M. C. N. S., & de Mello, J. M. (2017). Assessment of geostatistical features for object-based image classification of contrasted landscape vegetation cover. *Journal of Applied Remote Sensing*, *11*(3), 036004. https://doi.org/10.1117/1.JRS.11.036004.
15. Huo, L. Z., Boschetti, L., & Sparks, A. M. (2019). Object-based classification of forest disturbance types in the conterminous United States. *Remote Sensing*, *11*(5), 477. https://doi.org/10.3390/rs11050477.
16. Fan, F., Wang, Y., & Wang, Z. (2008). Temporal and spatial change detecting (1998–2003) and predicting of land use and land cover in Core corridor of Pearl River Delta (China) by using TM and ETM+ images. *Environmental monitoring and assessment*, *137*(1), 127-147. https://doi.org/10.1007/s10661-007-9734-y
17. Erfanian, M., Hossein, K. M., Alijanpour, A. (2013). Introduction to OLS and GWR Multivariate Regression Methods in Spatial Modeling of Land Use Effects on Water Quality. Journal of Watershed Management Promotion and Development, 1(1).

Advanced Remote Sensing

http://publish.mersin.edu.tr/index.php/arsej

e-ISSN 2979-9104

Evaluation of green areas with remote sensing and GIS: A case study of Yozgat city center

Alperen Erdoğan*[1], Mahmut Görken[1], Adem Kabadayi[1], Selin Temizel[2]

[1]*Yozgat Bozok University, Sefaatli Vocational School, Türkiye, alperen.erdogan@bozok.edu.tr; mahmut.gorken@bozok.edu.tr; adem.kabadayi@bozok.edu.tr*
[2]*Yozgat Bozok University, Faculty of Agriculture, Türkiye, selin.temizel@bozok.edu.tr*

Cite this study: Erdoğan, A., Görken, M., Kabadayı, A., & Temizel, S. (2022). Evaluation of green areas with remote sensing and GIS: A case study of Yozgat city center. Advanced Remote Sensing, 2 (2), 58-65

Keywords
Remote sensing
Green area
Classification
GIS

Research Article
Received: 05.09.2022
Revised: 28.11.2022
Accepted: 07.12.2022
Published: 28.12.2022

Abstract

Green spaces in urban areas play a critical role in the quality of life. The abundance of urban green spaces; They play an important role in the formation of quality living environments with their ecological, economic, social, physical and aesthetic functions. The fact that green areas or park areas in a city are at the level of human need have positive effects on the socio-psychological structure of the society living there, which has effects on the city in many dimensions such as physical, social, cultural and economic structure and livability, ecological sustainability, urban aesthetics, education, and recreation. makes an impact. It also has significant effects on the local microclimate and the regional climate of the city. In recent years, with the development of remote sensing technologies, many mapping techniques and analyzes have been developed. He has made great contributions to the analysis of urban green spaces. In this study, the direction of urban expansion and changes in urban open-green areas were investigated by using satellite images with high ground sample distance. Analyzes consist of satellite image classification, plant index generation and GIS-based analysis methods. The reliability of geospatial information from remote sensing data is often evaluated by actual verification or comparison with other reference data. In the study, active open green areas detected with the help of satellite images in the city center of Yozgat were compared with the data obtained in the field. More research is needed for thematic applications such as monitoring the changes in urban green spaces with remote sensing methods, assessing vegetation health, and carbon mapping.

1. Introduction

Remote sensing has long been an important and effective tool for monitoring land cover, with its ability to quickly provide broad, precise, unbiased and easily accessible information regarding the spatial variability of the land surface [1,2]. In remote sensing, the data source is an important factor for successful land cover classification. Landsat satellite data is widely used remote sensing data for land cover classification [2,3]. As a result of classification, by distinguishing land cover, roads, buildings and similar objects, thematic maps can be produced and transferred to geographic information systems (GIS).

People settled in certain places by forming social associations in order to survive on earth. With the increase in population and migration, these places have turned into urban spaces, which are accepted as the starting point of civilization. In the light of scientific and technological advances, the economic, cultural and social structures of cities and their physical appearance are changing day by day. With this change, open and green areas are neglected

among the construction activities carried out by ignoring environmental principles in parallel with the rapidly increasing population, especially in developing countries. As a matter of fact, the impact of these areas on the psychological renewal and social and cultural development of urban people, who are far from nature and under the influence of urban life, is too great to be underestimated. Open spaces are very important factors for the mental and physical development of children and young people. While children develop their own physical strength with outdoor games, they are involved in social and psychological actions, even if not as much as cultural activities [4]. From a social point of view, green spaces are areas where individuals, each of whom forms a different texture of the urban mosaic, come together and share their social and cultural characteristics.

From a social point of view, green spaces are areas where individuals, each of whom forms a different texture of the urban mosaic, come together and share their social and cultural characteristics. The rapid increase in the urban population, economic and political conditions bring with it increasing building and structural masses on the city surface. As a result, we rarely come across nature and natural life in our living environment. "On the other hand, the ability of a person to adapt to the environment according to physical and psychological conditions can only be achieved by establishing harmony not only with her own species but also with all living creatures" [5]. Green areas are of great importance in balancing the deteriorated relationship between nature and people and in creating a healthy urban texture. The data layers created in this process become easier to understand thanks to the advantages of mapping [6].

Parks and gardens, where people used to have fun in the past, have become a necessity after the increase in vertical architecture and the concentration of population in certain regions. Urban green spaces are defined as the surface areas of existing open spaces covered or combined with vegetative elements. In practice, it is divided into two as active green areas and passive green areas [7]. Active green areas are children's playgrounds, park areas and sports fields and are important physical components of urban life quality [8]. It has many functions in terms of economic, ecological, social, and physical (in terms of planning) [9-13]. Especially geographical information systems have an important contribution here [14].

In order to obtain sufficient sensitivity from images in remote sensing, a certain number of control points marked on the earth are needed [15]. These control points should be appropriately distributed over the terrain. In addition, it needs to be painted in certain dimensions in order to be visible in the satellite image [16-19]. At the beginning of the most important issues in which UA technology is used, agricultural ecosystem studies such as monitoring plant developments with the help of satellite images, tracking plant diseases and pests, biomass, evapotranspiration, product yield estimations, as well as land cover / land use types and especially agricultural product patterns.

It is necessary to analyze spatial, or in other words, geographical information in determining and solving problems that concern nature and natural life. As a result of developing computer technologies and sectoral demands, computer systems that collect, store, query and analyze spatial data have been developed. Thanks to Geographic Information Systems, different geographical formations and processes in the world can be mapped in the same environment and various analyzes can be made with these maps. Even the resulting maps can be presented in the WebGIS environment. WebGIS enables anyone to access geospatial data. It creates a fast and advanced environment without the limitations of space, time and high processing power and high client computer [20]. GIS technology greatly facilitates the inventory, evaluation, preservation, and documentation of sites and structures [21]. At the beginning of the most important issues in which UA technology is used, agricultural ecosystem studies such as monitoring plant developments with the help of satellite images, tracking plant diseases and pests, biomass, evapotranspiration, product yield estimations, as well as land cover / land use types and especially agricultural product patterns [22, 23].

The list of applications remote sensing and GIS is progressively growing; classification, visibility analysis, erosion modeling, surface hydrology, crop monitoring, watershed modeling, geomorphology, marine resource monitoring, land-sliding, and agriculture and ecosystem modeling, natural disaster warning, urban resource big data processing, land vegetation analysis, etc. are some examples [24].

This study was conducted to investigate the performance of Landsat 8 OLI data and to detect active green areas in Yozgat Center and to examine their changes compared to existing studies.

2. Material and Method

2.1. Study Area and Data

Yozgat (Figure 1) is located on the Bozok Plateau in the Central Central Anatolia Region. One of the trained classification methods on the satellite image dated 23/09/2020 08:21:21 of 176-32 path-row, which includes 34˚03'-36˚09' longitudes and 40˚ 15′-38˚ 57′ latitudes; It is classified by the closest distance and maximum probability methods. While the data consists of 7651x7781 pixels, its 915x580 pixel area covers the city center of Yozgat.

Landsat 8 Oli Satellite image bands and technical specifications of the study area are given in Table 1.

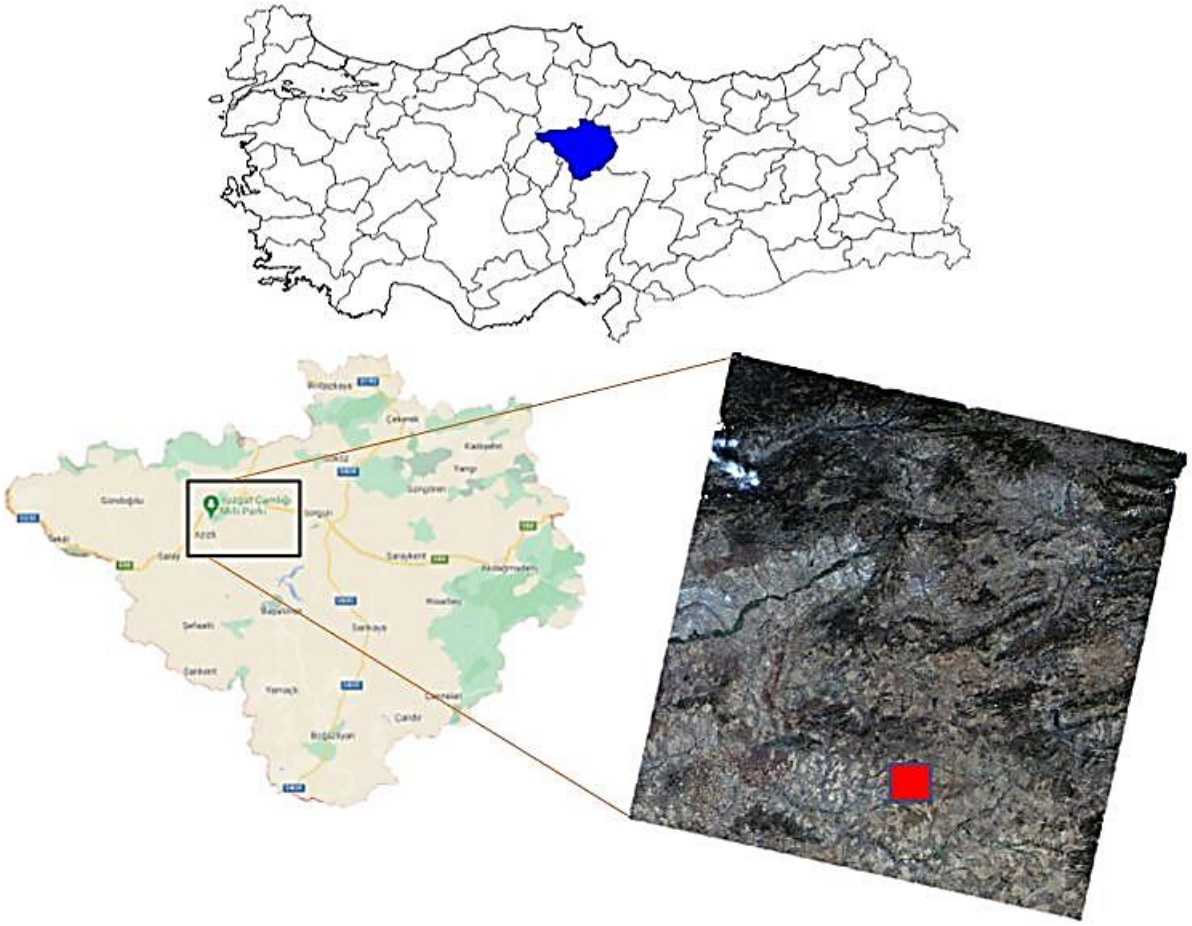

Figure 1. Study Area Turkey Map View

Table 1. Specifications of Landsat 8 OLI bands used

Band	Wavelength (μm)	Resolution (m)
Band 1 Coastal Aerosol	0.43-0.45	30
Band 2 Blue	0.45-0.51	30
Band 3 Green	0.53-0.59	30
Band 4 Red	0.64-0.67	30
Band 5 Near-Infrared	0.85-0.88	30
Band 6 SWIR-1	1.57-1.65	30
Band 7 SWIR-2	2.11-2.29	30
Band 8 Panchromatic (PAN)	0.50-0.68	15
Band 9 Cirrus	1.36-1.38	30

2.2. Classification of Images

Image classification refers to the classification of various objects in images, such as trees, people, crops, soil, minerals and bodies of water. Different objects or regions in the image must be identified and classified. The classification algorithm determines the accuracy of the result. It is usually based on a single image or sets of images. When image sets are used, the set will contain multiple images of the same object under different views and different conditions. Since the algorithm can accommodate a variety of conditions such as background differences, lighting or appearances, it will be more efficient at classification than with single images. It can also be invariant for image rotation and other transformations [10].

Using the spectral subset in ENVI software, selected regions of interest (ROI) were selected as training pixels. 6 classes were selected as park, national park (pine grove, road, structure, soil, high-speed train line) (Table 2).

Table 2. Pixel numbers and classes used as training data

ROI Summary	Pixel Count
Park	135
Pine Grove	184
Structure	153
Soil	405
High Speed Train Line	169
Asphalt	150

2.2.1. Atmospheric Correction and Radiometric Correction

Landsat image processing mainly includes radiometric calibration (Figure 2b) and atmospheric correction (Figure 2c). Landsat data radiometric calibration converts the value of digital numbers to luminance, and then atmospheric correction is performed to obtain the surface spectral reflection using the Fast Line-of-sight Atmospheric Analysis of Spectral Hypercubes (FLAASH) algorithm.

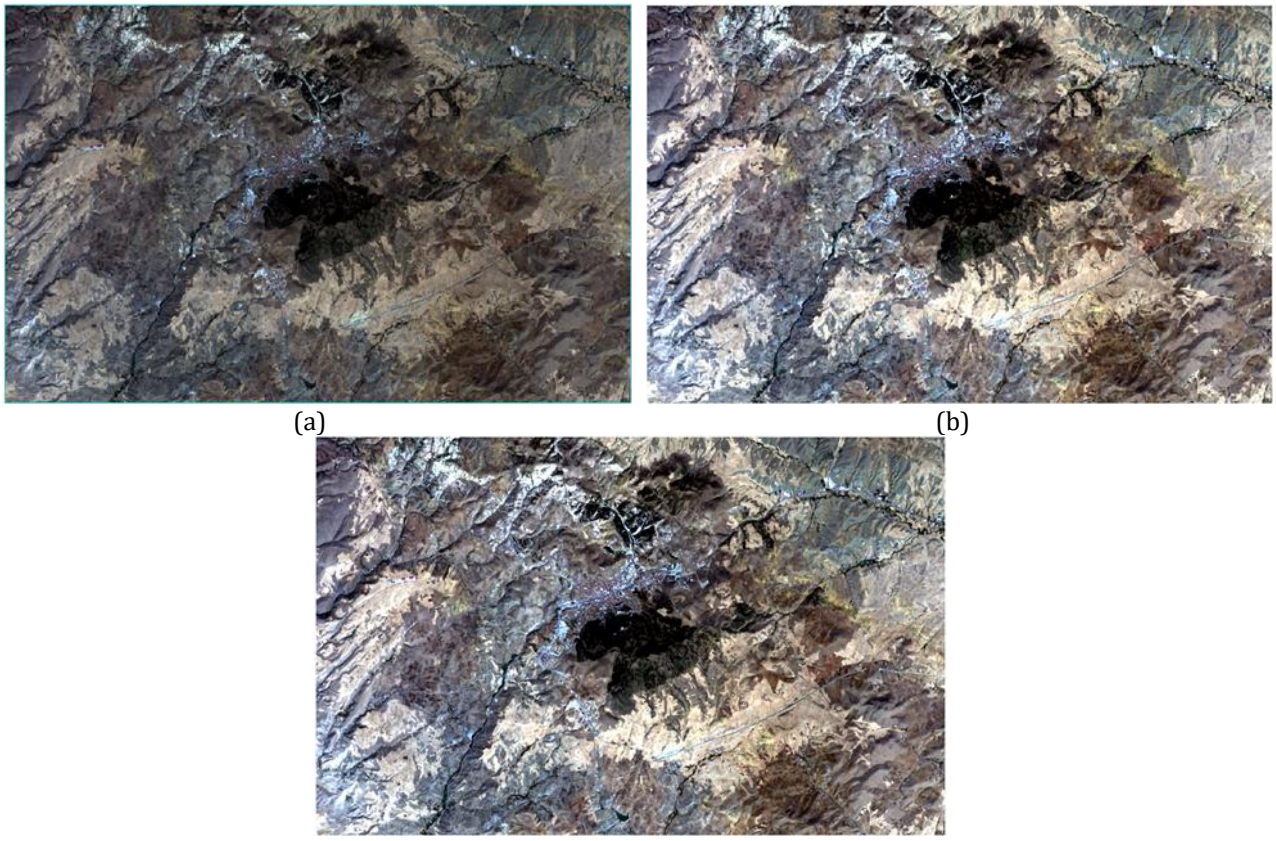

(a) (b)

(c)

Figure 2. (a) Working area image cut from satellite image, (b) Radiometrically corrected image, (c) Atmospherically corrected image

2.2.2. Minimum Distance Classification (MDC)

It assumes that the statistics for each class in each band are normally distributed and calculates the probability that a particular pixel belongs to a particular class (Figure 3). Each pixel is assigned to the class with the highest probability (i.e., maximum probability) [11]. After applying the Minimum Distance Classification method, the image (Figure 4) was produced.

2.2.3. Maksimum Likelihood Classification (MLC)

Among the pixel-based classification, the most frequently used and used method in the literature is the most similarity method. The main purpose of the method is to define the equiprobability curves for the classes and to assign the highest membership to the pixels to be classified [12]. After applying the Maximum Likelihood Classification method, the image (Figure 5) was produced.

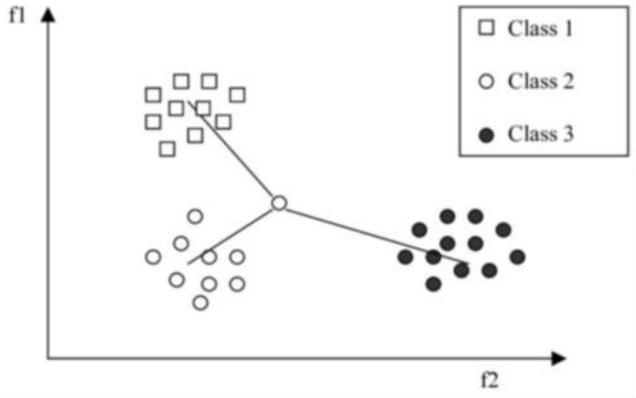

Figure 3. Minimum Distance Classification

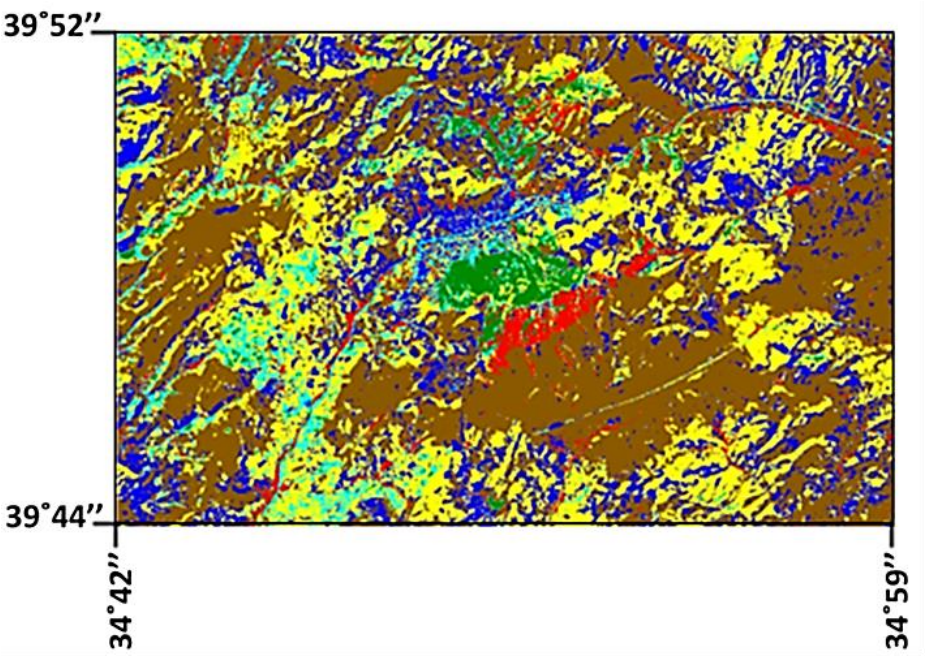

Figure 4. Thematic image formed after MDC

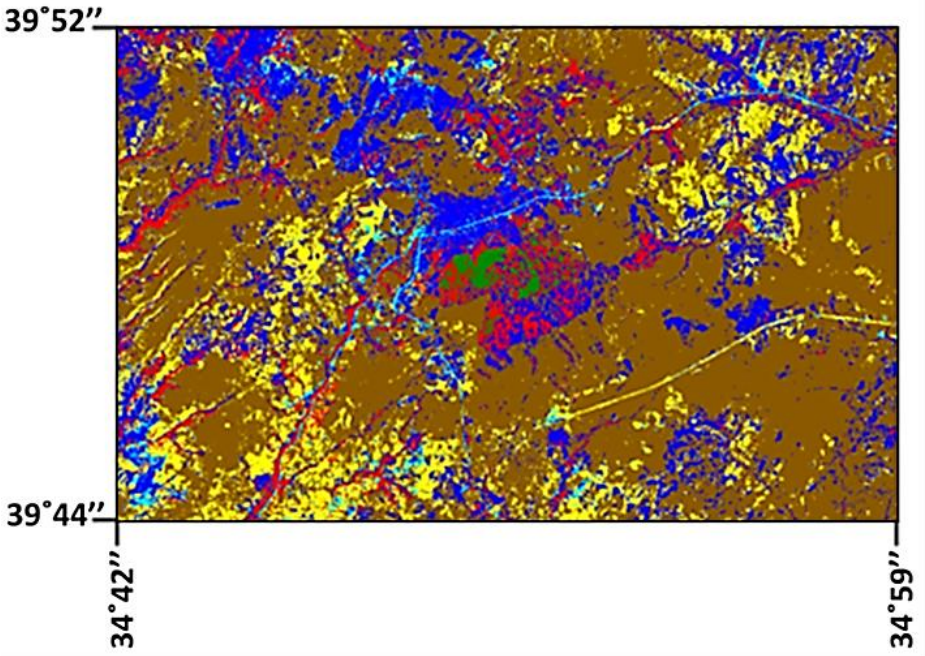

Figure 5. Thematic image created after MLC

2.2.4. Normalized Difference Vegetation Index (NDVI)

The normalized plant difference index (NDVI), which is the most widely used vegetation index in the field of remote sensing, is an expanded version of the band ratio. The basic equation for NDVI is the combination of infrared (Nır) and Red (R) band [13].

$$NDVI = (Nır - Red)/(Nır + Red)$$

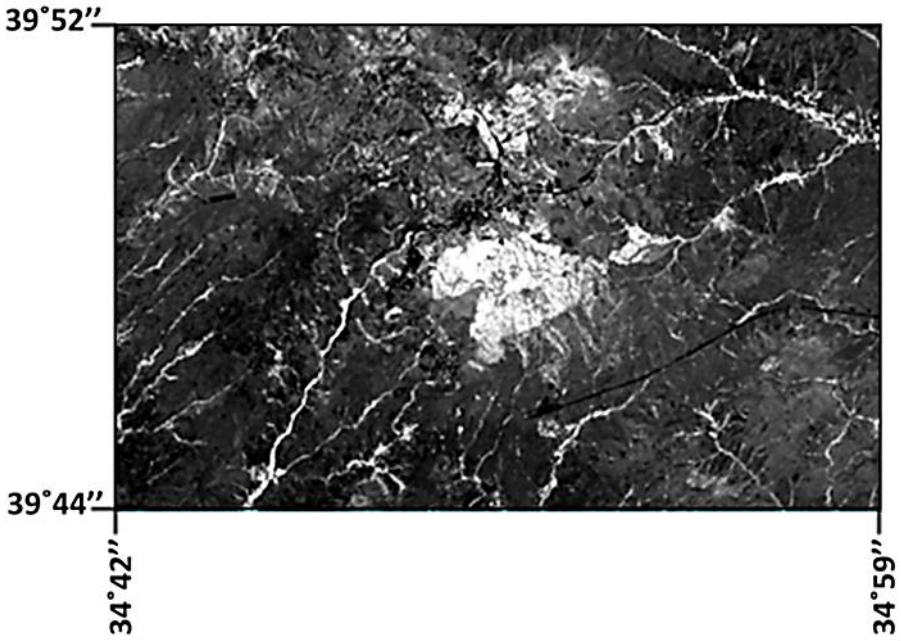

Figure 6. Thematic image formed after NDVI

3. Discussion

Landsat 8 Operational Land Imager (OLI) and Thermal Infrared Sensor (TIRS) images have a resolution of 30 m outside the panchromatic band in bands 1-9, reducing the classification success in residential areas. The file as a thematic map shape file obtained from the highest probability classification method with a higher accuracy rate was transferred to ARCGIS (Figure 7).

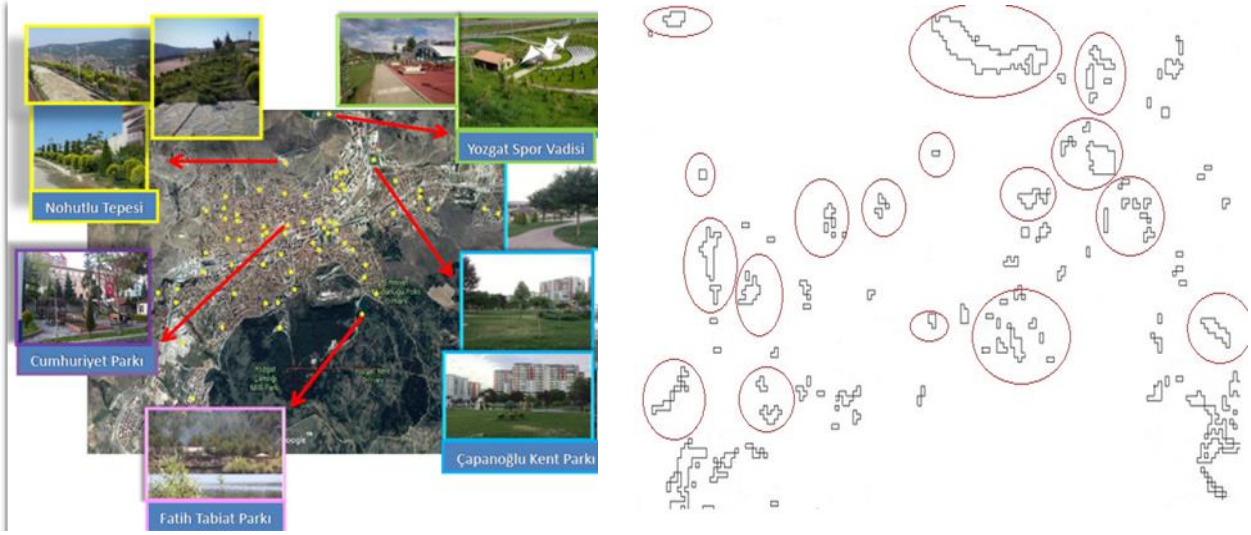

(a) (b)

Figure 7. (a) Image with active green areas marked, **(b)** Vector map produced from thematic maps

4. Conclusion

Accuracies of the produced thematic maps were calculated with the Confusing Matrix Using Ground Truth ROIs module in Envi 5.3 Program. In this module, comparisons of test data and training data are made.

Classification accuracy and kappa statistics were calculated based on validation samples. The overall performance of the MLC classifier (overall accuracy 80.4%; kappa coefficient: 0.71) was slightly lower than the MDC classifier (overall accuracy: 79.3%; kappa coefficient: 0.69). Since the building class and roads, Park and Çamlık classes have spectral signatures that are very close to each other, the most errors occurred in these two classes. All other class types have been observed to separate better from each other and have higher user and producer accuracies.

In this study, which was carried out in Yozgat city center, the total of active green areas was 627073 m^2. In the study, it was calculated as 680045 m^2. However, in the classification, a part of the Provincial Directorate of Agriculture, TOKİ garden and Governor's garden and Çamlık National Park located in the city center are classified as parks. These green areas cannot be considered as active green areas.

The social and demographic structure of the urban people must be taken into account in the planning and applications for green areas. According to the population projections to be made, green areas should be designed to meet the needs. Especially for the elderly, children and disabled people with walking distance limits, the standards should be taken into consideration in the planning.

Transferring green areas to future generations is as important as designing them. In this context, it is necessary to raise awareness of people about the protection and continuity of planned areas and natural greenery. Local government and non-governmental organizations should also take an active role in informing and raising awareness about green areas and their protection.

Funding

This research received no external funding.

Author contributions

Alperen Erdoğan: Data, Methodology, Software, Visualization. **Mahmut Görken:** Conceptualization, Data curation, Visualization. **Adem Kabadayi:** Writing-Original draft preparation, Software. **Selin Temizel:** Investigation, Writing-Reviewing and Editing.

Conflicts of interest

The authors declare no conflicts of interest.

References

1. Hansen, M. C., DeFries, R. S., Townshend, J. R., & Sohlberg, R. (2000). Global land cover classification at 1 km spatial resolution using a classification tree approach. *International journal of remote sensing*, *21*(6-7), 1331-1364.
2. Gong, P., Wang, J., Yu, L., Zhao, Y., Zhao, Y., Liang, L., ... & Chen, J. (2013). Finer resolution observation and monitoring of global land cover: First mapping results with Landsat TM and ETM+ data. *International Journal of Remote Sensing*, *34*(7), 2607-2654.
3. Gumma, M. K., Thenkabail, P. S., Hideto, F., Nelson, A., Dheeravath, V., Busia, D., & Rala, A. (2011). Mapping irrigated areas of Ghana using fusion of 30 m and 250 m resolution remote-sensing data. *Remote Sensing*, *3*(4), 816-835.
4. Yaşlica E, (1991). Konut Çevresi Açık Alan Kullanımına Yönelik Bir Araştırma, Türkiye'de 15. Dünya Şehircilik Günü, 3. Türkiye Şehircilik Kongresi, İzmir, Türkiye.
5. Bakan, K. & Konuk, G. (1987). Türkiye'de Kentsel Dış Mekanların Düzenlenmesi, Tübitak Yapı Araştırma Enstitüsü, Ankara, Türkiye.
6. www.dogadernegi.org/?sayfa=45 20/05/05-01/07/05
7. Karafakı, F. Ç. (2016). Niğde kent merkezindeki aktif yeşil alanların kentsel yaşam kalitesine etkileri. *Türk Tarım ve Doğa Bilimleri Dergisi*, *3*(3), 184-191.
8. Bağcı, Ö. (2010). Yenişehir (Mersin) Kentsel Alanında Peyzaj Mimarlığı Disiplini Kapsamında Kentsel Gönenç Araştırması. *Basılmamış Yüksek Lisans Tezi, Çukurova Üniversitesi, Fen Bilimleri Enstitüsü, Çukurova*.

9. Temizel S., Kılıç T., & Yazıcı K. (2018). Aktif Yeşil Alanlar Ve Kentsel Yaşam Kalitesi Üzerine Etkileri: Yozgat Örneği. 3rd International Bozok Symposium Regional Development and Socio-Cultural Structure.
10. Hemanth, D. J. & Estrela, V. V. (2017). Deep Learning for Image Processing Applications, IOS Press
11. Çolak E. (2018). Orman yangın alanlarının uzaktan algılama ve cbs entegrasyonu ile izlenmesi: İzmir, Menderes örneği, İstanbul Teknik Üniversitesi Fen Bilimleri Enstitüsü
12. Sabuncu, A., (2018). Yüksek Mekansal Çözünürlüklü Uydu/Uçak Platformlu Görüntüler ve CBS Teknolojisi Kullanılarak Van-Erciş Depremi Sonrası Bina Hasar Tespiti. Doktora Tezi. İstanbul Teknik Üniversitesi Fen Bilimleri Enstitüsü, İstanbul, 130.
13. Gündoğdu, K. S., & Bantchina, B. B. (2018). Landsat uydu görüntülerinden NDVI değer dağılımının parsel bazlı değerlendirilmesi, Uludağ üniversitesi ziraat fakültesi çiftlik arazisi örneği. *Bursa Uludağ Üniversitesi Ziraat Fakültesi Dergisi*, *32*(2), 45-53.
14. Erener, A., & Yakar, M. (2012). Monitoring coastline change using remote sensing and GIS technologies. *Lecture Notes in Information Technology*, *30*, 310-314.
15. Mutluoglu, O., Yakar, M., & Yilmaz, H. M. (2015). Investigation of effect of the number of ground control points and distribution on adjustment at WorldView-2 Stereo images. *International Journal of Applied Mathematics, Electronics and Computers*, *3*(1), 37-41.
16. Yilmaz, H. M., Yakar, M., Mutluoglu, O., & Yildiz, F. (2004, July). Selection of the most suitable sizes of ground control points in the satellite images. In *ISPRS Congress Istanbul* (Vol. 12, p. 13).
17. Mutluoğlu, Ö., Yakar, M., & Yilmaz, H. M. (2016). Investigation of spatial accuracy of high-resolution (50cm) Worldview-2 satallite images. *Selçuk Üniversitesi Mühendislik, Bilim ve Teknoloji Dergisi*, *4*(4), 321-329.
18. Mutluoğlu, Ö., & Yakar, M. (2005). Mono Ikonos Uydu Görüntülerinden Konumsal Verilerin Elde Edilmesinde Doğruluk ve Maliyet Analizi. *Selçuk Üniversitesi Mühendislik, Bilim ve Teknoloji Dergisi*, *20*(1), 27-34.
19. Mutluoglu, O., Yakar, M., & Yilmaz, H. M. (2008). Comparisation of spatial accuracy of data acquaried from mono and stereo images: A case study of campus area Konya–Turkey. International Archive of Photogrammetry and Remote Sensing, XXXVII (B4), 1045-1048
20. Şahin, M. A., & Yakar, M. (2021, June). WEBGIS Teknolojisi ve Mimarileri. In *International Geoinformatics Student Symposium (IGSS)* (Vol. 1, No. 1, pp. 48-51).
21. Doğan, Y., & Yakar, M. (2018). GIS and three-dimensional modeling for cultural heritages. *International Journal of Engineering and Geosciences*, *3*(2), 50-55.
22. Wesseling, J. G., & Feddes, R. A. (2006). Assessing crop water productivity from field to regional scale. *Agricultural Water Management*, *86*(1-2), 30-39.
23. Torunlar, H., Tuğaç, M. G., & Duyan, K. (2021). Nesne Tabanlı Sınıflandırma Yönteminde Sentinel-2A Uydu Görüntüleri Kullanılarak Tarımsal Ürün Desenlerinin Belirlenmesi; Konya-Karapınar Örneği. *Türkiye Uzaktan Algılama Dergisi*, *3*(2), 36-46.
24. Yakar, M., Yilmaz, H. M., & Yurt, K. (2010). The effect of grid resolution in defining terrain surface. Experimental Techniques, 34(6), 23-29.

Advanced Remote Sensing

http://publish.mersin.edu.tr/index.php/arsej

e-ISSN 2979-9104

DEM and GIS-based assessment of structural elements in the collision zone: Çağlayancerit, Kahramanmaraş (Türkiye)

Cihan Yalçın[*1]

[1]*Ministry of Industry and Technology, General Directorate of Industrial Zones, Ankara, Türkiye, cihan.yalcin@sanayi.gov.tr*

Cite this study: Yalçın, C. (2022). DEM and GIS-based assessment of structural elements in the collision zone: Çağlayancerit, Kahramanmaraş (Türkiye). Advanced Remote Sensing, 2 (2), 66-73

Keywords
Structural elements
Suture zone
Çağlayancerit
DEM
QGIS

Research Article
Received: 26.09.2022
Revised: 01.12.2022
Accepted: 13.12.2022
Published: 28.12.2022

Abstract

Topographic and linear data are precisely linked to the tectonic structure of the region. This relation can be identified both in the field and in satellite images. As it is recognized, high topographic areas are formed with the effect of the compression regime in the zones where different continents are sutured. There are traces of the suture zone in the northeast of Kahramanmaraş. Because of the closure of the Neotethys Ocean, a collision zone developed in and around Çağlayancerit, located in the northeast of Kahramanmaraş. Units in the Arabian Autochthonous and Taurus Orogenic belts came together in this district. Thrust belts and faults have been observed in this vicinity. In this region, there are different tectonostratigraphic sequences sliced on top of each other by the effect of compression. These slices and their structural features have caused different morphological traces in the region. Structural events have led to the development of linearity and topographic elevations, respectively. According to the in-situ observation and the digital elevation model (DEM) analysis results which were performed in the QGIS environment, the topographic elevations in the collision belt are relatively higher than the areas in the south. As a result of the north-south compression, the thrust lines formed definite linearity. Each fault characterized in the region controls the morphology directly.

1. Introduction

Many geological studies utilize lineament and topographic components as ancillary indicators [1-2]. Depending on the geological development of a region, basins and orogenic belts are observed. In this situation, regional lineaments and morphological data have their ultimate form under tectonic and sedimentation control [3-5].

Remote sensing (RS) and geographic information systems (GIS) are platforms for the map-based evaluation of geological structures. With technological advances and recent developments in spatial analysis techniques, large-scale linearity and morphological analyses have become relatively practicable [6]. These studies use numerical data such as satellite images and Digital Elevation Model (DEM). Such studies interpret morphological and linear structures [7-9].

Structural elements (fault, lineament, fracture, joint, etc.) cause the emergence of geomorphic expressions. These relationships are revealed by using reliefs and slopes on the DEM image. Satellite images are matched with the data obtained in the field and structural features are revealed. Thus, using many factors, the geological boundary relations, tectonics, and structural geology of the regions are revealed [10-11].

In terms of its geological structure, Kahramanmaraş is a complex region where different tectonic units are observed together. Many thrust and fault zones associated with the closure of the southern branch of the Neotethys Ocean are observed in this region [12]. Suture belts were formed by the closure of this ocean and the convergence

of the Tauride and Arabian plates as a result [13-14]. With the depletion of the ocean floor, allochthonous units were thrust onto the Arabian platform in the south, and a suture belt was formed between these two continents [15-16].

Gül [17] explained that the Anatolian and Arabian plates collision occurred in the Late Cretaceous and that a compressional regime was active in the region during the Paleocene-Early Eocene period. Yılmaz and Yiğitbaş [18] stated that as a result of the movement of the Arabian continent towards the Anatolian plate between the Late Cretaceous-Miocene, the region gained a nappe character.

Rigo De Righi and Cortesini [19] divided the tectonostratigraphic units in the Southeast Anatolian Region into four primary tectonic belts: the Taurus Orogenic Belt, the Margin Fold Belt, the Folded Belt, and the Foreland, respectively.

On the other hand, Gül [20] described Kahramanmaraş and its vicinity as Orogenic Belts. Yalçın [21] mapped the rocks of different origins in Çağlayancerit and its west and revealed the deformation structures of the region. This region still has an active fault, such as the East Anatolian Fault (EAF). It is recognized that this main fault affects many morphological formations. In this region, distinctive morphological structures have cropped up due to the coexistence of rocks belonging to two different plates and the presence of different tectonic sequences on the thrust zones.

Yalçın and Kop [22] stated that there are different types of rock groups developed in the Paleozoic-Quaternary age range in the region. They stated that Malatya Metamorphics, Suture Belt, and Arabian Autochthonous units are located in this region, which is located in the collision zone, from north to south, and that there are different tectonostratigraphic sequences sliced on each other with the effect of compression. Yalçın [23] stated that the structural elements in this region are effective in shaping the morphology of the region and that these lineaments can be revealed/identified using the remote sensing method.

2. Material and Method

The study area is located in the Çağlayancerit region, approximately 60 km northeast of Kahramanmaraş province (Figure 1a), in the Eastern Taurus Orogenic Belt. This region and its vicinity were named Engizek Askuşağı by Gül [20] (Figure 1b). Just south of this belt is the marginal fold belt of the Arabian plate.

In this region, allochthonous Malatya Metamorphites form the Berit Metaophiolite, Ziyaret Tepe, and Kaleköy Tectonic Slices from bottom to top, respectively, due to nappes. Sedimentary and volcanic units belonging to the Suture Belt were sliced on the thrust front just south of these slices. In the areas south of the Suture Belt, autochthonous rock assemblages representing the Arabian Platform and also called the margin fold belt crop out [21-22]. Structural elements show that the compression regime continues for a long time in this region.

2.1. Geology

Different stratigraphic sequences have emerged due to the coexistence of rock groups of different origins in the study area and allochthonous rocks overlying nappes and younger rocks in large areas. Allochthonous rocks, Suture Belt, and Autochthonous units were defined from north to south [21].

In the study area, the tectonic slices present an imbricated structure, and the units belonging to different plates come together, indicating a very complex structural position in the region (Figure 2). According to the structural elements examined, it can be said that the region has been under the influence of an N-S oriented compression for a long time.

In the NW of Çağlayancerit (Kahramanmaraş), around Kaleköy and Hombur districts, lithostratigraphic units representing different environments and facies from Paleozoic to Quaternary crop out [22]. Because the region is located in the continent-continent collision belt, allochthonous rock groups were dragged over the autochthonous units in the nappe and frontal thrusts. For this reason, the rock assemblages outcropping in the study area were classified into two main groups autochthonous and allochthonous according to their location. Allochthonous rocks, on the other hand, are considered in two main groups the Suture Belt and the Malatya Metamorphites located in the Taurus Orogenic Belt, taking into account their origin.

Allochthonous units, which are widely distributed in Kaleköy, Hombur, and Zorkun regions in the study area, consist of Malatya Metamorphites and Suture Belt units. From north to south, Malatya Metamorphites were emplaced as nappes on each other and on Suture Belt units along the approximately E-W trending lines (Figure 2, Figure 3). As a result of these nappes, different lithological and stratigraphic sequences emerged, and tectonic slices were formed [21-22].

Considering the locations and contact relationships of allochthonous rocks, it was determined that the rocks from north to south were sliced to form an annealed structure. These slices are defined under the names of Berit Metaophiolite, Kaleköy, and Ziyaret Tepe Tectonic Slices respectively [21-29].

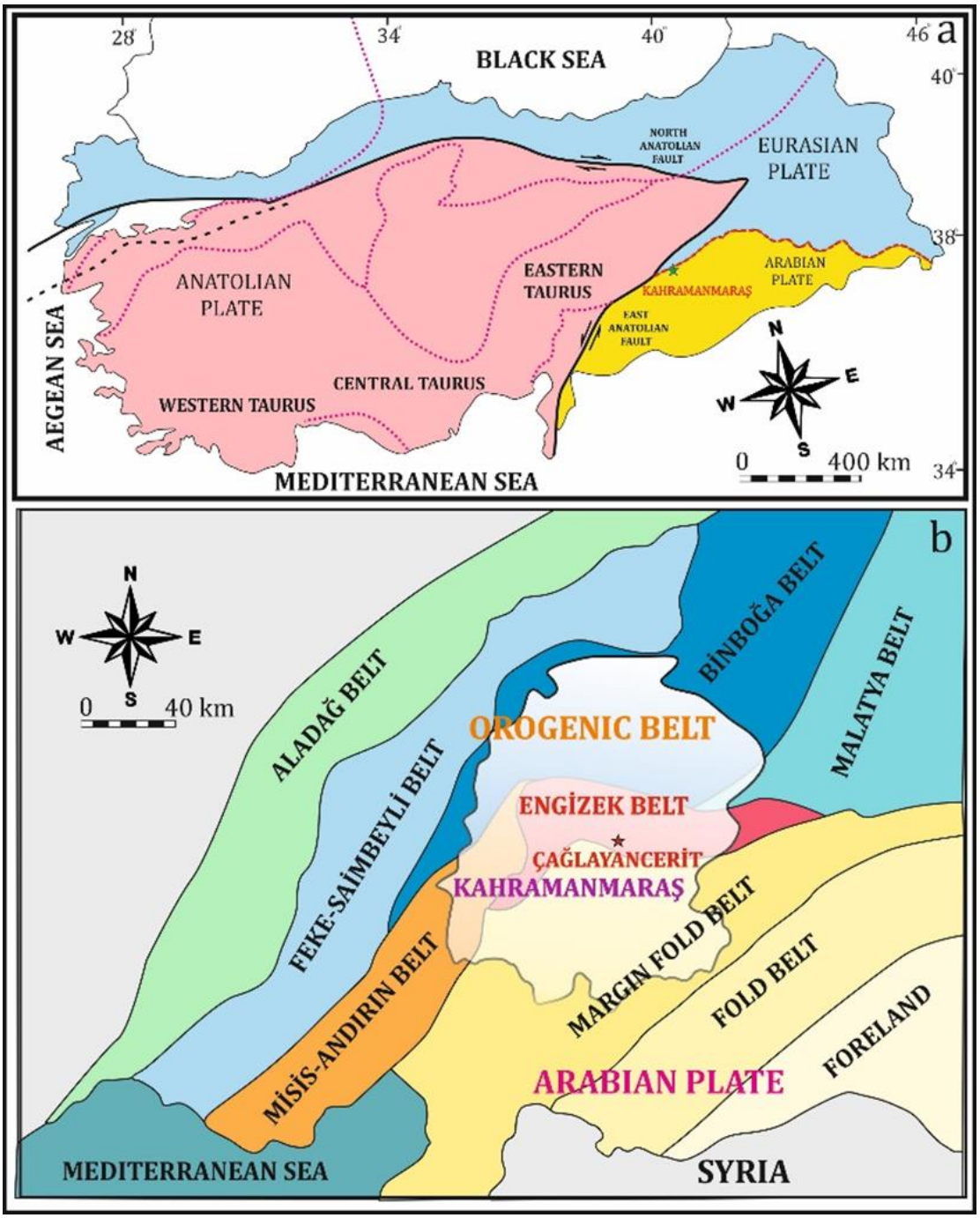

Figure 1. a) Tectonic location of the study area (Modified from [30]) **b)** Location of the study area according to tectonic belts. (Modified from Gül, [20]).

2.2. GIS-based analysis

Topographical approaches were obtained with the DEM of Çağlayancerit and its vicinity, a tectonically active region and an important belt where two different continents collide. ASTER GDEM data provided by JPL (Jet Propulsion Laboratory) was used to derive topographic approximations.

The DEM of this geologically significant region has been downloaded from the United States Geological Survey (USGS) website [31] (Earthexplorer, https://earthexplorer.usgs.gov). GIS-based structural analyses were performed in the QGIS environment, an open-source Geographical Information System. Aspect and slope analyses were performed in order to define the structural elements of the study area. The combination of raster/vector output of this analysis, in-situ measurements, and visual lineaments analysis were used in multi-layer-based decisions. In addition, active faults in the region are placed on these layers. The DEM and the active faults in the region overlapped (Figure 4).

The processing steps of GIS-based structural elements determination used in the QGIS environment, respectively, are as follows;

1.DEM data was classified and colored in the QGIS environment with a single-band pseudocolor application (Figure 5a).
2.The relief image for the slope map of the region and the slope image on it were overlaid, revealing the slope map (Figure 5b). The red-colored areas represent the areas with the highest topographic elevation.
3.A view map of the region was created. According to the field studies, it has also been revealed with DEM that the slopes generally face south because there are thrusts from north to south (Figure 5c).
4.A 3D map of the region was created to obtain a more understandable image. The most important linearity obtained according to this image belongs to EAF. Other important linearities are thrust zones and dip-slip faults that form the boundary of the thrust front and autochthonous units (Figure 5d).

Considering that there are different active and inactive faults in and around Çağlayancerit, the region's morphology is quite rugged, and the topographic elevations are relatively lower in the southern areas. According to these DEM data, some important lineaments have been determined, which are structures generally affected by faults.

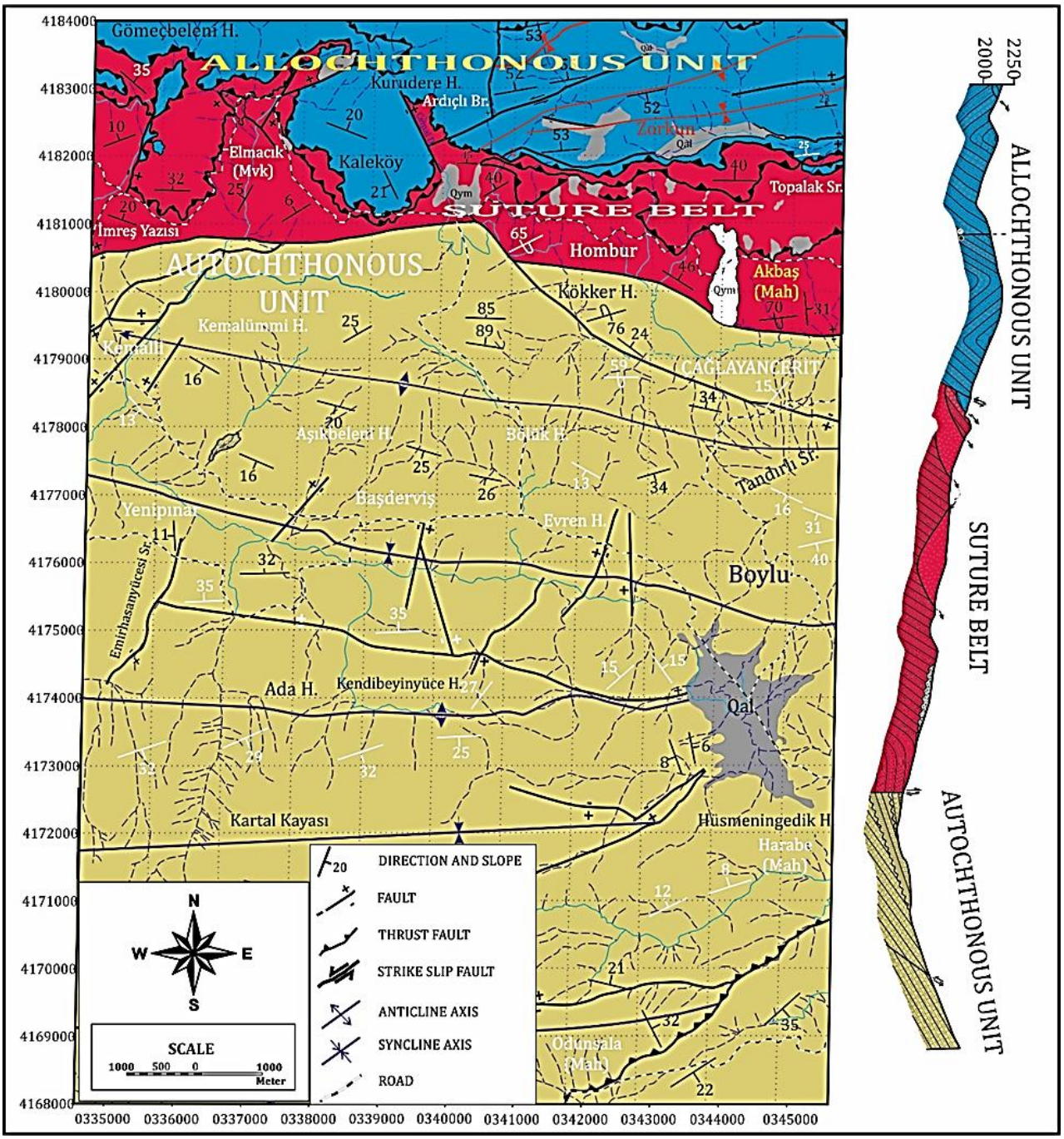

Figure 2. Structural map of the study area (Modified from [21]).

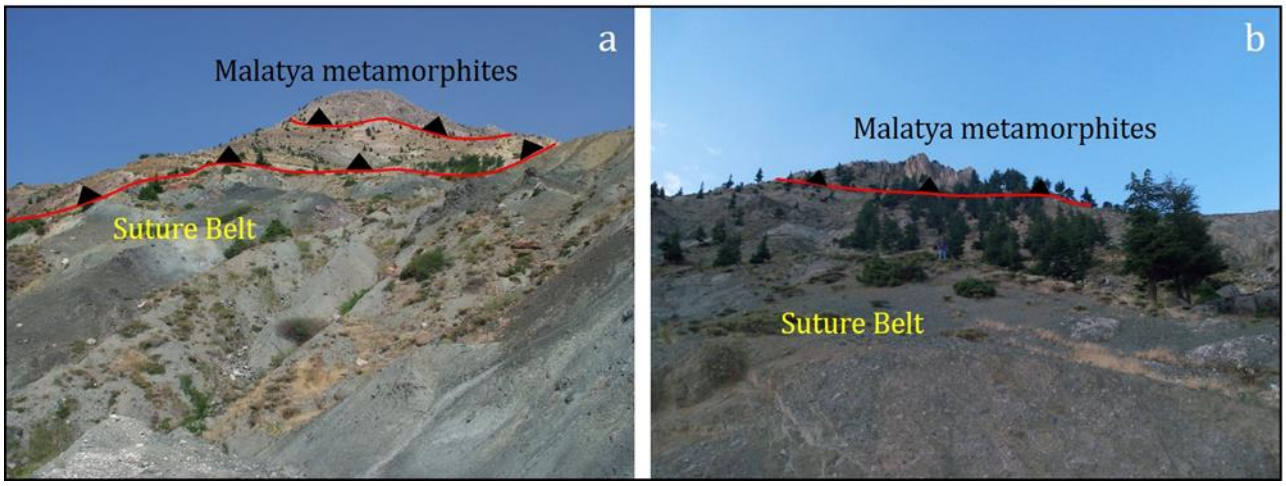

Figure 3. General view of thrust faults and allochthonous units.

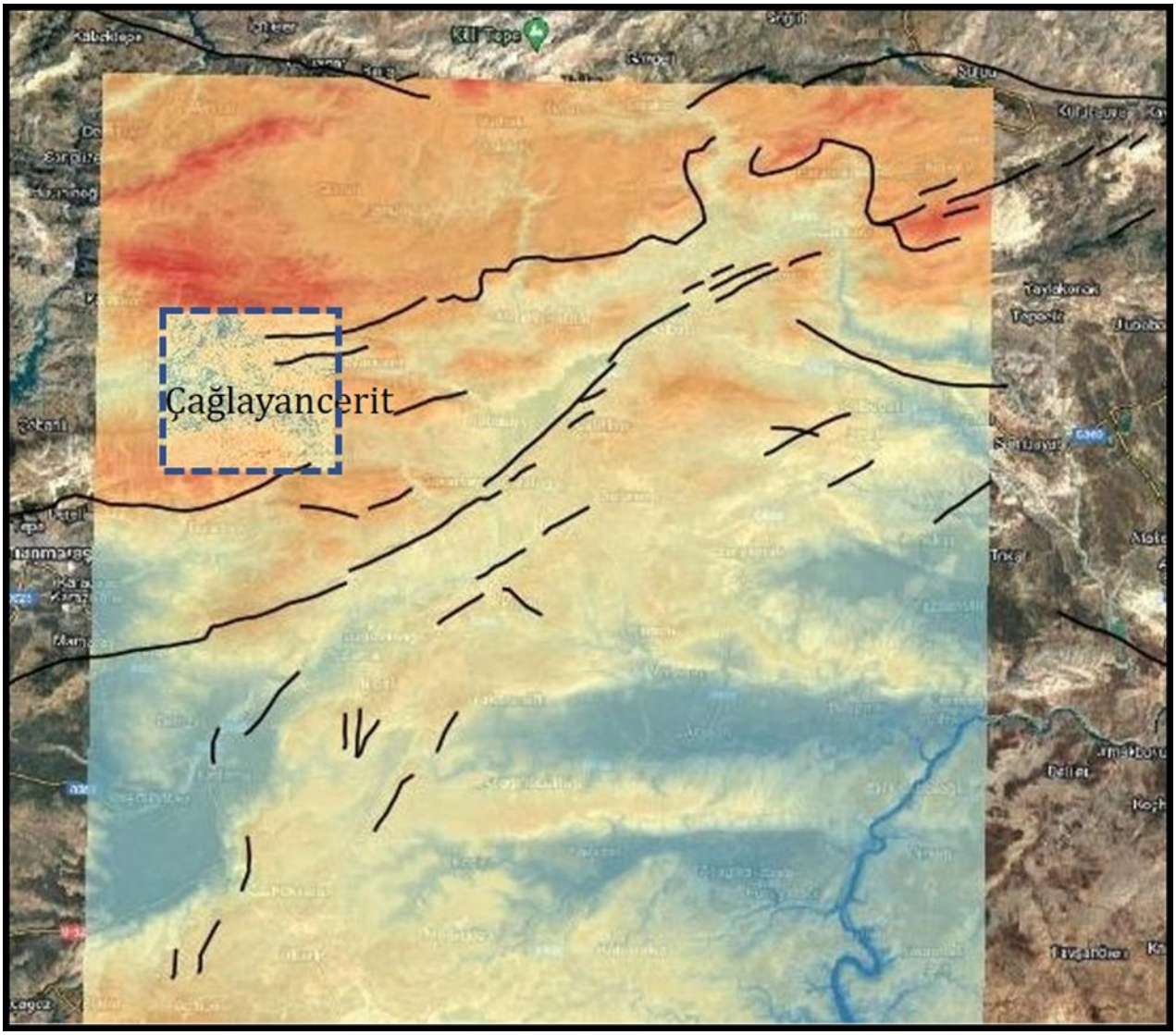

Figure 4. Satellite and DEM image of the study area.

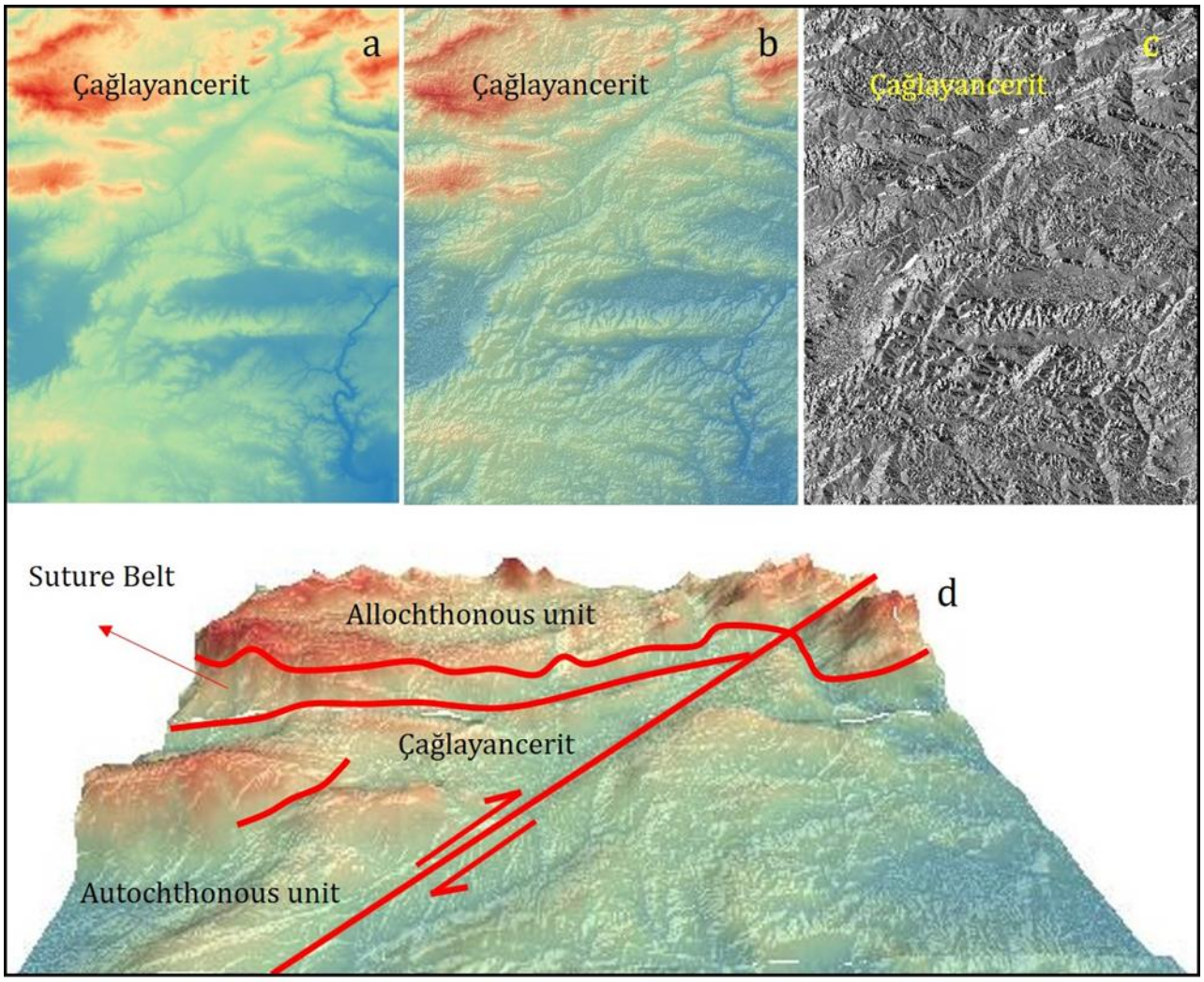

Figure 5. a. DEM **b.** slope, **c.** aspect **d.** 3D image of the study area.

3. Results

Geological lineaments are an important element to reveal the paleo or neo-tectonic features of a region. The use of remote sensing data to describe the lineaments of these tectonic features has been applied in many geological settings [32].

The study area is an important region where Arabian plate and allochthonous units come together. In the study area, there are lithostratigraphic units deposited in the Upper Permian-Quaternary age range. From north to south, Malatya Metamorphics, Suture Belt and Arabian Autochthonous Units are located. Thrust zones were developed by the closure of the southern branch of the Neotethys Ocean [12] and then by the convergence of the Tauride plate and Arabian plate [13, 33].

In these thrust belts, allochthonous units were thrust over the northern margin of the Arabian platform in the south. As a result of this pushing movement, both allochthonous rocks were sliced and frontal charges were formed between the Taurus Orogenic belt and Arabian Autochthonous [15-16]. The Arabian Platform consists of a thick marine sedimentary succession and is a belt compressed between nappes in the thrust zone [34]. In the nappe regions, ophiolitic rocks and Malatya Metamorphites caused the formation of the regional orogeny. Later, as a result of the collision of the nappes with the Arabian plate in the Late Miocene, the present successions were formed [34]. The tectonostratigraphic slices identified from Yalçın and Kop [22] study also support the theory of the development of this orogenic belt.

At the end of the compression system in the region reached a level that could no longer be met by thrusts, the Eastern Anatolian Fault and other strike-slip faults in the region developed in this period, which is called the Neotectonic phase [35]. The region started to undergo deformation under the control of strike-slip faults since the Upper Miocene. Such Miocene-Present units are bounded by left-lateral strike-slip faults known to be active (such as the Sürgü fault) [36].

In the research prepared by Yalçın [21], it was stated that the units belonging to the collision belt in Çağlayancerit and its west came together, and deformation structures belonging to different periods developed in the region. The region's structural elements and surroundings were re-evaluated in this study with remote sensing

methods. Topographic data and linear structures reveal that tectonic forces in the region are effective in geomorphology. In supplement, the faults in the structural map obtained in the field study are in harmony with the satellite images.

4. Conclusion

Tectonic lineaments are important parameters of any structural geological study. Linear structures help in mapping and tracing fault structures related to geological hazards. Lineaments in DEM have topographic relief and/or tonal features on the earth.

The maps prepared for tectonic and structural purposes can still be verified with GIS-based techniques. Morphological changes are the most common, especially in tectonically active areas where different continents come together. Very high topographic data is obtained in the thrust belts. In this study, the units of the Arabian Autochthonous and Taurus Orogenic belts collided, and then the position of the EAF was evaluated together. DEM and field data can be compared by evaluating them in the GIS environment. Other parameters/variables such as hydrological factors, lithology, and shading should be used and specified in such research.

Acknowledgement

This study was partly presented at the 4th Intercontinental Geoinformation Days [23].

Funding

This research received no external funding.

Conflicts of interest

The authors declare no conflicts of interest.

References

1. Guild, P. W. (1974). Distribution of metallogenic provinces in relation to major earth features. In *Metallogenetische und Geochemische Provinzen/Metallogenetic and Geochemical Provinces* (pp. 10-24). Springer, Vienna.
2. Masoud, A., Koike, K., & Teng, Y. (2007, August). Geothermal reservoir characterization integrating spatial GIS models of temperature, geology, and fractures. In *Proc. 12th Conference of International Association for Mathematical Geology, Beijing, China, August* (pp. 26-31).
3. Oakey, G. (1994). A structural fabric defined by topographic lineaments: Correlation with Tertiary deformation of Ellesmere and Axel Heiberg Islands, Canadian Arctic. *Journal of Geophysical Research: Solid Earth*, *99*(B10), 20311-20321.
4. Fichler, C., Rundhovde, E., Olesen, O., Sæther, B. M., Rueslåtten, H., Lundin, E., & Doré, A. G. (1999). Regional tectonic interpretation of image enhanced gravity and magnetic data covering the mid-Norwegian shelf and adjacent mainland. *Tectonophysics*, *306*(2), 183-197.
5. Austin, J. R., & Blenkinsop, T. G. (2008). The Cloncurry Lineament: Geophysical and geological evidence for a deep crustal structure in the Eastern Succession of the Mount Isa Inlier. *Precambrian Research*, *163*(1-2), 50-68.
6. Masoud, A. A., & Koike, K. (2011). Auto-detection and integration of tectonically significant lineaments from SRTM DEM and remotely-sensed geophysical data. *ISPRS journal of Photogrammetry and Remote sensing*, *66*(6), 818-832. https://doi.org/10.1016/j.isprsjprs.2011.08.003
7. Morris, K. (1991). Using Knowledge-Base Rules to Map the Three-Dimensional Nature of Geological. *Photogrammetric Engineering & Remote Sensing*, *57*, 1209-1216.
8. Suzen, M. L., & Toprak, V. (1998). Filtering of satellite images in geological lineament analyses: an application to a fault zone in Central Turkey. *International journal of remote sensing*, *19*(6), 1101-1114.
9. Tripathi, N. K., Gokhale, K. V. G. K., & Siddiqui, M. U. (2000). Directional morphological image transforms for lineament extraction from remotely sensed images. *International Journal of Remote Sensing*, *21*(17), 3281-3292.
10. Blakely, R. J. (1996). *Potential theory in gravity and magnetic applications*. Cambridge university press.
11. Miller, H. G., & Singh, V. (1994). Potential field tilt—a new concept for location of potential field sources. *Journal of applied Geophysics*, *32*(2-3), 213-217.
12. Şengör, A. C., & Yilmaz, Y. (1981). Tethyan evolution of Turkey: a plate tectonic approach. *Tectonophysics*, *75*(3-4), 181-241.

13. Robertson, A. H. F., & Dixon, J. E. (1984). Introduction: aspects of the geological evolution of the Eastern Mediterranean. *Geological Society, London, Special Publications*, *17*(1), 1-74.
14. Robertson, A. H., Parlak, O., & Ustaömer, T. (2012). Overview of the Palaeozoic–Neogene evolution of neotethys in the Eastern Mediterranean region (southern turkey, cyprus, Syria). *Petroleum Geoscience*, *18*(4), 381-404.
15. Yılmaz, Y. (1984). Amanos dağlarının jeolojisi: İ. Ü. Müh. Fak. (TPAO Arş. No. 1920, İstanbul).
16. Yılmaz, Y., Gürpınar, O., Kozlu, H., Gül, MA., Yiğitbaş, E., Yıldırım, M., Genç, C. & Keskin, M. (1987). Maraş kuzeyinin jeolojisi (Andırın- Berit-Engizek-Nurhak-Binboğa Dağları) yapı ve jeolojik evrimi. İstanbul Üniversitesi, Mühendislik Fakültesi.
17. Gül, M.A. (1987). Kahramanmaraş Yöresinin Jeolojisi ve Petrol Olanakları. T.P.A.O. Rap. No: 2359, (Yayınlanmamış), Ankara.
18. Yilmaz, Y., & Yiğitbaş, E. (1990). SE Anadolu'nun farklı ofiyolitik-metamorfik birlikleri ve bunların jeolojik evrimdeki rolü, Türkiye 8. *Petrol Kong. Bild*, 128-140.
19. De Righi, M. R., & Cortesini, A. (1964). Gravity tectonics in foothills structure belt of southeast Turkey. *AAPG Bulletin*, *48*(12), 1911-1937.
20. Gül, M. A. (2000). Kahramanmaraş yöresinin jeolojisi. Hacettepe Üniversitesi, Fen Bilimleri Enstitüsü, Doktora Tezi, 304 s.
21. Yalçın, C., (2012). Çağlayancerit (Kahramanmaraş) batısının tektono-stratigrafisi ve yapısal evrimi. Kahramanmaraş Sütçü İmam Üniversitesi Fen Bilimleri Enstitüsü, Yüksek Lisans Tezi, 129s.
22. Yalçın, C., & Kop, A. (2022). Kaleköy-Hombur (Çağlayancerit-Kahramanmaraş) civarının tektono-stratigrafik özellikleri, Geosound, 55 (1), 37-60
23. Yalçın, C. (2022). Evaluation of structural elements in the collision zone by remote sensing method. Intercontinental Geoinformation Days, 4, 5-8.
24. Waldhoff, G., Bubenzer, O., Bolten, A., Koppe, W., & Bareth, G. (2008). Spectral analysis of ASTER, Hyperion, and Quickbird data for geomorphological and geological research in Egypt (Dakhla Oasis, Western Desert). *Int. Arch. Photogramm. Remote Sens. Spat. Inf. Sci*, *37*, 1201-1206.
25. Rani, K., Guha, A., Pal, S. K., & Vinod Kumar, K. (2018). Comparative analysis of potentials of ASTER thermal infrared band derived emissivity composite, radiance composite and emissivity–temperature composite in geological mapping of proterozoic rocks in parts of Banswara, Rajasthan. *Journal of the Indian Society of Remote Sensing*, *46*(5), 771-782. https://doi.org/10.1007/s12524-017-0737-z.
26. Chattoraj, S. L., Prasad, G., Sharma, R. U., van der Meer, F. D., Guha, A., & Pour, A. B. (2020). Integration of remote sensing, gravity and geochemical data for exploration of Cu-mineralization in Alwar basin, Rajasthan, India. *International Journal of Applied Earth Observation and Geoinformation*, *91*, 102162. https://doi.org/10.1016/j.jag.2020.102162.
27. Jain, S., Bhu, H., & Kothyari, G. C. (2021). Quaternary deformation in south-western Luni-Sukri basin, Rajasthan, India. *Arabian Journal of Geosciences*, *14*(15), 1-12. https://doi.org/10.1007/s12517-021-07710-2.
28. Guha, A., Kumar Ghosh, U., Sinha, J., Pour, A. B., Bhaisal, R., Chatterjee, S., ... & Rao, P. V. (2021). Potentials of Airborne Hyperspectral AVIRIS-NG Data in the Exploration of Base Metal Deposit—A Study in the Parts of Bhilwara, Rajasthan. *Remote Sensing*, *13*(11), 2101. https://doi.org/10.3390/rs13112101.
29. Pandey, A., & Purohit, R. (2022). Impact of Geological Controls on Change in Groundwater Potential of Recharge Zones due to Watershed Development Activities, Using Integrated Approach of RS and GIS. *Journal of Scientific Research*, *66*(1), 53-62
30. Işık, V. (2016). Torosların jeolojisi; Türkiye Jeolojisi Ders Notu. Ankara Üniversitesi, Jeoloji Mühendisliği Bölümü, Ankara.
31. https://earthexplorer.usgs.gov
32. Abdelkareem, M., Bamousa, A. O., Hamimi, Z., & Kamal El-Din, G. M. (2020). Multispectral and RADAR images integration for geologic, geomorphic, and structural investigation in southwestern Arabian Shield, Al Qunfudhah area, Saudi Arabia. *Journal of Taibah University for Science*, *14*(1), 383-401.
33. Elmas, A., & Yilmaz, Y. (2003). Development of an oblique subduction zone—tectonic evolution of the Tethys suture zone in southeast Turkey. *International Geology Review*, *45*(9), 827-840.
34. Yılmaz, Y. (2019). Southeast Anatolian Orogenic Belt revisited (geology and evolution). *Canadian Journal of Earth Sciences*, *56*(11), 1163-1180.
35. Şengör, A. M. C., & Yılmaz, Y. (1983). Türkiye'de Tetis' in evrimi: Levha tektoniği açısından bir yaklaşım. *Türkiye Jeoloji Kurumu Yerbilimleri Özel Dizisi*, *1*, 75.
36. Yiğitbaş, E., Yılmaz, Y., & Genç, Ş. C. (1992). Güneydoğu Anadolu orojenik kuşağında Eosen nap yerleşmesi. *Türkiye*, *9*, 307-318.

Advanced Remote Sensing

http://publish.mersin.edu.tr/index.php/arsej

e-ISSN 2979-9104

Spatio-temporal assessment of mangrove cover in the Gambia using combined mangrove recognition index

Bambo Bayo [1], Warda Habib [1], Shakeel Mahmood [*1]

[1]Government College University Lahore, Department of Geography, Pakistan, bayo.bambo@gmail.com, wardahabib419@gmail.com, shakeelmahmoodkhan@gcu.edu.pk

Cite this study: Bayo, B., Habib, W., & Mahmood, S. (2022). Spatio-temporal assessment of mangrove cover in the Gambia using combined mangrove recognition index. Advanced Remote Sensing, 2 (2), 74-84

Keywords
Mangrove Cover
Degradation
Change Detection
Remote sensing
GIS
CMRI

Research Article
Received: 09.10.2022
Revised: 30.11.2022
Accepted: 15.12.2022
Published: 28.12.2022

Abstract

This study is an effort to assess mangrove cover in The Gambia utilizing Landsat Data. The gradual land use and land cover variations along the coastal estuarine area of The Gambia provoked this paper to assess variation on the mangrove forest cover. The aim of this research is to do spatiotemporal monitoring and mapping to detect changes in mangrove forest cover of the Gambia from 2000 to 2020. For analyzing change, the technique of supervised classification with CMRI was applied on three multi-temporal Landsat images. Combined Mangrove Recognition Index (CMRI) approach is used in this research which is an index for distinction of mangrove forest from non-mangrove area. In this study, mangrove forest cover decline has been found to be approximately from 1811km^2 to 853km^2 in the last two decades. The main vegetation being deforested in Greater Banjul Area is mangroves. This impact has significantly increased the vulnerability of residents to flash floods after heavy rainfalls especially in towns like Serrekunda, Tallinding, Bundung, New Jeshwang and even the Capital City, Banjul. These findings can be significant for conservation authorities and research groups. The maps presented in this analysis will be a valuable guide and provide soft grounds for coastline regulatory body to formulate better sustainable development strategies for this region. Alongside, it a matter of global concern because its deforestation has not only threatened the mangrove ecosystem but also increased vulnerability of the nearby communities and fish breeding grounds. The results of the study will help environmental protection agency, agriculture and forest departments to design location specific strategies to reduce mangrove cover degradation.

1. Introduction

Globally, mangroves are distributed in more than one hundred countries, but in the past four decades, mangrove forests have suffered an intense decline [1]. Mangroves offer a wide range of functions and advantages to humans and wildlife; therefore, their loss is significant [2]. Woody plants known as mangroves are found in tropical and subtropical areas and once covered an area of around 18.8 million hectares [3]. However, deforestation has caused mangroves to shrink to 13.7 million hectares and later to 8.3 million hectares [4-5]. The mangrove ecology is in danger due to this alarmingly quick decline. Additionally, it is a cause for concern on a worldwide scale because deforestation has increased the vulnerability of the local communities and fish spawning grounds in addition to endangering the mangrove environment.

Following a mapping of the current extent of mangrove vegetation cover in South Asia from 2000 to 2012, the mangrove forest shift was noted [6]. In total, 1,187,476 ha of mangroves have been lost, which is equivalent to 7% of the world's total [7]. Conversion to other land uses, pollution, overharvesting, flooding, a decrease in the

availability of freshwater, coastal erosion, a decrease in silt deposition, and disturbances from tropical cyclones and tsunamis are the main causes of deforestation in South Asia [8].

At a global level, loss of mangrove vegetation cover according to Hamilton et al. [9] was mainly due to population growth and coastal development. Jayakumar, [10] opined those specific factors to mangrove vegetation cover loss includes urbanization, aquaculture, conversion to agricultural activities such as rice cultivation, and vegetable gardening, road construction, and overexploitation for timber and fuel wood. Mangroves are highly protective ecosystem that provides numerous functions and services including food, spawning ground and refuge for numerous faunas, and a sink for contaminants, a trap for fine sediments, coastal sediments, coastal protection, and carbon sequestration [11].

The mangroves are widely distributed throughout the tropical world, making it challenging, time-consuming, and perhaps impossible to monitor these ecosystems through ground surveys. As a result, many remote sensing technologies and satellite imagery have been employed [12]. The MCL (maximum land cover) with NDVI approach was used to detect changes in mangrove density in Matang Forest, Malaysia. The findings suggest that the mangrove forest cover has decreased by roughly 8017.3 hectares. The causes of this loss were discovered to include erosion, tree harvesting, and illicit agricultural activities [13]. Using remote sensing technology and Landsat data, the extent and density of mangroves in Pongok, Indonesia, were mapped. In that study, Path/Row: 123/062 Landsat data that were collected on July 24th, 2019, were used. The density of mangroves was determined by utilising the NDVI formula, which uses a vegetation index approach and has a range of values from -1 to 1. The findings show that mangrove density can be divided into three classes: dense (NDVI range: 0.42-1; equal to 1,500 Trees/Ha), sparse (NDVI range: -1- 0.33; equal to 1,000 Trees/Ha), and moderate (NDVI range: 0.33-0.42; equal to 1,000 to 1,500 Trees/Ha) (Sabai, 2019). Supervised classification and Vegetation indexing approach has the potential to quantify mangrove extent and density within the area in temporal and spatial scale [14].

Mangrove control on the coast is essentially what the Indus Delta's coastal zone management is all about. Mangrove forests once covered the deltaic region entirely, having an indirect or direct impact on its fauna and vegetation [15-16]. The 600,000 acres of mangroves over a coastline of around 240 km were listed as the fifth or sixth largest arid climate mangroves. Their growth is rapid on islands and in the creeks, however mangroves are vanishing speedily due to extreme meddling of the environment, and overexploitation by man [17].

Several consultancy projects on mangroves occurred in The Gambia such as National Environment Agency's (NEA) assessment of mangrove dieback (NEA, 2014), and West African Bird Study Association's (WABSA) survey on mangrove restoration and identification of the different species of mangroves in The Gambia [18]. The extensive scientific study on mangrove vegetation in The Gambia was conducted on Tambi Wetland Forest. The research revealed that two main types of mangroves exist in the wetland, Avicenna germananes and rhizophora mangle [19]. Like in many parts of the globe, anthropogenic activities such as fishing, oyster collection, farming, tourism, and wood collection are reported as the major causes of mangrove forest depletion in The Gambia. In contrast to the late 1980s loss in mangrove cover, which was attributed to the 1960–1974 Sahelian droughts, Fent et al. [20] reported that mangrove vegetation cover had grown recently. The apparent decrease in mangrove vegetation cover may be the result of an imbalance between local resource demands and the ecosystem's ability to meet those demands. Mangroves must not only be maintained but also reforested in order to reap the many ecological benefits they provide in order to meet the Sustainable Development Goals (SDGs), particularly Goal 15 (Life on Land). It places a focus on managing forests sustainably, stopping deforestation, reversing land degradation, and preserving biodiversity. The wetlands in The Gambia, where mangroves are found has approximately 108 mammal species and over 540 bird species of which a third is palearctic migrants. The loss of these habitats will result in endangering this biodiversity. SDG 13 (Climate Action) is generally believed to be a hinderance to the achievement of the agenda 2030 due to increasing levels of global temperatures and its consequent effects on both living and non-living systems. SDG 13 emphasizes on an urgent action to combat climate change and its impacts. Achieving all other SDGs will be much more challenging without urgent climate action, including those related to poverty, hunger, access to water, terrestrial and marine ecosystems, health, gender equality and the empowerment of women and girls, among others. Floods, the most frequent hazard in The Gambia, can be decreased and habitats protected by the presence of mangroves. Floods are projected to increase in the coming years due to consequences of climate change, such as sea level rise [21]. REDD+ (Reducing Emission from Deforestation and Forest Degradation), which is based on Article 5 of the Paris Agreement, is really encouraged by SDG 15 [22] for countries to implement.

Monitoring and charting the amount of the mangrove cover is therefore essential for both restoration and gaining a thorough understanding of the mangrove ecosystem. The goal of this study is to do spatiotemporal monitoring and mapping in order to find changes in The Gambia's mangrove forest cover between 2000 and 2020. This study uses geospatial approaches to conduct exploratory research on the change analysis of mangrove cover. The main objectives of this paper are to determine the spatial extent of mangrove vegetation cover changes; compare these changes in the spatial extent of mangroves cover and evaluate the causes of these changes within the two decades.

2. Study Area

The Gambia is located on the extreme west coast of Africa and extended from 13˚N to14˚N latitude and 13º to 17º West longitude. It has a total area of 11,295 km^2. The country has about 80 km coastline on the Atlantic Ocean. River Gambia is the main physical feature in the study area. It divides the country into north and south banks. The Gambia has a tropical climate with distinct dry and wet season. In the dry season, the temperatures are cool and dry varying from 70˚F(21˚C) to 80˚F (27˚C) and a relative humidity of 30% and 60%. The wet season starts in summer from June and October. Annual rainfall is between 800mm and 1000mm [23].

From the coast to about 250 km inland, the ocean salt water intrudes. It is on these banks where majority of the mangroves are found. Being halophytic, mangroves are found in the brackish waters along the banks and tributaries of the river, and the intertidal estuarine areas of the coast. Up to about 200 km inland, there is a continuous stretch of mangrove vegetation. Of the eight species of mangroves in Africa, seven are all found in The Gambia. The Gambia has three Ramsar sites comprised of mangroves: Bao Bolong Wetland Reserve, Tambi Wetland Complex, and Niumi National Park. The geographic location of the country and the presence of wetland systems support the diverse ecosystems for the several species of plants and animals [21].

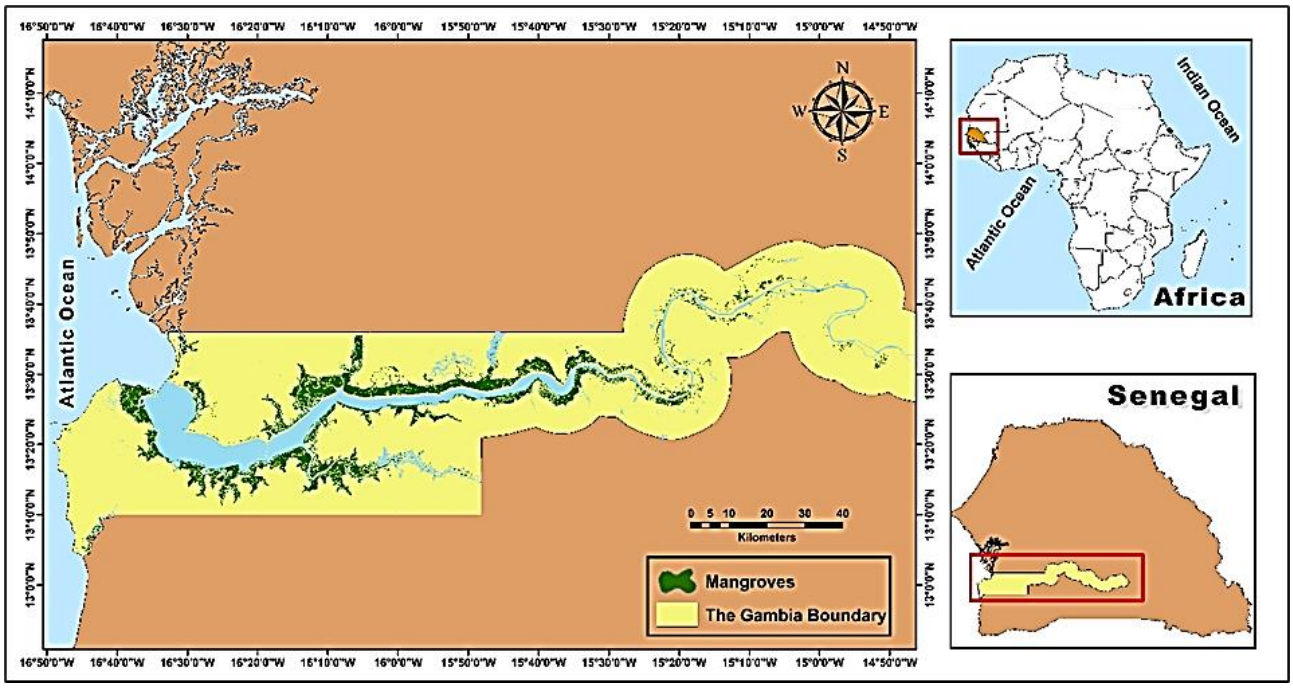

Figure 1. Representation of mangrove forest area in The Gambia

3. Material and Methods

The ideas behind change detection analysis are not new, but with the development of new imaging sensors and geospatial technologies, there is now a demand for image processing methods that can combine data from a range of sensors and datasets in order to map, detect, and monitor forest resources. The overall objective of this study was to map out and analyze the structural changes of mangrove forest cover using Landsat imageries of the study area. A supervised classification and CMRI index approach was performed on three multi-temporal satellite images.

3.1. Data Acquisition

Multispectral satellite images of the past twenty years (2000-2020) were downloaded for 2000, 2010 and 2020 with temporal resolution of 10 years from United States Geological Survey (USGS) [24] to geo-visualize mangrove cover changes in The Gambia. Specifications of the satellite data are given in Table 1.

Table 1. Characteristics of Acquired Satellite Images

Satellite Data	Year of acquisition	Number of Bands	Spatial Resolution	Month
L7 ETM+	2000	8		
L7 ETM+	2010	8	30m	October
L8 OLI/TIRS	2020	11		

3.2. Image Pre-processing

Satellite image pre-processing before change detection phenomenon is very important. The satellite data will be imported into ERDAS imagine software for stacking, mosaicking, extraction of AOI and for geometric correction.

3.3. Data Analysis and Techniques

Geographic Information System (GIS) techniques such as Supervised Classification and Combined Mangrove Recognition Index (CMRI) were performed to analyze changes in mangrove forest cover in the past 20 years.

3.4. Supervised Classification

The maximum likelihood algorithm was used to perform supervised classification on the images. It is a sort of image classification where the analyst itself controls the majority of the process by choosing the pixels that best represent the targeted classes. As images were spectrally strong and with ground truth information it was easy to do visual interpretation of all categorized classes. Targeted object texture, tone, color made it more precise to determine required classes like Agriculture cover represents less thickness as compared to mangrove cover. Also, field survey and indigenous knowledge of study area help analyst to select samples more accurately. Built-up Area, Agriculture, Mangrove Cover, Water Body, Dry Fields, and Barren Land were the categories that were defined. Each class was given a distinct identity and given a specific color to help them stand out from one another. Training samples were chosen for each of the preset land cover/use types. The pixels contained by these polygons were used to record the spectral signatures for the various land cover types that were obtained from the satellite data.

3.5. Combined Mangrove Recognition Index

The Combined Mangrove Recognition Index (CMRI) incorporates three bands (Red Band, Green Band, and Near Infra-Red Band) for evaluating solely the mangrove forest cover utilizing information like greenness and water content (succulence).

MRI (Mangrove Recognition Index) was applied in Beilunhekou (National Nature Reserve Area of China) for differentiating mangrove vegetation cover from non-mangrove cover area. Changes are observed in spectral values during conditions like both high and low tides, that's why this index used green and wet values of satellite images. The need for an index that is not dependent on such variables arises from the fact that factors like tides, salinity, and the variety of nearby vegetation cover vary globally. In compared to other vegetation indexes, CMRI index offers much improved results because it is primarily utilized to identify mangrove forest cover. In our study, mangrove vegetation cover was identified using CMRI. The formula of Combined Mangrove Recognition Index is shown in Equation 1.

$$\textbf{CMRI} = [(\text{NIR-RED}) / (\text{NIR+RED})]- [(\text{GREEN-NIR}) / (\text{GREEN+NIR})] \quad (1)$$

3.6. Accuracy assessment

Accuracy assessment is an important step for the validation of image classification process. In this research, accuracy of user, producer, and O A (overall accuracy) was done through Equation 2.

$$\text{OA}= \frac{Correctly\ classified\ no.of\ sampling\ classes}{No.of\ reference\ sampling\ classes} \quad (2)$$

Precision of classified image or validity with reference information is measured by kappa (K) values. Numerical statement of kappa (K) is stated in Equation 3.

$$\text{K}= \frac{Observed\ Accuracy - Chance\ Assessment}{1 - Chance\ Agreement} \quad (3)$$

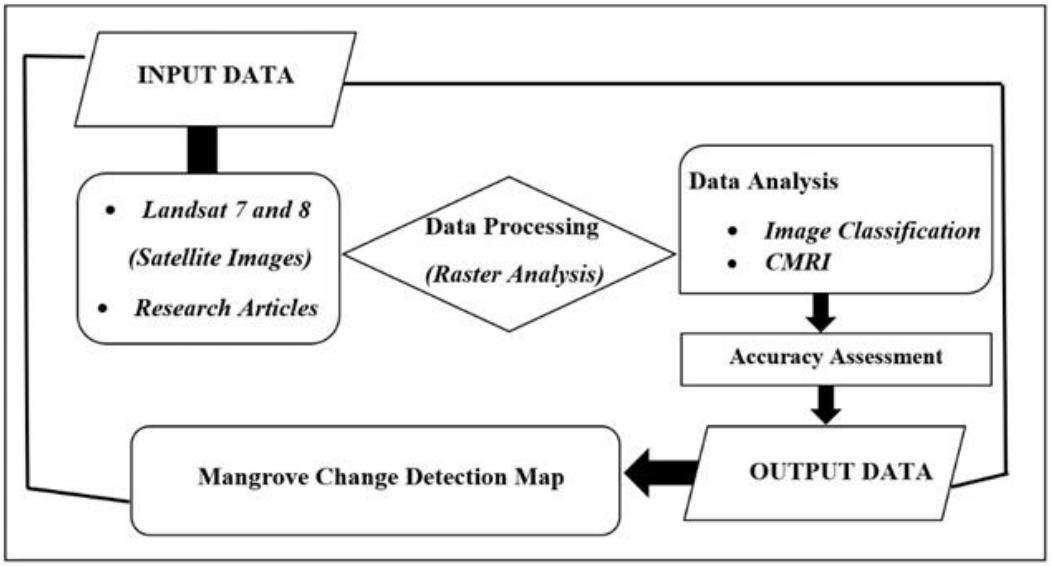

Figure 2. Research Methodology

4. Results and Discussion

4.1. Image Classification

The analysis of mangrove cover change done using supervised classification and CMRI techniques on satellite images from 2000 to 2020. In green cover most of the area is covered by mangrove and significant decline has been observed in the past two decades.

4.2. Spatial Analysis of Mangrove Cover Change

The mangrove vegetation occupied roughly 1181 square kilometers (16 %) of the total land area in 2000. 1381kilometer squares (or 12 %) was made up of agricultural land, whereas 1.4 % was occupied by built-up areas. There were more dry fields and barren ground than anything else, making up 35% and 27% of the total area, respectively. A total of 571 km^2 of built-up land can be seen in the 2010 image (5 %). In 2010, there was 4.2 % agricultural land, down from 12 % in 2000. This decrease is reflected in both built-up and bare land, which increased from 4036 (36%) in 2000 to 6567 (58%) in 2010. Mangrove cover, however, saw a reduction in forestry from 16 to 13 %. According to an analysis of 2020 imagery, the area covered by barren land is 33 %, the greatest percentage among the other classes, including dry fields (8 %), built-up areas (15 %), and mangrove cover (7 %).

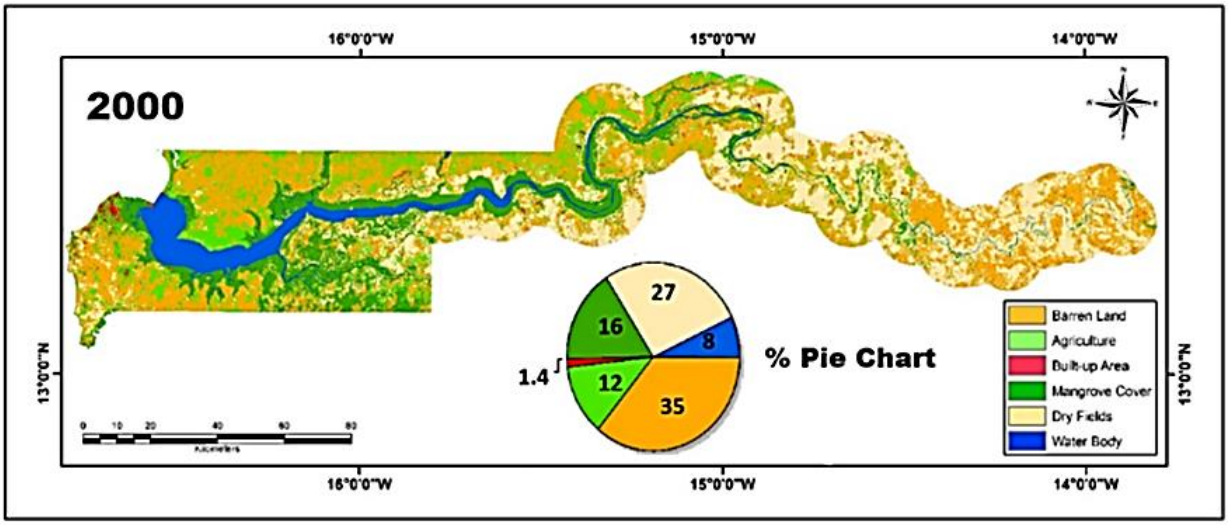

Figure 3. Classification of 2000

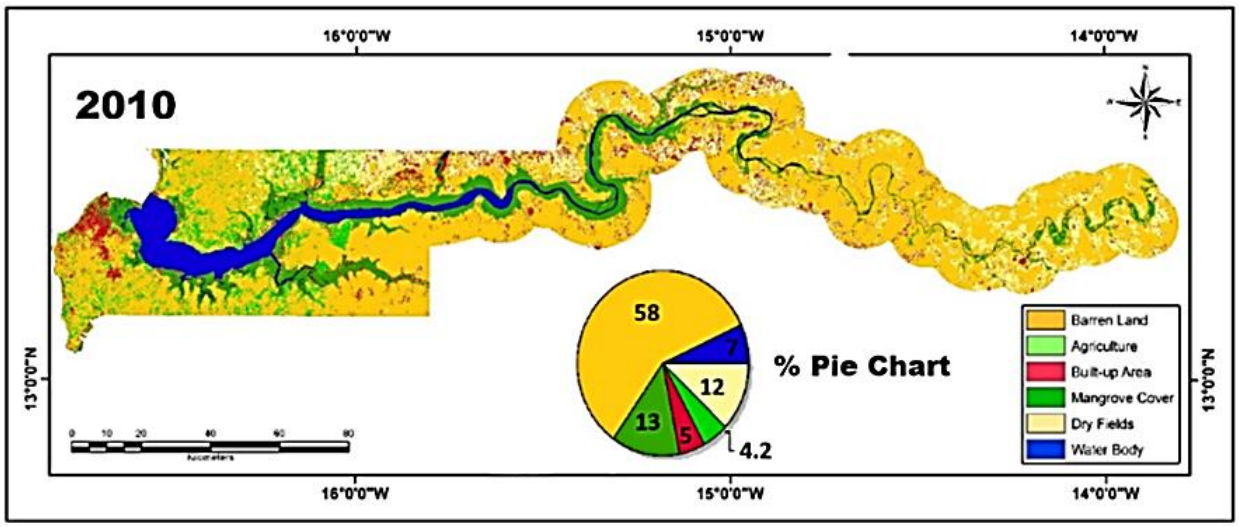

Figure 4. Classification of 2010

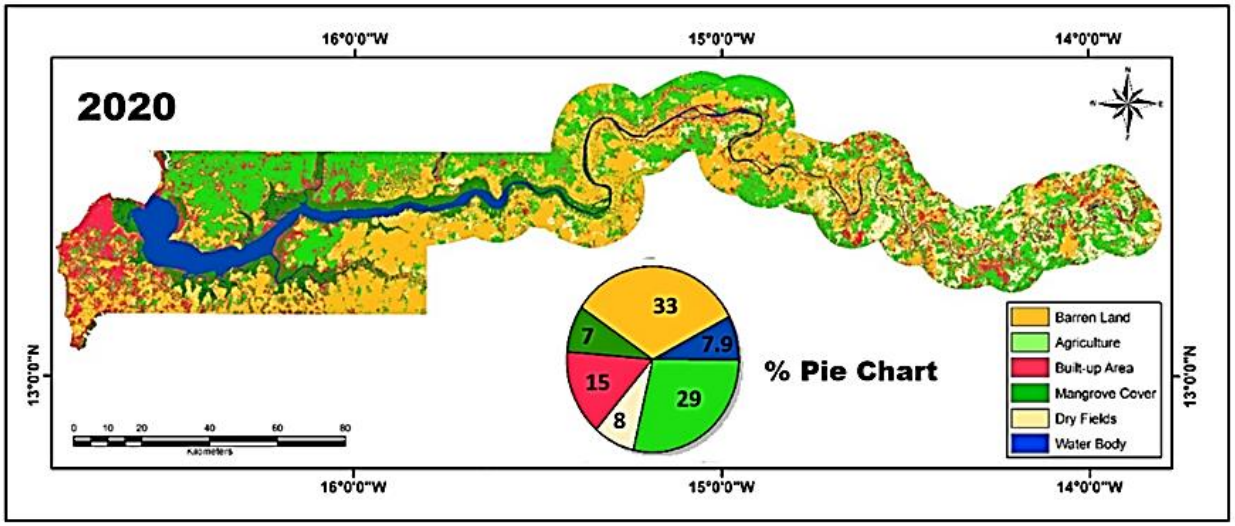

Figure 5. Classification of 2020

4.3. Combined Mangrove Recognition Index Changes

The extent of the mangrove cover pattern may be readily detected from the images analysis carried out utilizing CMRI technology. On the banks of the river Gambia and its tributaries, the mangrove cover is depicted as a dark green color. Compared to the 2000 image, the 2020 photographs revealed a considerable reduction in mangrove cover (853 km^2) (1811 km^2). This explains a decrease of mangrove vegetation cover of 958 km^2 (more than 100%) during a period of 20 years. Between 2000 and 2020, there was a rising trajectory in the built-up area. The expansion of the built-up area clearly has a deleterious impact on both the mangrove cover and other land uses. Due to a variety of circumstances, including the temperature, closeness to the sea, concentrated government facilities and services, private enterprises, urbanization, and others, this is particularly pronounced in the western region of the country. The accompanying figure clearly highlights variations in mangrove forest cover and displays the spatiotemporal scope of the mangrove cover pattern.

In 2020, the built-up area and agricultural land areas are seen to grow the most. The degradation of mangroves is mostly brought about by these two anthropogenic factors. On New Jeshwang, Tallinding, and Faji Kunda, one can see vegetable and rice farms being grown. The construction and expansion of the West Field-Banjul Highway has caused the degeneration of the mangrove cover along this area and further attracted the construction of buildings along the highway.

Mangroves across the entire country were the subject of this study. Hence detailed matters such as major deforested areas may not be highlighted. An area-specific study and field observations can help one gain a better knowledge of the situation by revealing the facts on the ground and helping to pinpoint areas where the mangrove vegetation cover is increasing or decreasing.

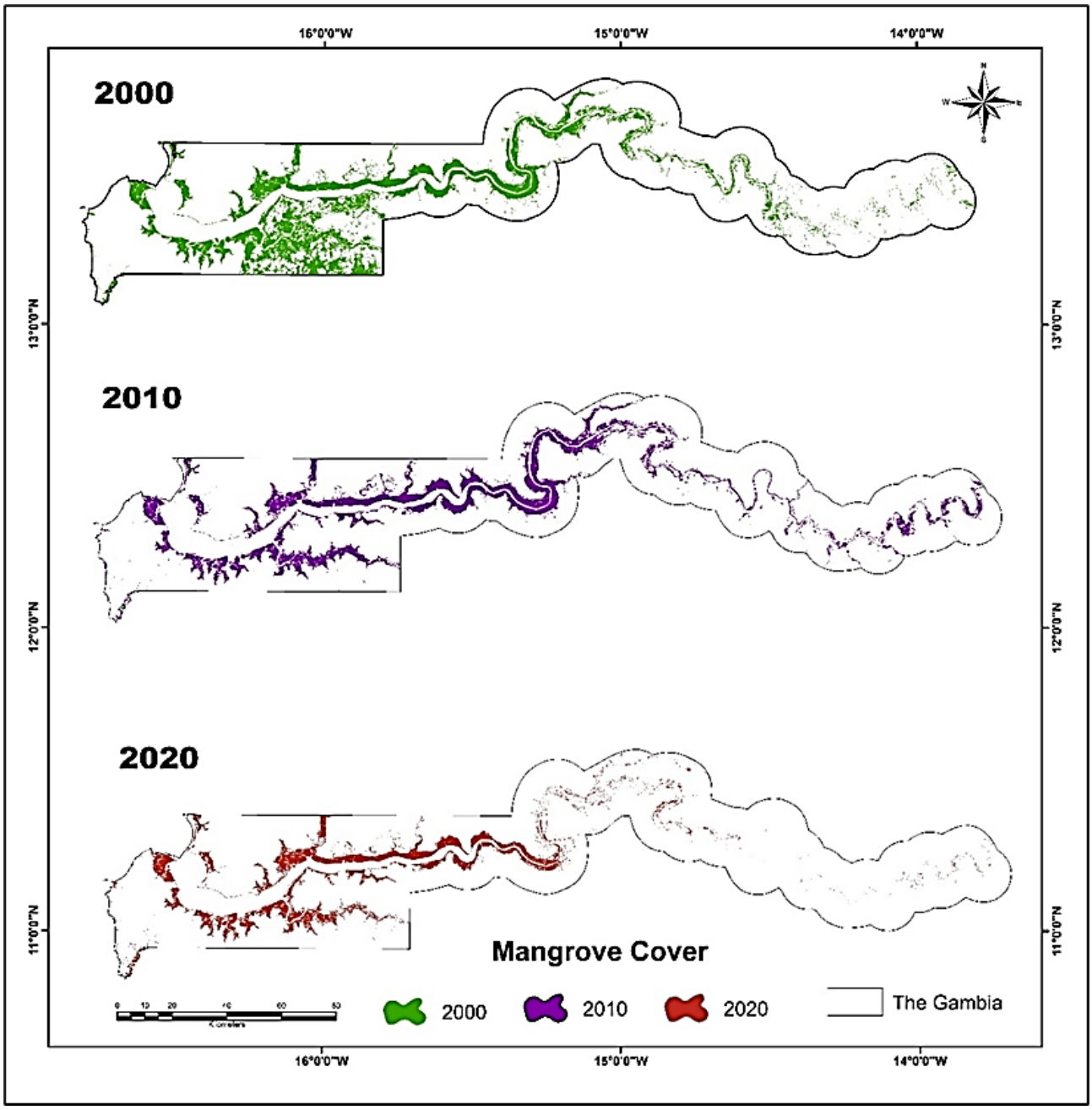

Figure 6. Change Detection of Mangrove Cover

4.4. Temporal Analysis of Mangrove Cover Change

Figure 5. presents abrupt change in built-up area which is 1664 km2 from 159 km^2 area and barren land is approximately decreased from 4036 km^2 to 3688 km^2 in 20 years. In this research, mangrove forest cover decline has been found to be approximately from 1811 km2 to 853 km^2 between 2000 and 2020 as shown in Table 2.

Table 2. Area Statistics of the land use land cover units from 2000 to 2020 of The Gambia

Categories	2000		2010		2020	
	Area (km^2)	Area (%)	Area (km^2)	Area (%)	Area (km^2)	Area (%)
Built up Area	159	1.4	571	5	1664	15
Mangrove Cover	1811	16	1418	13	853	7
Barren Land	4036	36	6567	58	3688	33
Dry Fields	3042	27	1396	12	928	8
Agriculture	1381	12	479	4.2	3258	29
Water body	763	7	762	7	803	8

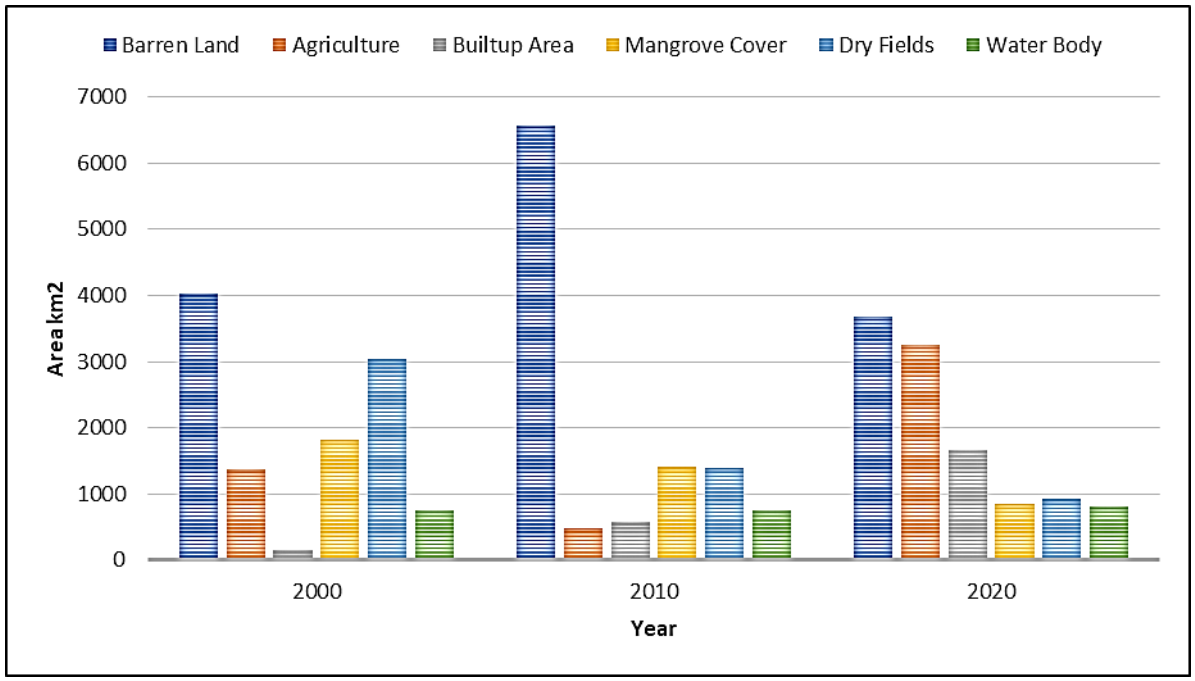

Figure 7. Temporal Analysis of Mangrove Cover Change

4.5. Accuracy assessment

K (kappa) values along with user's and producer's accuracy of delineated classes for the years 2000, 2010 and 2020 are shown in Table 3.

Table 3. Summation of producer's and user's accuracy and kappa (K) coefficients

Classes	Producer's Accuracy (%)							User's Accuracy (%)							Overall Accuracy	K
	1	2	3	4	5	6	Avg.	1	2	3	4	5	6	Avg.		
2000	89	86.7	84.6	80.2	83.1	80.4	88.1	87.8	88	86	86.7	83.6	86.4	88.5	0.83	0.80
2010	90.4	91.3	87	89.1	84	83	89.5	89.8	90	83.7	84.2	86.2	84.7	89.9	0.88	0.85
2020	87.7	95.5	88.2	87.4	86	87	87.4	84.7	82.5	84.7	85.5	86.8	85.8	87.6	0.86	0.82

The map makers (producer) accuracy is the accurateness of the map while the accuracy of users is the accuracy from the perspective of map user not mapmaker. The two accuracies in our data were within a reasonable extent, indicating less mistakes in findings.

4.6. Mangrove Deforestation and Challenges

Mangrove deforestation has global significance because very few mangrove ecosystems are surviving and fighting anthropogenic actions. There are numerous environmental problems and a depletion of natural resources in The Gambia. Extreme forest degradation and soil degradation are the two main problems. According to reports, the percentage of mangrove forests has decreased from 16 to 7%. Without a doubt, this loss will make areas more susceptible to hydrometeorological hazards.

The Gambia is divided into two different Representative Territorial Units (RTUs). In contrast to the North Bank Region, which is rural and dependent on subsistence agriculture, the Greater Banjul Area is located in the western coastal regions and is more developed and urbanized.

The North Bank RTU is mainly affected by deforestation and soil erosion. Being an agrarian region, these hazards have a negative consequence on food security and livelihood activities. The Greater Banjul Area is confronted mainly by coastal erosion, flood, and deforestation. Deforestation is more severe in The Kanifing Municipality as commercial and industrial activities and urbanization have increase demand for land. Coastal erosion is another major environmental hazard in GBA. In some areas, the beach is retreating at a rate of 1-2 meters annually. Sectors such as tourism (second major contributor to the economy of The Gambia), artisanal fisheries and other livelihoods will be affected due to sea level rise and other hydrometeorological events.

The main vegetation being deforested in Greater Banjul Area is mangroves. This impact has significantly increased the vulnerability of residents to flash floods after heavy rainfalls especially in towns like Serrekunda, Tallinding, Bundung, New Jeshwang and even the Capital City, Banjul. Over 35,000 people, 2,371 houses and unaccounted food and cash crops were damaged by flash floods in 2010 rainy season alone.

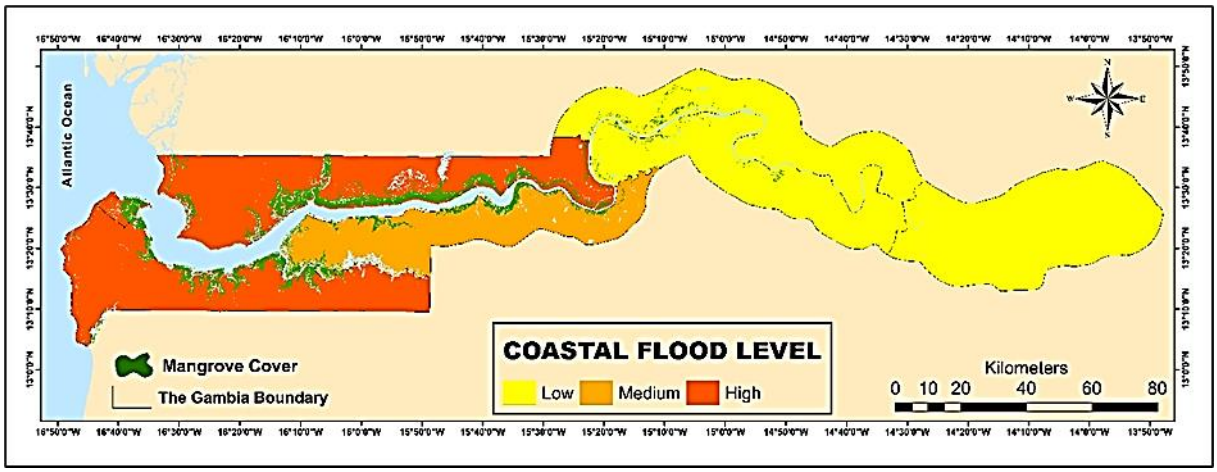

Figure 8. Zonation of Coastal flood-Hazard Level (Source: Mapbox)

Mangroves have both environmental and societal impacts. The effectiveness of mangroves in hydrometeorological risk reduction has been well documented in coastal setting where they exist. Mangrove belts are effective in attenuating storm surges during cyclones (typhoons/ hurricanes) hence, protecting lives and properties. For example, the 2004 Indian Ocean tsunami, hamlets in the Indian Tamil Nadu region did not lose a single life attributed mainly to the impact of mangroves. Another impact is that mangroves have the potentials to reduce flood extent in low-lying areas as it serves as a buffer between marine and terrestrial ecosystems. Mangrove roots bind the soil, reducing erosion and carbon storage. This accretion acts as a carbon sink and helps to reduce coastal erosion. Deforestation reduces the potential of mangroves in these environmental impacts. Mangroves have the potential to increase community resilience to hydrometeorological impacts [25].

Socially, as highlighted in previous chapters mangrove forests serve as a good source of livelihood to locals in the forms of fishing, crap, oyster and wood collection, herb, medicinal purposes and recreation functions. The absence of mangroves will severely affect these livelihood services.

Due to the Greater Banjul and North Bank regions' vulnerability to climate-related dangers, mangrove belt restoration and afforestation are essential. In some places of the world, increasing mangrove forest cover has been accomplished through public awareness campaigns, replanting, reforestation, and even legal action. This would lessen The Gambia's vulnerability to climate-related disasters and enhance its ability to adapt.

The United Nation Environment Program (UNEP) office Banjul has launched "Gambia Ecosystem-based Adaptation 2017-2023" in line with SDG 15 (Life on Land) where it targets the rehabilitation of 10,400 ha of degraded forest, savanna and mangroves and an additional 3000 ha of farmland. According to UNEP (nd), it has already planted 10million mangrove propagules within the first 2 years. These mangroves are expected to serve as a buffer against storm surges to protect coastal settlements and also provide habitat for many fish species. In line with SDG 1 (No Poverty), the project also targets increasing the income of 11,550 household through horticulture and vegetable gardening. This will reduce the overdependence of inhabitants on the forest on which they get fuelwood and wood for income generation. The significant function of mangroves in carbon sequestration, preventing soil erosion, controlling the effects of sea level rise can be very instrumental in attaining SDG 13 (Climate Action). As argued by [23] that the need to participate in the production of knowledge in order to achieve Goal 15 of the Sustainable Development Goals on the preservation and restoration of terrestrial ecosystems, monitoring of changes in vegetation cover is necessary.

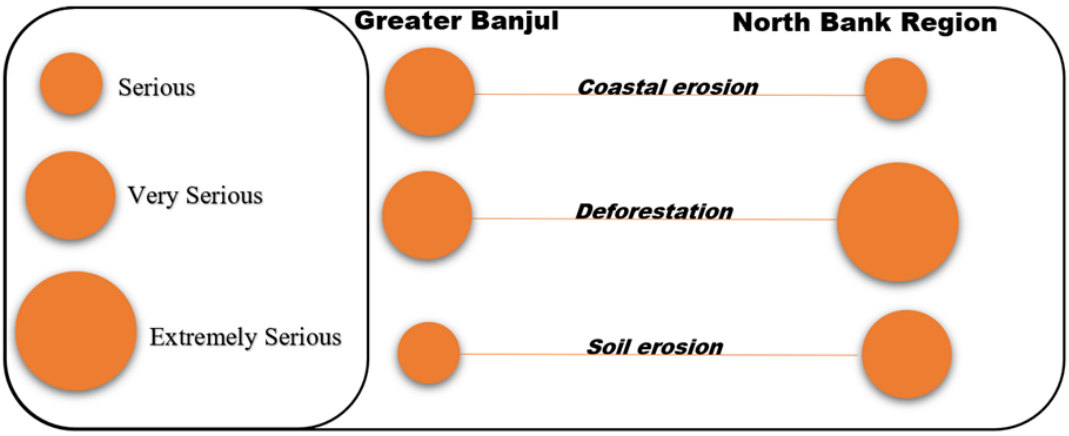

Figure 9. Challenges in Greater Banjul Area and North Bank Region (Source: DARA)

5. Conclusion

Mangrove forest are decreasing due to rapid deforestation. The main causes of these are attributed to both anthropogenic factors such as urbanization and agriculture/aquaculture activities, wood collection, etc. and natural factors such as cyclones, rising sea levels, and climate changes impacts. In The Gambia, the main cause of mangrove degradation is attributed to anthropogenic activities mainly farming, oyster collection, wood collection, urbanization, and damming of distributaries which prevent water reaching some areas. Natural factors such as drought and increasing salinity are the main causes of mangroves dieback.

The importance of mangroves in both coastal protection and ecological services cannot be over emphasized. This research found that, The Gambia has experienced a significant decrease of mangrove cover within two decades. Therefore, there is a need to curb the deforestation trend to benefit from mangrove vegetation functions. Tambi Wetland Reserve and areas along the Bintang Creek need more protection and restoration activities respectively. Mangroves in the Tambi Wetland Reserve are exposed to urban expansion effects while those along the Bintang Creek suffer from local wood collection and dieback due to climate change impact. Mangrove forests should be protected through public awareness campaigns and, where possible, through litigation. Indeed, for sustainable management, mangrove vegetation healthiness and cover should be constantly monitored, not only to maintain existing ones but also to increase the area covered by mangroves.

Funding

This research received no external funding.

Author contributions

Bambo Bayo: Conceptualization, Analysis, Geo-visualization **Warda Habib: Analysis:** Preparation of manuscript. **Shakeel Mahmood:** Methodology, writing, reviewing and editing.

Conflicts of interest

The authors declare no conflicts of interest.

References

1. Elmahdy, S. I., Ali, T. A., Mohamed, M. M., Howari, F. M., Abouleish, M., & Simonet, D. (2020). Spatiotemporal mapping and monitoring of mangrove forests changes from 1990 to 2019 in the Northern Emirates, UAE using random forest, Kernel logistic regression and Naive Bayes Tree models. *Frontiers in Environmental Science*, *8*, 102.
2. Bryan-Brown, D. N., Connolly, R. M., Richards, D. R., Adame, F., Friess, D. A., & Brown, C. J. (2020). Global trends in mangrove forest fragmentation. *Scientific reports*, *10*(1), 1-8.
3. Gao, J., Lundquist, C. J., & Schwendenmann, L. (2018). Characterizing landscape patterns in changing mangrove ecosystems at high latitudes using spatial metrics. *Estuarine, Coastal and Shelf Science*, *215*, 1-10.
4. Dan, T. T., Chen, C. F., Chiang, S. H., & Ogawa, S. (2016). Mapping and change analysis in Mangrove Forest by using Landsat imagery. *ISPRS Annals of Photogrammetry, Remote Sensing & Spatial Information Sciences*, *3*(8), 109-116
5. Basheer, M. A., El Kafrawy, S. B., & Mekawy, A. A. (2019). Identification of mangrove plant using hyperspectral remote sensing data along the Red Sea, Egypt. *Egyptian Journal of Aquatic Biology and Fisheries*, *23*(1), 27-36.
6. Sari, S. P., & Rosalina, D. (2016). Mapping and monitoring of mangrove density changes on tin mining area. *Procedia Environmental Sciences*, *33*, 436-442.
7. Lucas, R., Otero, V., Van De Kerchove, R., Lagomasino, D., Satyanarayana, B., Fatoyinbo, T., & Dahdouh-Guebas, F. (2021). Monitoring Matang's Mangroves in Peninsular Malaysia through Earth observations: A globally relevant approach. *Land Degradation & Development*, *32*(1), 354-373.
8. Jia, M., Wang, Z., Zhang, Y., Mao, D., & Wang, C. (2018). Monitoring loss and recovery of mangrove forests during 42 years: The achievements of mangrove conservation in China. *International journal of applied earth observation and geoinformation*, *73*, 535-545.
9. Hamilton, S. E., Castellanos-Galindo, G. A., Millones-Mayer, M., & Chen, M. (2018). Remote sensing of mangrove forests: Current techniques and existing databases. In *Threats to Mangrove Forests* (pp. 497-520). Springer, Cham.

10. Jayakumar, K. (2019). Managing mangrove forests using open source-based webgis. In *Coastal management* (pp. 301-321). Academic Press.
11. Andrieu, J., Cormier-Salem, M. C., Descroix, L., Sané, T., & Ndour, N. (2019). Correctly assessing forest change in a priority West African mangrove ecosystem: 1986–2010 An answer to Carney et al. (2014) paper "Assessing forest change in a priority West African mangrove ecosystem: 1986–2010". *Remote Sensing Applications: Society and Environment*, *13*, 337-347.
12. Wang, L., Jia, M., Yin, D., & Tian, J. (2019). A review of remote sensing for mangrove forests: 1956–2018. *Remote Sensing of Environment*, *231*, 111223.
13. Saravanan, S., Jegankumar, R., Selvaraj, A., Jennifer, J. J., & Parthasarathy, K. S. S. (2019). Utility of landsat data for assessing mangrove degradation in Muthupet Lagoon, South India. In *Coastal zone management* (pp. 471-484). Elsevier.
14. Nguyen, L. D., Nguyen, C. T., Le, H. S., & Tran, B. Q. (2019). Mangrove mapping and above-ground biomass change detection using satellite images in coastal areas of Thai Binh Province, Vietnam. *Forest and Society*, *3*(2), 248-261.
15. Zhang, X., Treitz, P. M., Chen, D., Quan, C., Shi, L., & Li, X. (2017). Mapping mangrove forests using multi-tidal remotely-sensed data and a decision-tree-based procedure. *International journal of applied earth observation and geoinformation*, *62*, 201-214.
16. Navarro, J. A., Algeet, N., Fernández-Landa, A., Esteban, J., Rodríguez-Noriega, P., & Guillén-Climent, M. L. (2019). Integration of UAV, Sentinel-1, and Sentinel-2 data for mangrove plantation aboveground biomass monitoring in Senegal. *Remote Sensing*, *11*(1), 77.
17. Pham, T. D., Yokoya, N., Bui, D. T., Yoshino, K., & Friess, D. A. (2019). Remote sensing approaches for monitoring mangrove species, structure, and biomass: Opportunities and challenges. *Remote Sensing*, *11*(3), 230.
18. West African Bird Study Association (2020). A Report on survey on the distribution, identification and suitable sites for mangrove enrichment and restoration in LRR and CRR. Mangrove survey report, Banjul, The Gambia.
19. Satyanarayana, B., Bhanderi, P., Debry, M., Maniatis, D., Foré, F., Badgie, D., ... & Dahdouh-Guebas, F. (2012). A socio-ecological assessment aiming at improved forest resource management and sustainable ecotourism development in the mangroves of Tanbi Wetland National Park, The Gambia, West Africa. *Ambio*, *41*(5), 513-526.
20. Fent, A., Bardou, R., Carney, J., & Cavanaugh, K. (2019). Transborder political ecology of mangroves in Senegal and The Gambia. *Global Environmental Change*, *54*, 214-226.
21. Rivera, J., Ceesay, A. A., & Sillah, A. (2020). Challenges to disaster risk management in The Gambia: A preliminary investigation of the disaster management system's structure. *Progress in Disaster Science*, *6*, 100075.
22. Dampha, N. K. (2021). Change detection (1985-2020): Projections on land-use land cover, carbon storage, sequestration, and valuation in Southwestern Gambia. *Sustainable Environment*, *7*(1), 1875556.
23. Solly, B., Jarju, A. M., Sonko, E., Yaffa, S., & Sawaneh, M. (2021). Detection of recent changes in Gambia vegetation cover using time series MODIS NDVI. *Belgeo. Revue belge de géographie*, (1).
24. https://www.glovis.usgs.gov
25. Estoque, R. C., Myint, S. W., Wang, C., Ishtiaque, A., Aung, T. T., Emerton, L., ... & Fan, C. (2018). Assessing environmental impacts and change in Myanmar's mangrove ecosystem service value due to deforestation (2000–2014). *Global change biology*, *24*(11), 5391-5410.

Advanced Remote Sensing

http://publish.mersin.edu.tr/index.php/arsej

e-ISSN 2979-9104

Water budget estimation using remote sensing observations and GLDAS-CLSM for Limpopo River Basin

Motasem Alfaloji *[1]

[1]*Istanbul Technical University, Graduate School, Geomatics Engineering Program, Türkiye, alfaloji20@itu.edu.tr*

Cite this study: Alfaloji, M. (2022). Water budget estimation using remote sensing observations and GLDAS-CLSM for Limpopo River Basin. Advanced Remote Sensing, 2 (2), 85-93

Keywords
Water Budget Estimation
GLDAS
Remote sensing
GPM-IMERG
MODIS
River Basin
Limpopo

Research Article
Received: 15.11.2022
Revised: 21.12.2022
Accepted: 24.12.2022
Published: 28.12.2022

Abstract

River Basin Management is heavily reliant on satellite remote sensing technologies. Keeping track of a basin's water supply and demand is essential for efficient and sustainable water resource management. In this study, The Limpopo River Basin's monthly water budget components for the 2019 wet and dry seasons were determined using satellite measurements and the GLDAS-2.1 CLSM model. The water budget components, which include Precipitation, Evapotranspiration, Terrestrial Water Storage, and Runoff, were obtained from several satellite-based sources (GPM-IMERG, MODIS, GRACE & GRACE-FO). Runoff was calculated as a residual from the water balance equation because it could not be directly determined from remote sensing measurements. The datasets were prepared, investigated, and evaluated. The effectiveness of satellite remote sensing for estimating the water budget was assessed. The results showed good stability for the Precipitation and Evapotranspiration, but there were significant ambiguities in the Terrestrial Water Storage and Runoff. The precipitation results for the 2019 wet season were close from GPM-IMERG (~ 108 BCM) and GLDAS (~ 119 BCM). Both MODIS and GLDAS showed similar results for the Evapotranspiration for the 2019 dry season (18 BCM, 15 BCM respectively) The study demonstrated the benefits and drawbacks of GLDAS-2.1 CLSM models with satellite-based remote sensing for calculating water budgets. Since human impact is not considered in remote sensing and modeled data, caution should be used when employing them in ungauged areas. Given the limitations in GLDAS and remote sensing datasets, these data can be extremely helpful, especially in areas with limited data, for assessing seasonal and inter-annual changes in water components and river basin management.

1. Introduction

The availability of water is a significant issue in the twenty-first century [1]. Understanding the hydrologic cycle and how water travels through Earth's atmosphere, land surface, and subsurface is necessary for ensuring sustainable water supplies [2]. Hydrologists and users can quantify the hydrologic cycle by using water budgets [3]. An evaluation of the rates of water flow and the change in water storage in the entire atmosphere, land surface, and subsurface is known as a "water budget" [4]. Water budgets are straightforward in concept, but they could be challenging to calculate precisely. To assess how much water may be available for human and environmental demands, it is critical for the public and decision-makers to understand the uncertainties that exist in water budgets and their relative relevance [5].

A river basin is an area of land that drains water into a river and its tributaries. A river basin collects rain or snow, and it drains into a common outlet such as a stream or a tributary lake or wetland, where it eventually flows

into the river. River Basin is major source of fresh water for drinking and agricultural activities, which makes it the lifeblood of the area surrounding it. Moreover, there are 263 trans-boundary river basins covering about half the earth's surface [6]. About 145 states have territory within trans-boundary lakes or river basins, and 30 countries lie entirely within trans-boundary rivers, and it has been noted that since 1948 there have been 37 incidents of acute conflict over water [7,8]. The components of water budget include Precipitation, Evaporation, and transpiration (Evapotranspiration), infiltration, Total water Storage (Soil moisture, reservoirs, and groundwater storage) and Runoff [9].

Surface-based gauges (rain gauges) and remote sensing measurements can be used to measure Precipitation. But since gauge-based observations are dependent on points, the uncertainty in Precipitation values grows as one gets further away from the measuring station [10,11]. Evapotranspiration is the total of all evaporation and transpiration processes that transport water from the ground surface to the atmosphere. When using in situ methods to measure Evapotranspiration at large scales, spatial variability is typically substantial. Numerous factors (such as solar radiation at the surface, air and ground temperatures, surface winds, humidity, soil conditions, and vegetation cover and types) affect Evapotranspiration [12]. Runoff is water that runs off into the stream and eventually out of the watershed or sub-basin. Hydrological stations can be used to monitor Runoff variations, although many basins across the world have a dearth of or a patchy distribution of these stations [13]. A crucial part of the hydrological cycle, which encompasses all types of surface and subsurface water, is Terrestrial Water Storage (TWS). Surface measurements are still very important but point measurements have non-uniform coverage and data void regions. Although point measurements have non-uniform coverage and data empty zones, surface measurements are still very useful [14].

The management of water resources is increasingly dependent on satellite remote sensing technologies. When opposed to ground-based nonuniform observations [15], satellite remote sensing offers global coverage and spatially uniform data. One of the key benefits of earth-observing satellites is their ability to give reliable Precipitation estimates on a global scale with high spatial and temporal precision. This capability includes providing Precipitation data over data-restricted regions [16]. Several researchers have recently investigated how well satellite-based rainfall estimates perform. Remotely sensed Precipitation products have been suggested as an alternative in terms of time and space for data-scarce areas because of the encouraging findings that have been reported [17-20]. This paper aim to estimate the Limpopo River Basin terrestrial water budget from GLDAS 2.1-CLSM and remote sensing observations and compare the results to assess how well satellite remote sensing performs in estimating water budgets, and to examine and contrast the spatial patterns between satellite data and earth system model data.

2. Material and Method

In this study, earth system modeling and remote sensing datasets (Table 1) were utilized for evaluating the water budget in the 2019 wet and dry seasons in the Limpopo River basin (December 2015-February2016) and (June2016-August2016) respectively. The Shuttle Radar Topography Mission (SRTM) provided a Digital Elevation Model (DEM) for the research area with a 1 arc-sec (~ 30 m) grid resolution. The basin and its network of streams were defined using the DEM. Due to the GLDAS-2.1 CLSM model's ability to represent groundwater and the high performance of the data assimilation framework, it was chosen to be used with their Level-4 monthly output data for comparative comparison. Datasets from GLDAS 2.1 are accessible at 1° spatial resolution. The model's outputs for Surface Runoff (R), Terrestrial Water Storage (TWS), Evapotranspiration (ET), and Precipitation (P) on a monthly average were retrieved from NASA's Goddard Earth Sciences Data and Information Services Center. To test the water budget estimation utilizing solely remote sensing data, satellite-based hydrological datasets from several sources were acquired.

2.1. Study Area

Southern Africa is home to the Limpopo River basin, which includes parts of Botswana, Mozambique, South Africa, and Zimbabwe. The Limpopo River Basin is situated between the latitudes of 20°S and 26°S and the longitudes of 25°E and 35°E in Southern Africa as shown in Fig. 1. There are several problems in the Limpopo River watershed, but one of the biggest is water scarcity. The Limpopo River basin drains an area of around 408,000 Km^2. The Limpopo River flows from the junction of the Marcio and Crocodile Rivers in South Africa to the Indian Ocean at Xai Xai in Mozambique across more than 1,750 km. Before entering Mozambique at Pafuri, the river forms the border between Botswana and South Africa, then between Zimbabwe and South Africa. The climate of the Limpopo River basin varies along the path of the river from the temperate climate of the Western basin to the subtropical environment at the river mouth in Mozambique. The minimum and maximum summer temperatures within the catchment range from 14°C to 25°C, whereas the minimum and maximum winter temperatures range between 0°C and 17°C, respectively, during the chilly winter months [21]. The basin receives 530 mm of rain on average annually, with rainfall varying from 1200 mm in the Southeast to 200 mm in the central-West [22]. Due to the climate's wildly erratic rainfall patterns, there are both relatively dry years and years with floods. With rates

ranging from 1,000 mm/year in the Southern half of the basin to 2 000 mm/yr in the north, Evapotranspiration across the basin is high in comparison to rainfall according to the Food and Agriculture Organization (FAO) [23].

Table 1. List of hydrological variables used in this study.

Variable	Product	Spatial resolution	Temporal resolution	Time Span	Website
Precipitation	GPM IMERG V6	0.1°	Monthly	06/2000-Present	https://giovanni.gsfc.nasa.gov/giovanni/
	GLDAS-2.1 CLSM output	1°	Monthly	01/1981-Present	https://daac.gsfc.nasa.gov/
Evapotranspiration	MOD16A2	500m	8-day	12/1999-Present	https://appeears.earthdatacloud.nasa.gov/
	GLDAS-2.1 CLSM output	1°	Monthly	01/1981-Present	https://daac.gsfc.nasa.gov/
TWS	GRACE	0.1°	Monthly	03/2002-Present	https://grace.jpl.nasa.gov/
	GLDAS-2.1 CLSM output	1°	Monthly	01/1981-Present	https://daac.gsfc.nasa.gov/
Runoff	GLDAS-2.1 CLSM output	1°	Monthly	01/1981-Present	https://daac.gsfc.nasa.gov/

2.2. Methods

First, the DEM data was used to delineate the basin and its stream network using Arc Hydro Tools within the ArcGIS environment. The hydrological raster data were then subjected to image pre-processing to prepare them for analysis. The Raster Calculator function was then used to change the variable units to millimeters each month. The values for each variable were then retrieved from the monthly basin averages using Zonal Statistics. The monthly data were compiled for the basin water budget calculation, and calculations were made using the general water balance equation. To produce the overall seasonal quantities, the seasonal accumulated components were finally multiplied by the basin area. Below is provided the general water balance equation.

$$P=ET+R+\Delta S$$

Where P is Precipitation, ET is Evapotranspiration, R is Runoff, and $\Delta S=ds/dt$ is change in surface and subsurface water storage. It is important to note that the water balance calculation does not explicitly account for water quantities used for agriculture or other residential purposes, due to the lack of a mechanism for estimating such values that is universally consistent. Studies are typically carried out to ensure the accuracy and caliber of observations both before and after the launch of earth observation satellites and the introduction of new services. By contrasting the findings with remotely sensed data, and model outputs, validation studies can be carried out. Utilizing in situ research and other techniques, all the data used in this study have undergone comprehensive validation. Many academics have separately assessed remote sensing Precipitation datasets like TRMM and GPM. Various studies have evaluated Evapotranspiration data from MODIS. Multiple studies have validated the forcing data as well as the GLDAS outputs.

3. Results

For each season, the amounts of Precipitation, Evapotranspiration, Runoff, and Change in Terrestrial Water Storage were estimated. In this part, satellite-based water budget elements are assessed by comparing them with model results and measured data.

3.1. Precipitation

The regional distribution of total Precipitation for the wet and dry seasons is depicted in Fig. 2 using data from remote sensing observations (GPM IMERG) and the GLDAS model (CLSM). Due to the limited spatial resolution of GLDAS outputs, extracting raster by mask can result in loss of data; to address this problem, the shape extent coordinates were employed. then the Zonal Statistics tool in ArcGIS was used to get the area average data. IMERG data underestimates Precipitation over the Northeast region in the wet season, While GLDAS showed underestimation only on the East region. GLDAS offered higher Precipitation rates than IMERG. The variations in the datasets may result from the models' use of various forcing data.

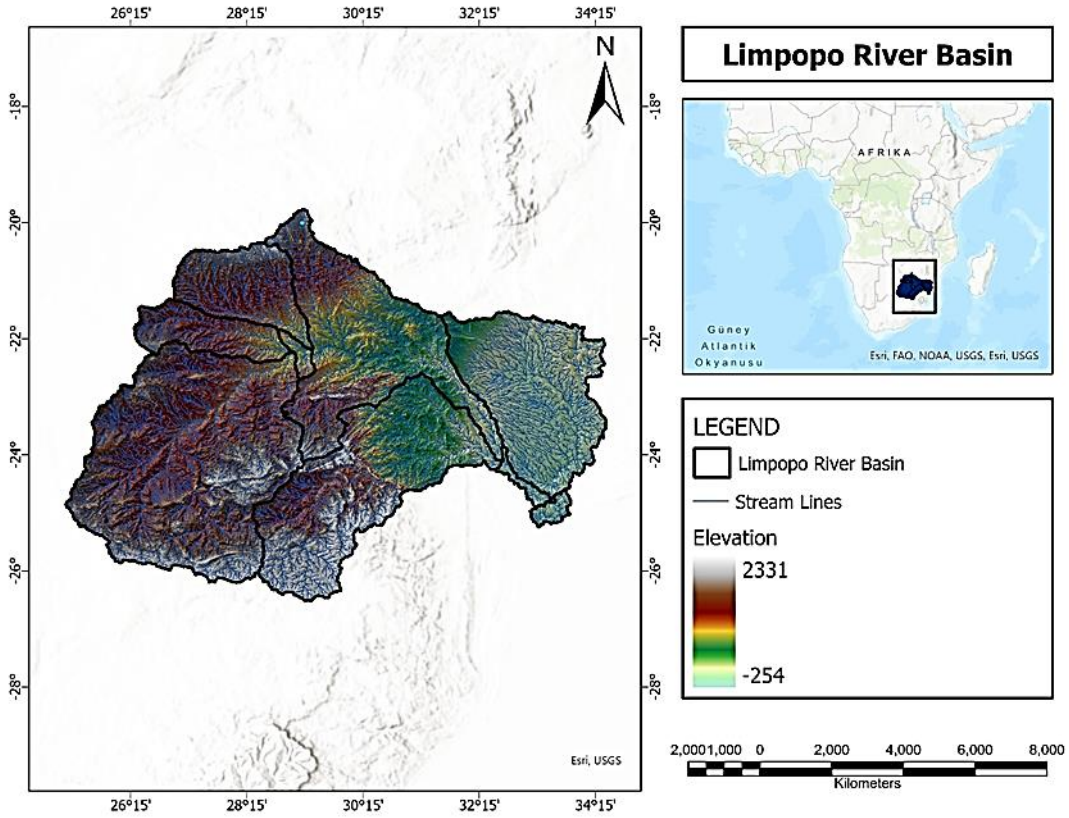

Figure 1. Study Area- Limpopo River Basin

3.2. Evapotranspiration

Using data from remote sensing observations and GLDAS CLSM, Fig. 3shows the seasonal area-averaged total Evapotranspiration for the water in the wet and dry season for the Limpopo River Basin. MODIS and GLDAS data show High rates of Evapotranspiration on the North, South, East regions in the wet season. Even while ET maps produced from GLDAS outputs have relatively low spatial resolutions, certain similarities can be seen in the patterns.

3.3. Terrestrial Water Storage Change

The water cycle relies heavily on Terrestrial Water Storage. The difference of monthly TWS over the study period was used to calculate the values of DTWS derived from the GRACE and GLDAS models. Change in TWS derived from two model outputs and GRACE product are shown in Figure 4. Most of the regions show discrepancies between the GLDAS outputs and GRACE DTWS. The variations could result from a variety of factors such as Spatial signal-leakage from adjacent areas is probable due to GRACE's coarse resolution (330 x 330 km), particularly at the sea boundary. The monthly grids have greater inaccuracies when the orbit is close to an exact repeat, which leads to incorrect gravity field estimations. Additionally, uncertainty in P, ET, and R results in uncertainty in TWSC. Another reason for the differences between the GRACE TWSC and GLDAS models could be that the GLDAS model does not take lake and river modules into account. It is GRACE's and GLDAS's primary drawback.

3.4. Runoff

Figure 5 illustrates the seasonal total Runoff derived using the GLDAS-CLSM model and the residual (P-ET-TWS) from the water balance equation for the 2019 wet and dry seasons. We calculated the residuals to determine if we can interpret those numbers as Runoff in the basin as R cannot be determined directly from satellite data. This study's objective is to evaluate each component's behavior over the Limpopo River basin rather than to resolve the water balance. Figure 5 shows that exact R values cannot be determined, not even from model output residuals.

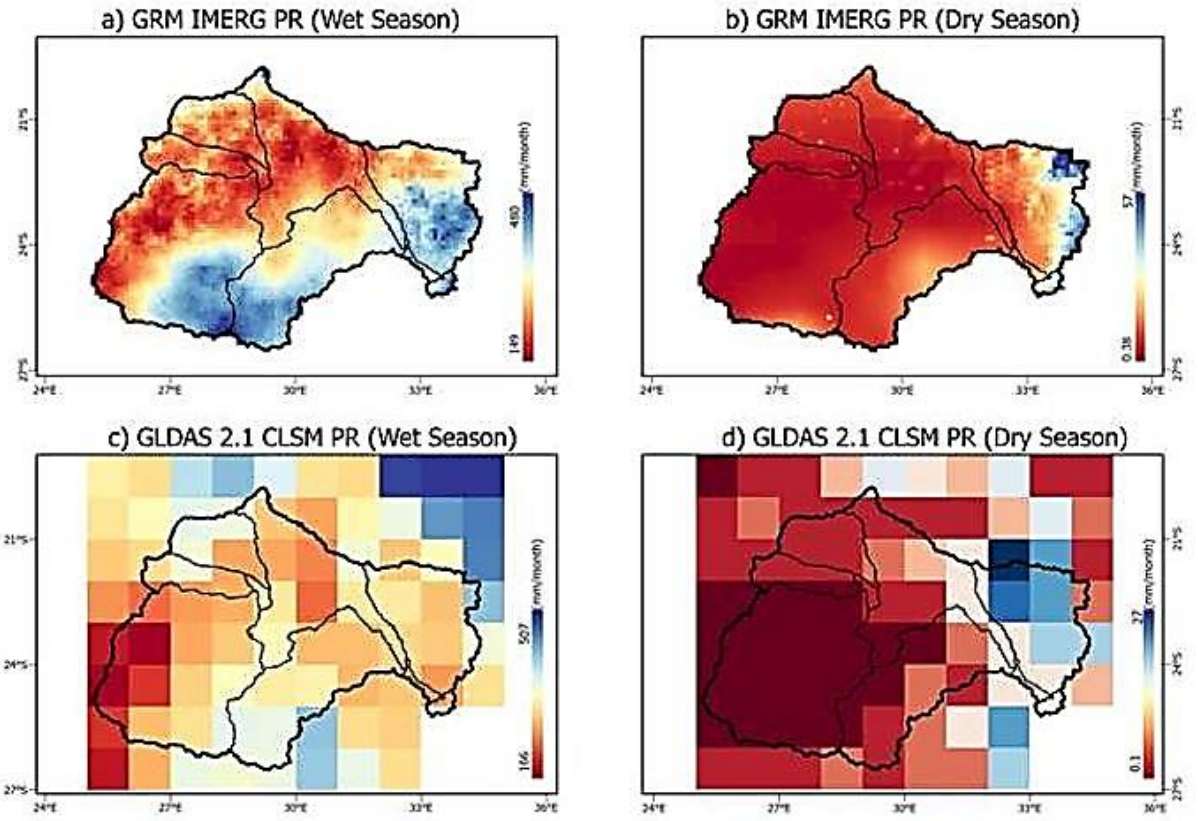

Figure 2. Average total Precipitation for the Wet and Dry season in 2019 a and b GPM IMERG (remote sensing observation), c and d GLDAS CLSM

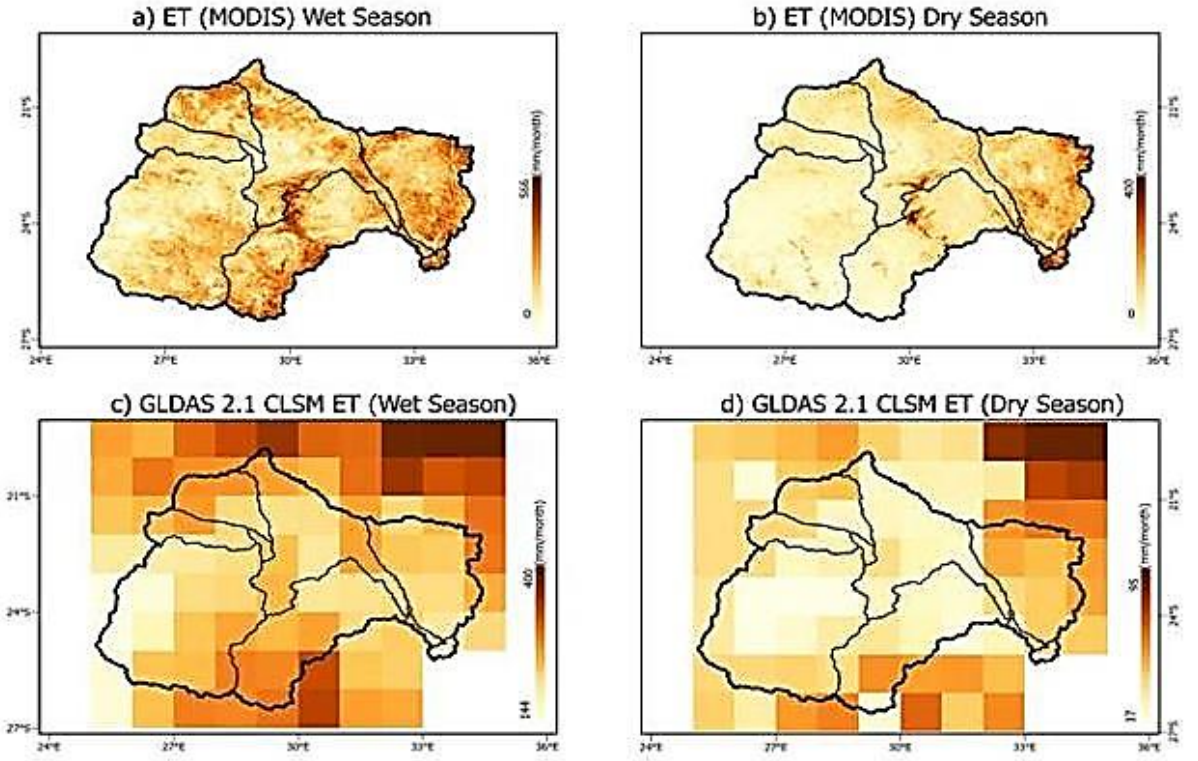

Figure 3. Average total Evapotranspiration for the Wet and Dry season in 2019 a and b GPM IMERG (remote sensing observation), c and d GLDAS CLSM

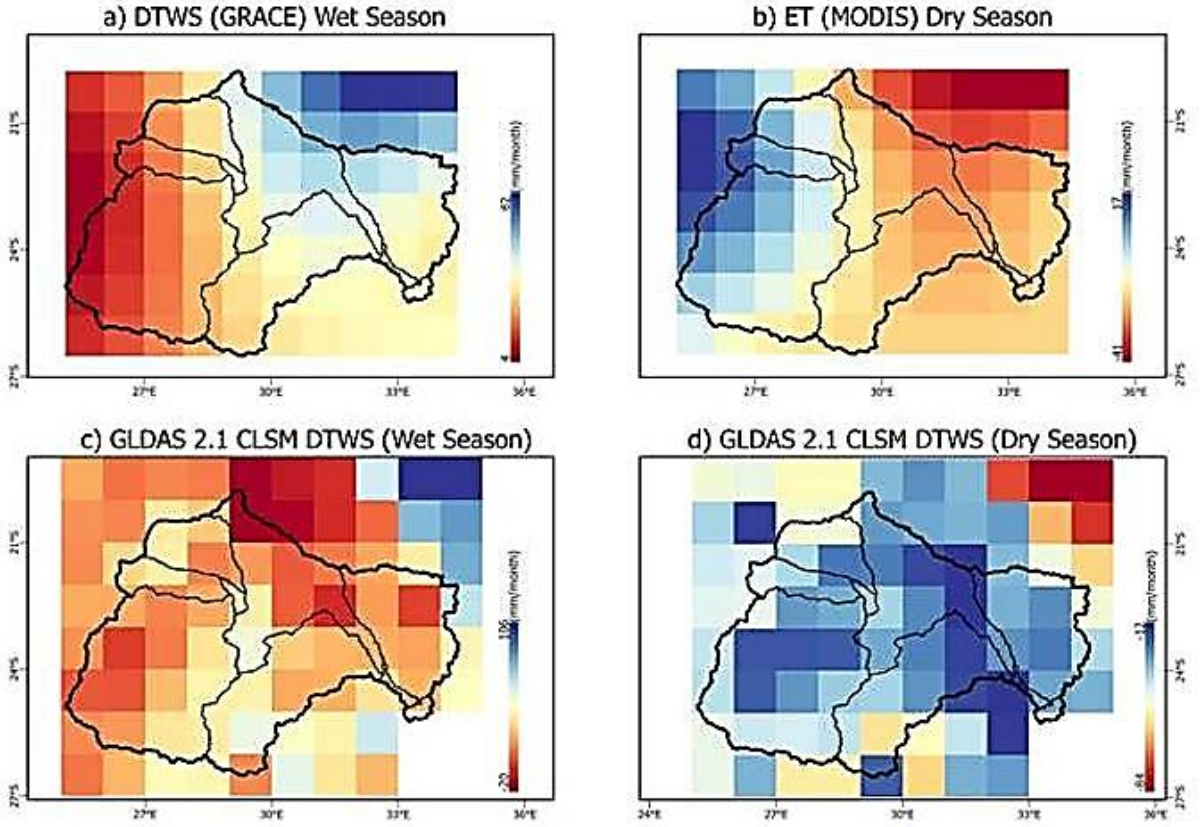

Figure 4. Total Difference Terrestrial Water Storage (DTWS) for the Wet and Dry season in 2019 a and b GPM IMERG (remote sensing observation), c and d GLDAS CLSM

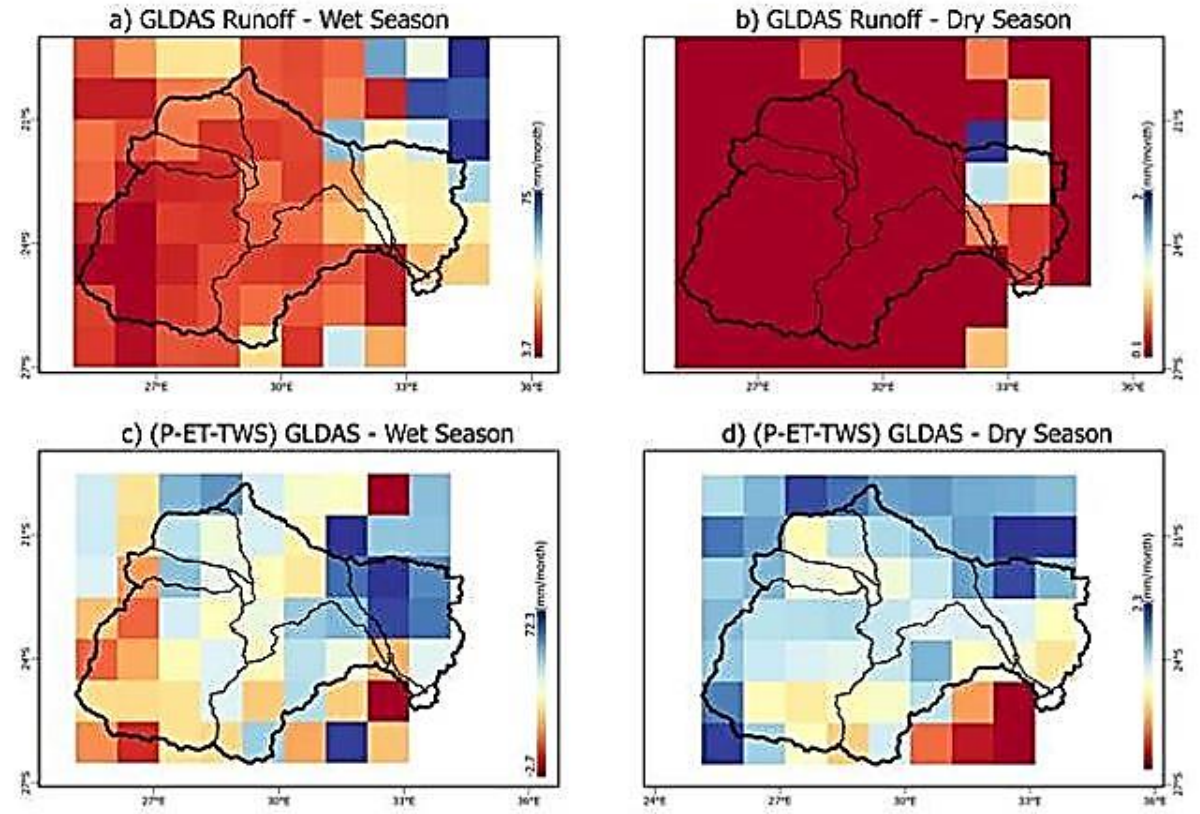

Figure 5. Total Runoff (R) for the Wet and Dry season in 2019 a and b GLDAS-CSLM for 2019 wet and dry Season, c and d water residual calculated from using water balance equation (P-ET-TWS) for 2019 wet and Dry Season

3.5. Evaluation of Water Budget Estimation

Figure 6 depicts the Limpopo Basin's basin-averaged water budget components in billion cubic meters for both the wet and dry seasons in 2019. It shows the total Seasonal P, ET, R, and TWSC calculated using the GLDAS models and observations from remote sensing. For R, ET and TWS, the results between IMERG and GLDAS were close to each other for both seasons. However, there was a noticeable difference in the Runoff observation. GLDAS Seems to underestimate the runoff values. The GLDAS-2.1 simulations do not incorporate stream flow routing; hence the modeled R has significant inaccuracies relative to the observed values.

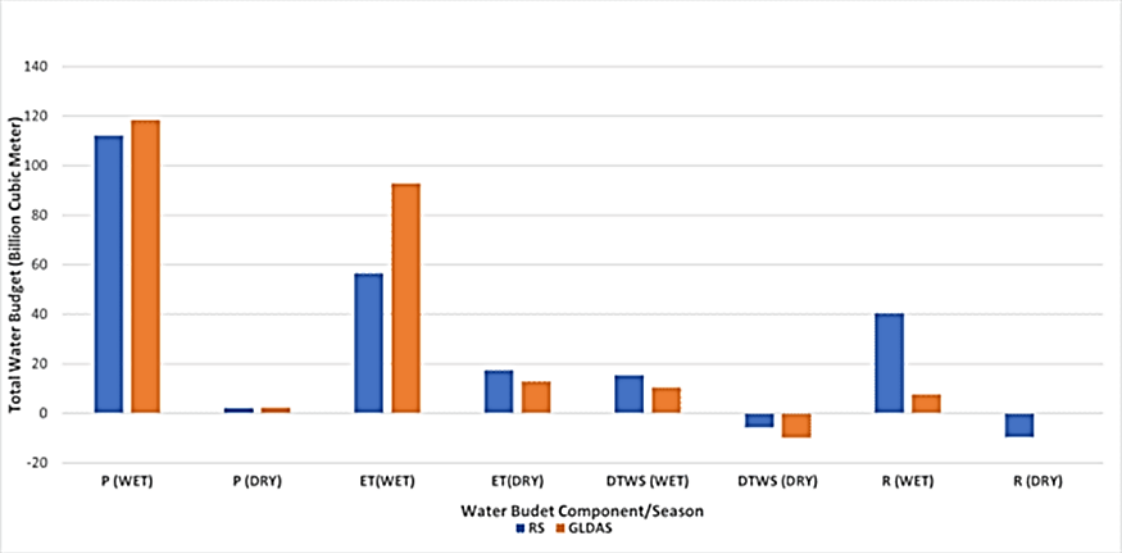

Figure 6. Seasonal water budget components of the Limpopo River Basin for the 2019 wet and dry seasons

4. Conclusion

This study used publicly available monthly satellite data and GLDAS model output products for the wet and dry seasons of 2019 to analyze GIS data over the Limpopo River Basin and assess the primary water balance components (P, ET, R, and TWSC). GPM-IMERG, MODIS, GRACE, and GLDAS-2.1 CLSM products were used to determine the amounts of Precipitation, Evapotranspiration, Runoff, and change in Terrestrial Water Storage. The findings showed how the basin's overall water budget components changed on a seasonal basis. The results showed some similarities especially for the Precipitation and Evapotranspiration. The change in Terrestrial Water Storage was estimated with the greatest degree of uncertainty. The modeled Runoff products varied greatly from one another. The residual from the water balance equation (P-ET-TWSC) was interpreted as Runoff in order to investigate the indirect approach because precise Runoff cannot be determined using remote sensing. When the residual quantities were compared to the Runoff levels predicted by the model, the findings revealed sizable disparities. Due to numerous uncertainties, including the limited resolution of GRACE & GRACE-FO and large mistakes in MODIS Evapotranspiration, closing water balance continues to be difficult. Due to the difficulty of modeling/observing all the water components in a basin, there are limits in determining the overall water budget utilizing the outputs of the GLDAS model and satellite-based remote sensing data. For instance, groundwater pumping, irrigation, and stream flow.

Acknowledgement

I would like to express my special thanks The National Aeronautics and Space Administration (NASA) and the United States Geological Survey (USGS) for supplying satellite data.

Funding

This research received no external funding.

Conflicts of interest

The authors declare no conflicts of interest.

References

1. Gleick, P. H. (2000). A look at twenty-first century water resources development. *Water international*, *25*(1), 127-138. https://doi.org/10.1080/02508060008686804
2. Chahine, M. T. (1992). The hydrological cycle and its influence on climate. *Nature*, *359*(6394), 373-380. https://doi.org/10.1038/359373a0
3. Li, X., Cheng, G., Ge, Y., Li, H., Han, F., Hu, X., ... & Cai, X. (2018). Hydrological cycle in the Heihe River Basin and its implication for water resource management in endorheic basins. *Journal of Geophysical Research: Atmospheres*, *123*(2), 890-914. https://doi.org/10.1002/2017jd027889
4. Robertson, D. M., Perlman, H. A., & Narisimhan, T. N. (2022). Hydrological cycle and water budgets. Encyclopedia of inland waters, 19-27. https://doi.org/10.1016/b978-0-12-819166-8.00008-6
5. Healy, R. W., Winter, T. C., LaBaugh, J. W., & Franke, O. L. (2007). *Water budgets: foundations for effective water-resources and environmental management* (Vol. 1308, p. 90). Reston, Virginia: US Geological Survey. https://doi.org/10.3133/cir1308
6. Ahmadzai, S., & McKinna, A. (2018). Afghanistan electrical energy and trans-boundary water systems analyses: challenges and opportunities. Energy Rep. 4, 435–469. https://doi.org/10.1016/j.egyr.2018.06.003
7. Wolf, A. T. (2002). *Atlas of international freshwater agreements* (Vol. 4). UNEP/Earthprint.
8. Wolf, A. T., Yoffe, S. B., & Giordano, M. (2003). International waters: identifying basins at risk. *Water policy*, *5*(1), 29-60. https://doi.org/10.2166/wp.2003.0002
9. Kansoh, R., Abd-El-Mooty, M., & Abd-El-Baky, R. (2020). Computing the water budget components for lakes by using meteorological data. *Civil Engineering Journal*, *6*(7), 1255-1265. https://doi.org/10.28991/cej-2020-03091545
10. Ayivi, F., & Jha, M. K. (2018). Estimation of water balance and water yield in the Reedy Fork-Buffalo Creek Watershed in North Carolina using SWAT. *International Soil and water conservation Research*, *6*(3), 203-213. https://doi.org/10.1016/j.iswcr.2018.03.007
11. Kreklow, J., Tetzlaff, B., Burkhard, B., & Kuhnt, G. (2020). Radar-Based Precipitation Climatology in Germany—Developments, Uncertainties and Potentials. *Atmosphere*, *11*(2), 217. https://doi.org/10.20944/preprints202002.0044.v1
12. Habtie, T. Y. (2021). *Remote sensing and GIS based estimation of evapotranspiration to improve irrigation water management: In Koga, Ethiopia* (Doctoral dissertation).
13. Rao, W., & Sun, W. (2022). Runoff variations in the Yangtze River Basin and sub-basins based on GRACE, hydrological models, and in-situ data. *Earth and Planetary Physics*, *6*(3), 228-240. https://doi.org/10.26464/epp2022021
14. Pokhrel, Y., Felfelani, F., Satoh, Y., Boulange, J., Burek, P., Gädeke, A., ... & Wada, Y. (2021). Global terrestrial water storage and drought severity under climate change. *Nature Climate Change*, *11*(3), 226-233. https://doi.org/10.1038/s41558-020-00972-w
15. Sheffield, J., Wood, E. F., Pan, M., Beck, H., Coccia, G., Serrat-Capdevila, A., & Verbist, K. (2018). Satellite remote sensing for water resources management: Potential for supporting sustainable development in data-poor regions. *Water Resources Research*, *54*(12), 9724-9758. https://doi.org/10.1029/2017wr022437
16. Gebrechorkos, S. H., Hülsmann, S., & Bernhofer, C. (2019). Changes in temperature and precipitation extremes in Ethiopia, Kenya, and Tanzania. *International Journal of Climatology*, *39*(1), 18-30. https://doi.org/10.1002/joc.5777
17. Levizzani, V., & Cattani, E. (2019). Satellite remote sensing of precipitation and the terrestrial water cycle in a changing climate. *Remote sensing*, *11*(19), 2301. https://doi.org/10.3390/rs11192301
18. Nashwan, M. S., Shahid, S., & Wang, X. (2019). Assessment of satellite-based precipitation measurement products over the hot desert climate of Egypt. *Remote Sensing*, *11*(5), 555. https://doi.org/10.3390/rs11050555
19. Ullah, W., Wang, G., Ali, G., Tawia Hagan, D. F., Bhatti, A. S., & Lou, D. (2019). Comparing multiple precipitation products against in-situ observations over different climate regions of Pakistan. *Remote Sensing*, *11*(6), 628. https://doi.org/10.3390/rs11060628
20. Gado, T. A., Hsu, K., & Sorooshian, S. (2017). Rainfall frequency analysis for ungauged sites using satellite precipitation products. *Journal of hydrology*, *554*, 646-655. https://doi.org/10.1016/j.jhydrol.2017.09.043
21. Moeketsi, P., Nkhonjera, G. K., & Alowo, R. (2022, October). Changes in land use land cover within the Jukskei River basin and its implications on the water availability. In *IOP Conference Series: Earth and Environmental Science* (Vol. 1087, No. 1, p. 012035). IOP Publishing. https://doi.org/10.1088/1755-1315/1087/1/012035.
22. Domingos Sambo, S. (2021). Spatio-temporal drought characteristics in the Limpopo basin from 1918 to 2018-A case study based on analysis of the Standardized Precipitation Evaporation Index (SPEI). *Student thesis series INES*.

23. Blatchford, M. L., Mannaerts, C. M., Njuki, S. M., Nouri, H., Zeng, Y., Pelgrum, H., ... & Karimi, P. (2020). Evaluation of WaPOR V2 evapotranspiration products across Africa. *Hydrological processes*, *34*(15), 3200-3221. https://doi.org/10.1002/hyp.13791.